“I’m a slow learner, it’s true. But I learn…”

Sansa Stark.

A nonna Livia, un abbraccio da quaggiù.

SCUOLA DOTTORALE IN

GEOLOGIA DELL'AMBIENTE E DELLE RISORSE (SDiGAR)

XXX CICLO

Lateral vs vertical propagation of dikes through analogue modeling

Dottorando: _____

Stefano Urbani firma

Docente Guida: _____

Valerio Acocella firma

Coordinatore: _____

Claudio Faccenna firma

Co-Tutor: Dott.ssa Eleonora Rivalta, GeoForschungsZentrum (GFZ), Potsdam Germania

Revisori:

Dott. Nicolas Le Corvec: Universitè Blaise Pascal, Clermont Ferrand, Francia

Dott. Benoit Taisne: Earth Observatory of Singapore

Table of Contents

Abstract

The interest on the mechanisms governing dike propagation has been renewed by recent diking events showing lateral propagation along rift zones for tens of kilometers. Such laterally propagating dikes may feed eruptions far from their magma chamber, thus representing volcanic hazard in densely populated areas far from central volcanoes. It is therefore crucial to understand what mechanisms drive dike propagation and arrest in order to be eventually able to constrain the possible location of surface vents. In this regard, it is known that dikes may propagate both laterally and/or vertically at both a local (central volcanoes) and regional scale (rift systems), depending on several factors (such as regional stress, crustal layering, topography, buoyancy, magma solidification and gas exsolution, preexisting structures in the host rock, magma influx rate). However, so far these factors have been usually studied independently of each other. As in nature these factors may act contemporaneously, it is crucial to assess their relative importance by establishing a hierarchy.

The goal of this thesis is to address this latter issue by defining an hierarchy between a selection of these factors (crustal layering, topography, density ratio between host rock and magma, magma influx rate) through analogue models focusing on the conditions favoring lateral propagation. In the analogue experiments, each of the studied parameters has been varied systematically, fixing all the other variables, comparing semi-quantitatively the variations on dike shape and velocity. Two different sets of experiments with vertical (Set 1) and lateral (Set 2) injection have been performed. The results indicate that rigidity layering (i.e. a stiff layer overlying a weak one) and topography are the most efficient parameters that favor lateral propagation, while density layering, density ratio and magma influx rate show a subordinate role. Moreover, the observations made during the experiments of dike propagation testing the joint effect of rigidity layering and topography (i.e. downslope lateral dike propagation and arrest in front of an external relief) show interesting similarities with the 2014 Bardarbunga (Iceland) diking event, suggesting that our results should be taken into account to explain the lateral propagation observed in other recent diking events.

In nature, rigidity inversions (i.e. stiff layers above weak ones) may occur frequently. These inversions are usually due to alternating soft scoria layers and stiff lava flows (as in Afar), or to thermal weakening, which decreases host rock rigidity at higher depths (as observed in Iceland, Hawaii and Canary Islands). Such rigidity contrasts may be one order of magnitude higher than the contrasts imposed in the models, thus encouraging natural dikes to propagate laterally at the interface with the stiffer zones as observed in the models.

This approach to the investigation of the factors controlling dike propagation (i.e. systematic variations of the parameters and hierarchy definition) should be followed in future works adding the remaining processes that influence dike propagation (such as pre-existing structures in the host rocks, magma solidification, regional tectonic stresses, gas exsolution) not considered in this study.

Riassunto

L'interesse per i meccanismi che controllano la propagazione dei dicchi è stato rinnovato da recenti eventi eruttivi che hanno mostrato una propagazione laterale di dicchi per decine di chilometri. Tali dicchi a propagazione laterale, possono alimentare eruzioni a grandi distanze dalla loro camera magmatica di origine, rappresentando un fattore di rischio vulcanico in zone, densamente popolate, lontane dai vulcani centrali. È quindi fondamentale capire quali meccanismi controllano la direzione di propagazione e l'arresto dei dicchi per poter vincolare la possibile posizione delle bocche eruttive in superficie. A questo proposito, è noto che i dicchi possono propagarsi sia lateralmente e/o verticalmente sia a scala locale (vulcani centrali) che a scala regionale (sistemi di *rift*), in base alla variazione di diversi fattori come: lo stress tettonico regionale, la stratificazione crostale, la topografia, la spinta di galleggiamento, gli effetti del raffreddamento del magma e dell'essoluzione di gas, la presenza di strutture preesistenti nella roccia incassante, il tasso di afflusso di magma. Tuttavia, sino ad ora questi fattori sono stati studiati indipendentemente gli uni dagli altri. Poiché in natura questi fattori possono agire contemporaneamente, è cruciale valutare la loro importanza relativa stabilendo una gerarchia.

L'obiettivo di questa tesi è quello di affrontare quest'ultimo problema definendo una gerarchia tra una selezione di questi fattori (stratificazione crostale, topografia, rapporto di densità tra roccia incassante e magma, tasso di flusso magma) attraverso modelli analogici che si concentrano sulle condizioni che favoriscono la propagazione laterale. Negli esperimenti analogici, ciascuno dei parametri studiati è stato variato sistematicamente, fissando tutte le altre variabili, confrontando semi-quantitativamente le variazioni di forma e velocità del dicco. Sono stati eseguiti due differenti gruppi di esperimenti con iniezione verticale (Gruppo 1) e laterale (Gruppo 2). I risultati indicano che la stratificazione di rigidità (cioè uno strato rigido sovrastante uno strato più debole) e la topografia sono i parametri più efficaci che favoriscono la propagazione laterale, mentre la stratificazione di densità, il rapporto di densità roccia-magma ed il tasso di afflusso di magma mostrano un ruolo subordinato. Inoltre, le osservazioni fatte durante gli esperimenti, che testano l'effetto congiunto della stratificazione di rigidità e della topografia (ossia la propagazione laterale del dicco sotto un pendio e arresto dello stesso di fronte a un rilievo esterno), mostrano una stretta analogia con l'evento eruttivo del 2014-2015 al Bardarbunga (Islanda) suggerendo che i nostri risultati dovrebbero essere presi in considerazione per spiegare la propagazione laterale osservata in altri eventi eruttivi.

In natura, le inversioni di rigidità (cioè strati rigidi sopra quelli deboli) possono verificarsi frequentemente. Queste inversioni sono solitamente dovute ad una alternanza di strati morbidi di scoria e colate di lava rigide (come in Afar), o all'indebolimento termico, che fa diminuire la rigidità della roccia incassante a profondità più elevate (come osservato in Islanda, Hawaii e Isole Canarie). Tali contrasti di rigidità possono essere di un ordine di grandezza superiore rispetto ai contrasti imposti nei modelli, incoraggiando così i dicchi in natura a propagarsi lateralmente all'interfaccia con le zone più rigide come osservato nei modelli.

Questo approccio all'investigazione dei fattori che controllano la propagazione dei dicchi (cioè le variazioni sistematiche dei parametri e la definizione della gerarchia) dovrebbe essere seguito in lavori futuri aggiungendo i restanti processi che influenzano la propagazione dei dicchi (come le

strutture preesistenti nella roccia incassante, la solidificazione del magma, sforzi tettonici regionali, essoluzione dei gas) non considerate in questo studio.

Acknowledgments

Therefore, here I am at the end of a long journey that, as a student from the BSc to the PhD, lasted for such a long time at Roma Tre. I have many people to thank in the last 10 years since I started to get involved in geology finally focusing on Volcano-Tectonics, which I hope to continue to study for the coming years. First, I want to thank my supervisor, Valerio Acocella, which, since the Master degree, provided me countless opportunities to go to the field and present my research at conferences introducing me to various experienced and famous scientists, which I had the honor to work with and discuss about my research. I have learned a lot from Valerio during the meetings (sometimes harsh) at his office that improved all the presentations and writings made during the MSc and PhD.

Valerio made an incredible effort to push myself over my limits, not only on the scientific point of view but also about life, supporting me not only as a supervisor but also as a friend during the worst moments of my life.

I have also to thank my co-supervisor, Eleonora Rivalta, which has been of tremendous help in most of the mathematical stuff that was part of this thesis and for the understanding of the physics behind the processes observed in the lab. Moreover, she often provided a smile and nice words to cheer me up during the most stressful and bad times of this PhD.

Special thanks go to “the hammers et al.” (Marco, Matteo, Gabriele, Stefania, Silvia and Gaia) for all the time spent together hanging around in the last 10 years and for having shared the highs and lows of this long journey between lessons, exams and conferences. It was essential and helpful to support each other to overcome the obstacles and challenges we have faced many times.

Many thanks also to Giulia for all the time spent together inside and outside the laboratory discussing about science (and many other funny things) in front of a cup of coffee and a ginseng (and a damn cigarette).

Lastly, I thank my family, which funded my education before the beginning of the PhD.

Chapter 1

Introduction

The most efficient process to drive magma ascent within the Earth's lithosphere is the propagation of magma-filled fractures, called dikes [Rubin, 1995]. Although most of the dikes do not reach the surface, arresting at various crustal depths [Gudmundsson, 2011], nearly all eruptions are triggered and fed by those that make it to the surface.

During their ascent within the crust, dikes may propagate laterally or vertically (revealing the propagation direction of magma flow) implying that they can eventually feed eruptions within widespread areas. In particular, in the case of lateral magma flow, eruptions can occur far from the feeding chamber and the volcanic edifice, threating the population living at the base of the volcano [Cappello et al., 2012; Smets et al., 2015; Tadini et al., 2017a, 2017b].

Therefore, understanding dike propagation and emplacement is crucial not only to possibly forecast if an eruption will occur, but also to constrain the position of the surface vents fed by both lateral or vertical propagating dikes [Sparks, 2003; Brenguier et al., 2008; Kauahikaua and Poland 2012; Sparks et al., 2012; White and McCausland, 2016].

Lateral and vertical dike propagation have been previously inferred to deliver magma in both central volcanoes (Fig. 1a-b, [Geshi et al., 2008]) and rift systems (Fig. 8a-b, [Hartley and Thordarson, 2013]), suggesting that the factors that control dike propagation are scale independent. In this regard, the interest on dike propagation has been renewed by geophysical and geodetic data of recent diking events, revealing lateral dike propagation for tens of kilometers before the eruption, at Lake Natron (Tanzania) in 2007 [Biggs et al., 2009], Dallol and Dabbahu (Afar, Ethiopia) in 2004 and 2005-2010 [Ebinger et al., 2010; Nobile et al., 2012], Tolbachik (Kamchatka, Russia) in 2012-2013 [Caudron et al., 2015] and Bardarbunga (Iceland) in 2014-2015 [Sigmundsson et al., 2015].

Moreover, several recent eruptions at Etna (Italy) in 2001 [Acocella and Neri, 2003], Stromboli (Italy) in 2002-2003 and 2007 [Acocella et al., 2006b; Neri et al., 2008] and El Hierro (Canary Islands, Spain) in 2011-2012 [Martì et al., 2013, 2017] reveal that dikes may propagate both laterally and vertically, even changing their paths during the same eruption in response to the variations of the factors driving them (such as topography, regional stresses or rheological contrasts in the host rock). In these cases (except El Hierro), vertical dikes feed summit eruptions through a central conduit whereas lateral dikes, independent from the summit system, feed flank eruptions.

1.1 Lateral vs vertical dike propagation at central volcanoes

Models on dike propagation at central volcanoes, provide that lateral propagation occurs in a case of an open central conduit from which, a degassed and denser magma, intrudes laterally feeding flank eruptions (Fig. 1a [Geshi et al., 2008]). On the contrary, vertical propagation occurs in case of a closed central conduit with magma rising vertically from the chamber towards the flanks of the volcano (Fig.1b [Geshi et al., 2008]).

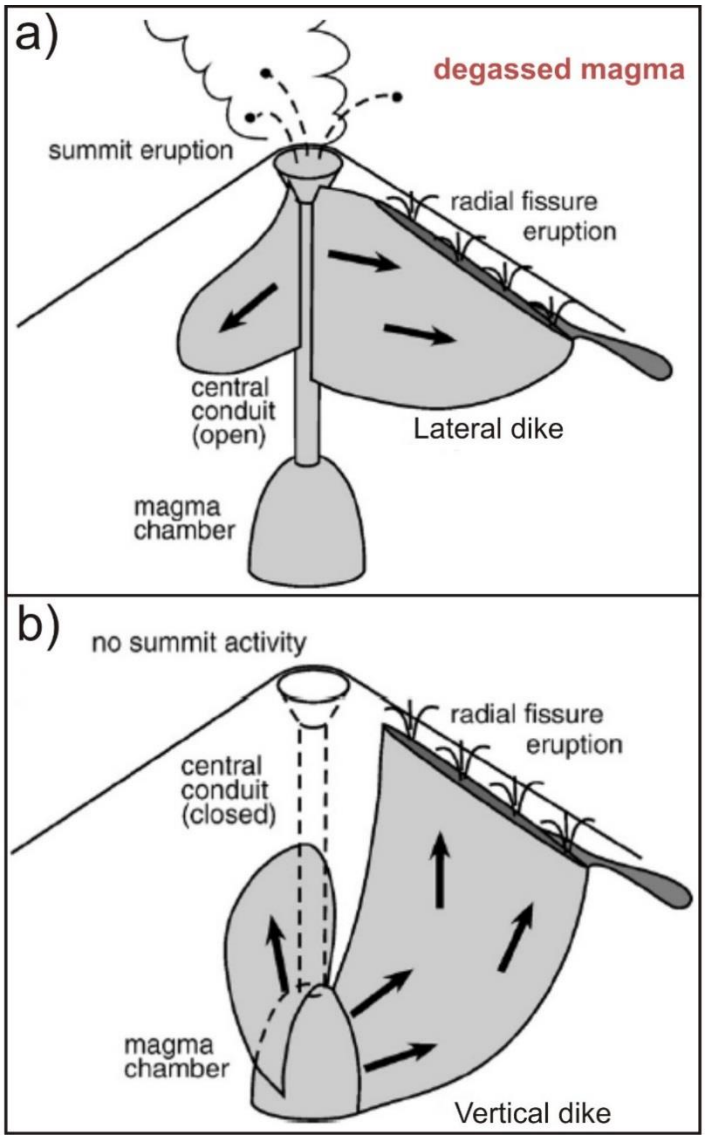

Fig.1. Schematic diagrams illustrating models of lateral (a) versus vertical (b) dike propagation at central volcanoes. a) With an open central conduit, a degassed and denser magma intrudes laterally from the conduit feeding fissure eruptions on the flank of the volcano. b) With a closed conduit, a less dense magma propagates vertically directly from the chamber towards the flank of the volcano. Modified from [Geshi et al., 2008].

In nature, lateral dike propagation has been repeatedly observed, as at Vesuvio (Italy) during the 1694 to 1944 fissure eruptions [Acocella et al., 2006a], Fernandina (Galapagos, Ecuador) in 1995, 2005 and 2009 [Chadwick et al., 2011; Bagnardi et al., 2013], Miyakejima (Japan) in 2000 [Ueda et al., 2005], Piton de la Fournaise (La Reunion, France) in 2000-2003 [Peltier et al., 2005, 2009], Etna

(Italy) in 2001 [Acocella and Neri, 2003], Stromboli (Italy) in 2002-2003 and 2007 [Acocella et al., 2006b; Neri et al., 2008], El Hierro (Canary Islands, Spain) in 2011-2012 [Martì et al., 2013], Tolbachik (Kamchatka, Russia) in 2012-2013 [Caudron et al., 2015].

All these eruptions will be briefly described following a chronological order.

At the Somma-Vesuvio volcanic complex, gravitational loading of the remnants of the Mt. Somma edifice, located in the northern border of the active Vesuvio cone, hindered lateral propagation of magma as suggested by the absence of dikes and fissure eruptions beyond Mt. Somma (Fig.2) [Acocella et al., 2006a].

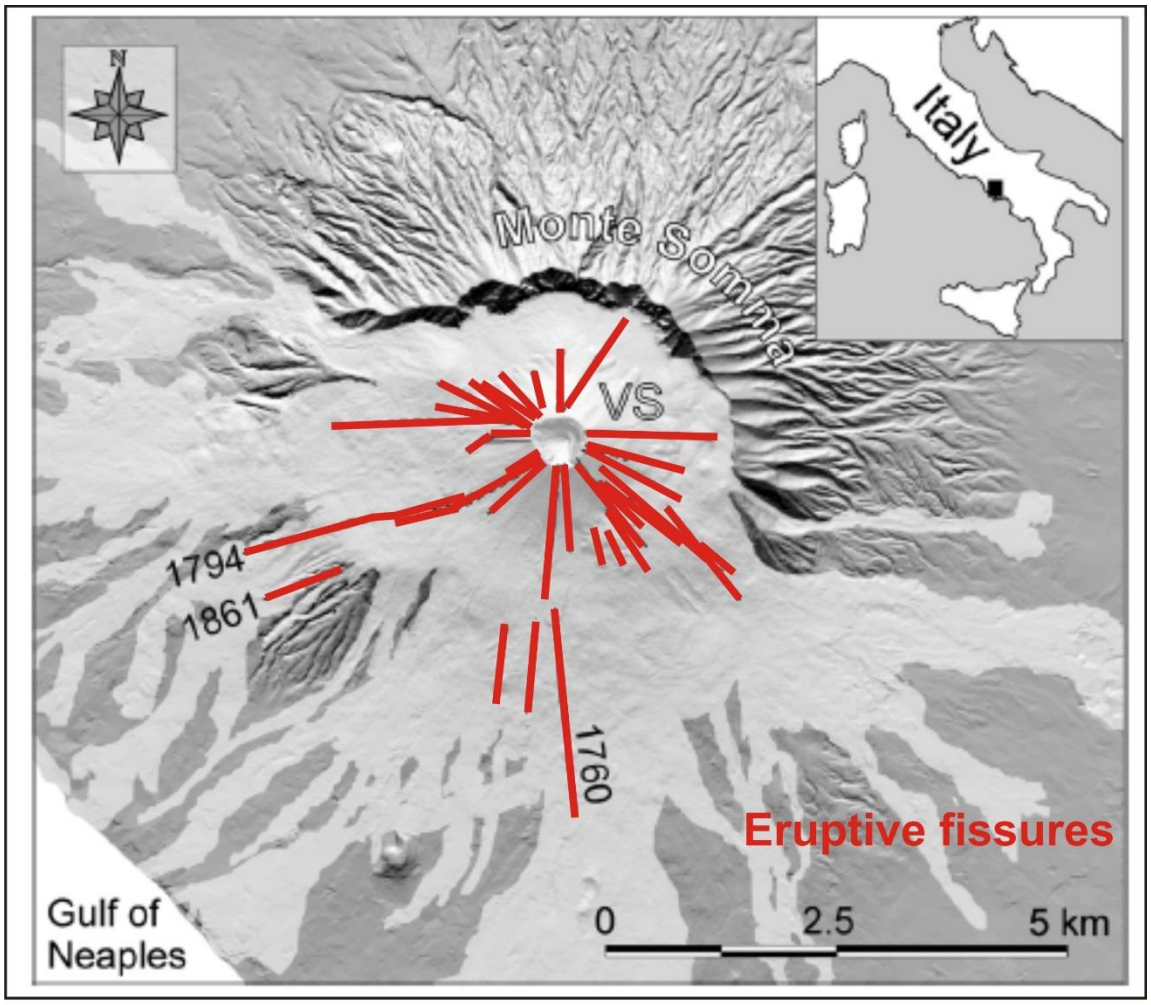

Fig.2. DEM of Somma-Vesuvio, showing the 36 fissures between 1694–1944 and the related lava field. VS = Vesuvio. From [Acocella et al., 2006a].

Modeling of GPS and InSAR data at Fernandina revealed that the circumferential fissures that opened parallel to the caldera rim in May 2005 were fed by a curved dike showing a complex "concave shell" shape connected to a shallow sill (~1 km depth, Fig.3a-b) [Chadwick et al., 2011]. Conversely, in the 1995 and 2009 eruptions two radial dikes, oriented NE-SW and NNE-SSW respectively, propagated from deeper sills (~2 km depth) towards the flanks of the volcano, feeding radial fissures (Fig.3c-d) [Bagnardi et al., 2013]. This two-fold intrusive pattern (i.e. alternating radial and circumferential dikes) is characteristic also of the other volcanoes in Western Galapagos [Chadwick and Howard, 1991] suggesting common processes controlling magma dynamics at a broader scale. It has been proposed that this pattern is due to a competition between caldera collapse (i.e. unloading), magma buoyancy and tectonic stresses, explaining all the observations described above [Corbi et al., 2015].

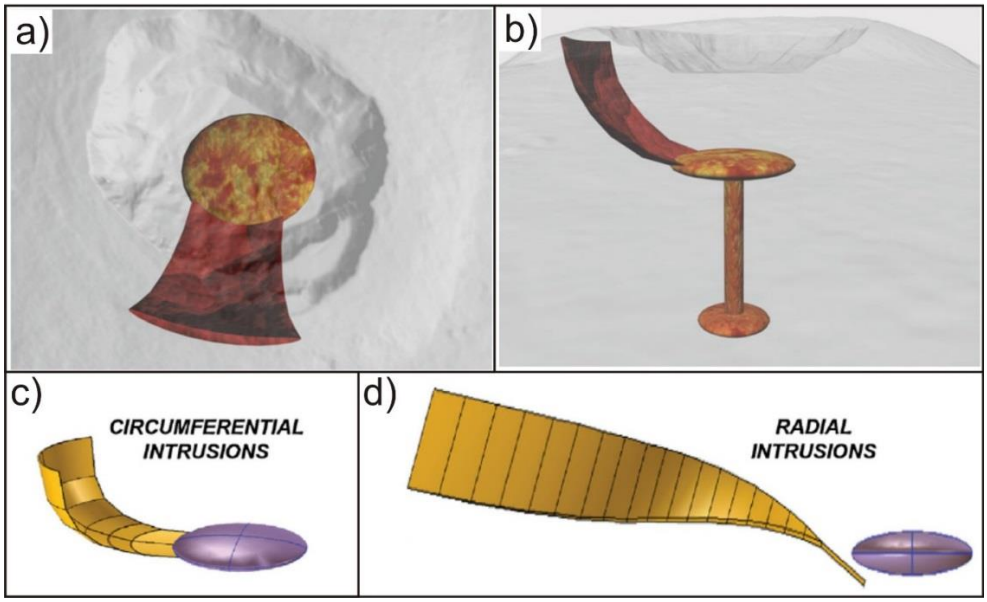

Fig.3. Top (a) and side (b) view of the three-dimensional representation of the curved circumferential dike that fed the 2005 eruption at Fernandina. A deep magma reservoir at 5 km depth feeds a shallower sill (1 km depth), which in turn feeds a curved circumferential dike with the shape of a concave shell. Dike thickness not to scale. Modified from [Chadwick et al., 2011]. Three-dimensional representation of circumferential (c) and radial (d) intrusions. The sill feeding the dikes are represented in purple and yellow respectively. Modified from [Bagnardi et al., 2013].

At Miyakejima, a dike propagated laterally from the volcanic edifice for ~30 km, stopping in correspondence of a strike slip system, oriented sub-perpendicular to the dike plane. It has been proposed that the dike arrest was due to the joint effect of the stress gradient induced by the topography and by the interaction with the strike slip fault (Fig.4a-b) [Maccaferri et al., 2016].

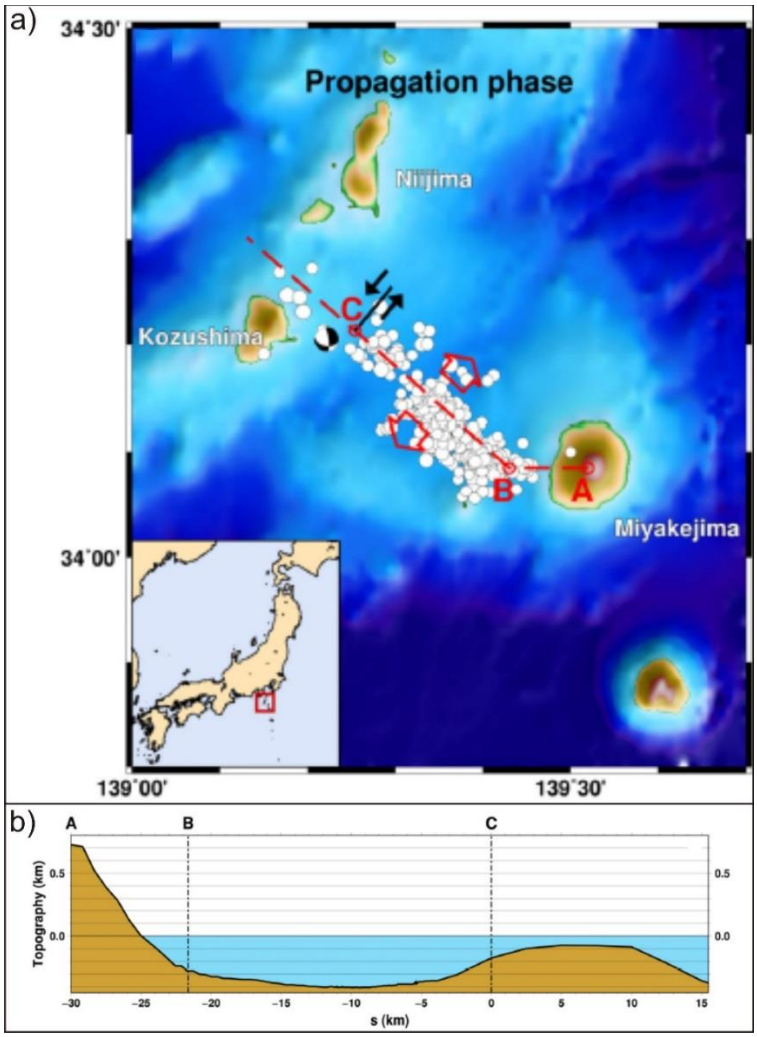

Fig.4. a) Map of the approximate path of the dike (dashed red line) during the 2000 Miyakejima eruption. A indicates the location of the summit of Miyakejima, B indicates the point changes its strike, C is the position where the dike comes close to the south-western tip of the strike-slip fault. The white dots indicate the epicenters of the seismicity related to the propagation of the dike. The black solid line indicates the strike-slip fault, with arrows indicating left-lateral slip. Inset: the red square indicates the focus area. b) Topography profile along the dike trajectory. Modified from [Maccaferri et al., 2016].

Seismic and geodetic data from 9 flank eruptions between 2000 and 2003 at Piton de la Fournaise show that dike intrusions are characterized by two phases: 1) a faster vertical dike propagation from the chamber to the surface and 2) a slower lateral propagation towards the flank of the volcano, feeding distal eruptions (Fig.5) [Peltier et al., 2005, 2009]. It has been proposed that the lateral magma migration is due to a dense fracture network that represent a preferential pathway that favors lateral propagation or, alternatively, to a high olivine content in the magma which increases its density [Peltier et al., 2005, 2009].

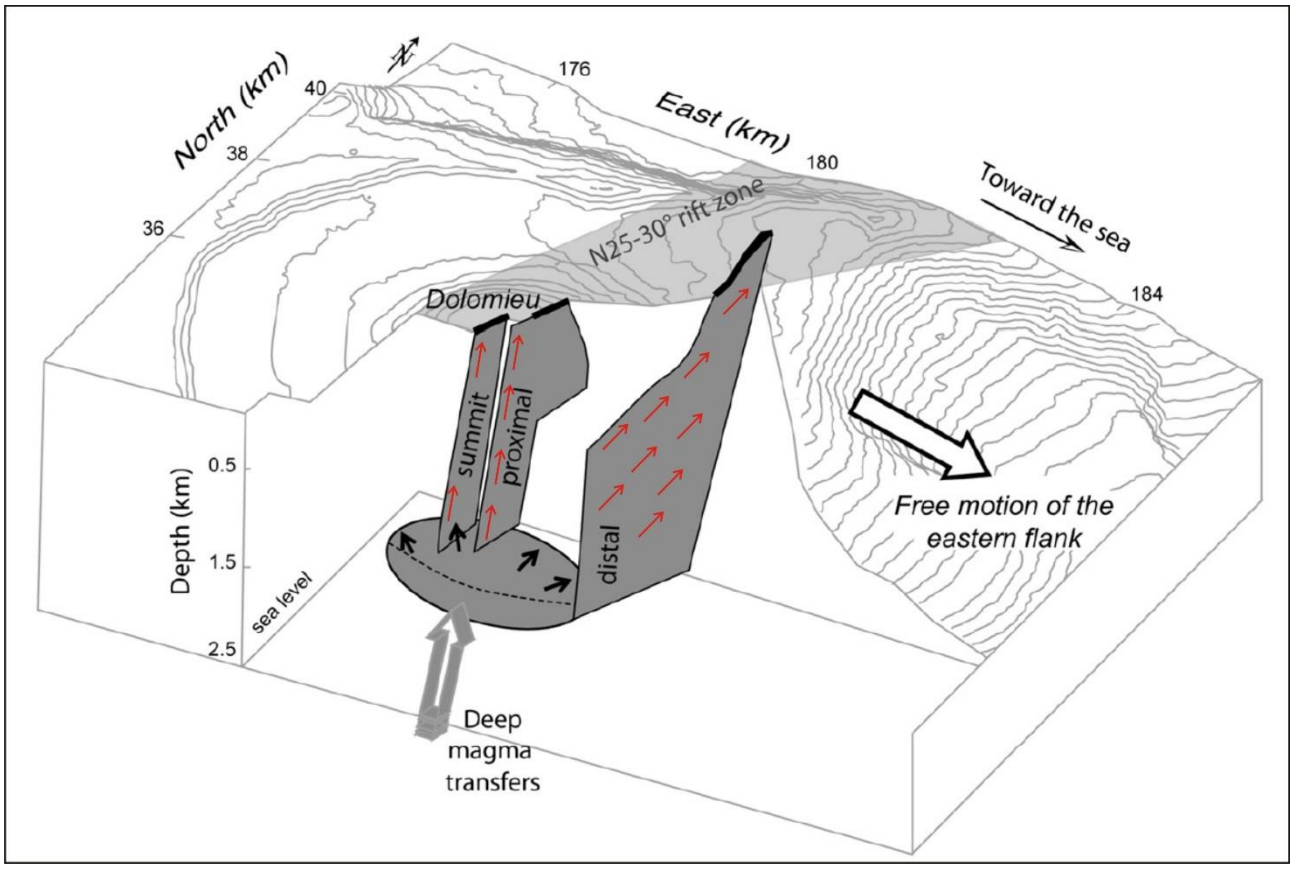

Fig.5. Schematic model of the shallow magmatic system of Piton de La Fournaise. Vertical propagating dikes feed the summit and proximal eruptions whereas lateral dikes feed the distal eruptions on the northern flank of the volcano. Modified from [Peltier et al., 2009]. The red arrows indicate the inferred direction of magma flow.

At Etna in 2001, both laterally and vertically propagating dikes were observed, feeding flank (i.e. central lateral) and peripheral eruptions respectively. It has been proposed that the rise of vertical

propagating dikes from the chamber was influenced by regional tectonic stresses, whereas gravitational stresses controlled the emplacement of the shallower lateral dikes (Fig.6) [Acocella and Neri, 2003].

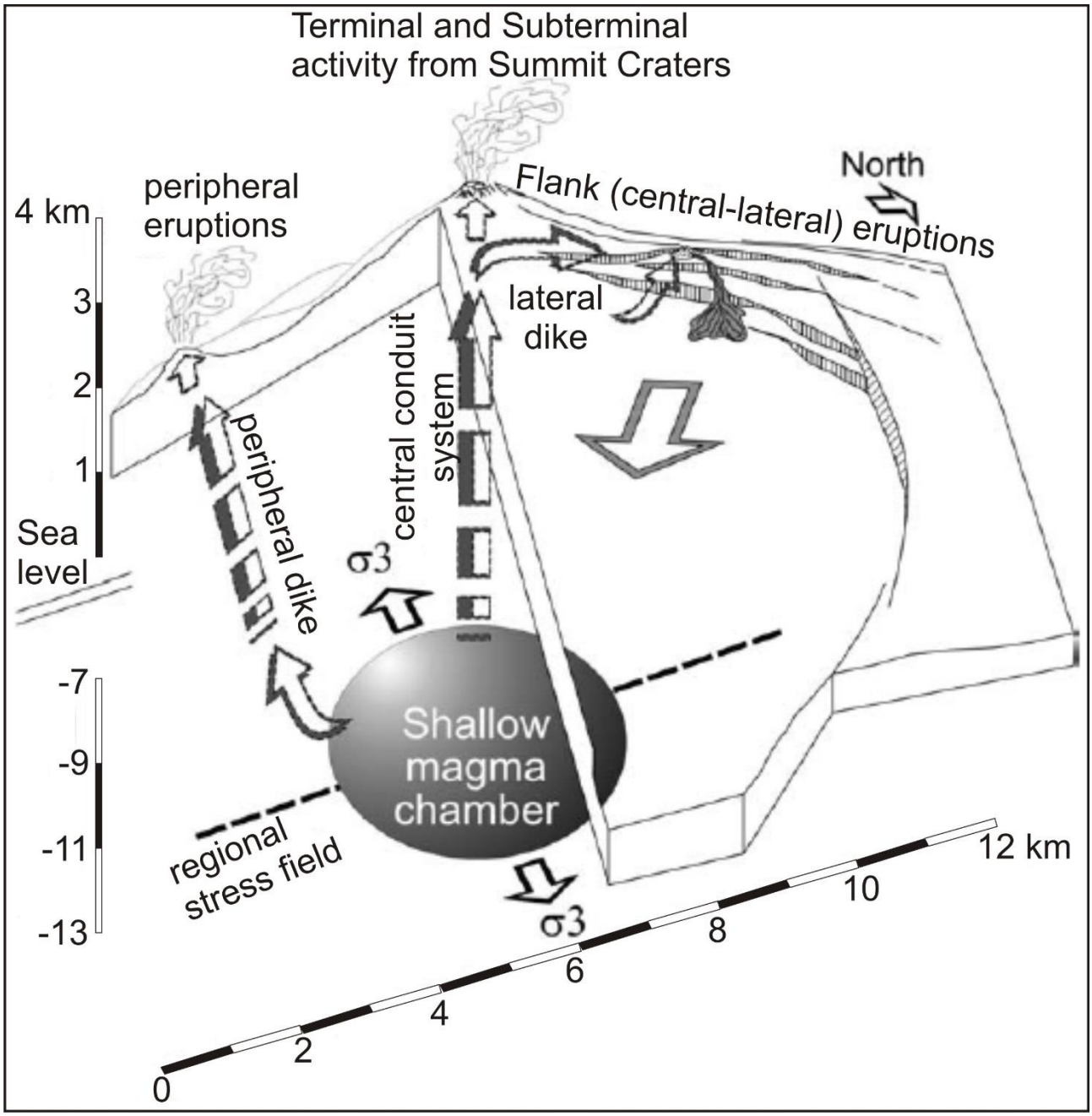

Fig.6. a) Schematic illustration for the proposed model, not to scale, of the control on the 2001 Etna eruption. From [Acocella and Neri, 2003].

Topographic effects influenced dike propagation also at Stromboli in both the 2002-2003 and 2007 eruptions. In these cases, dike emplacement was controlled by the gravitational stresses, so that the dikes intruded parallel to the slope of the Sciara Del Fuoco (Fig.7) [Acocella et al., 2006b; Neri et al., 2008].

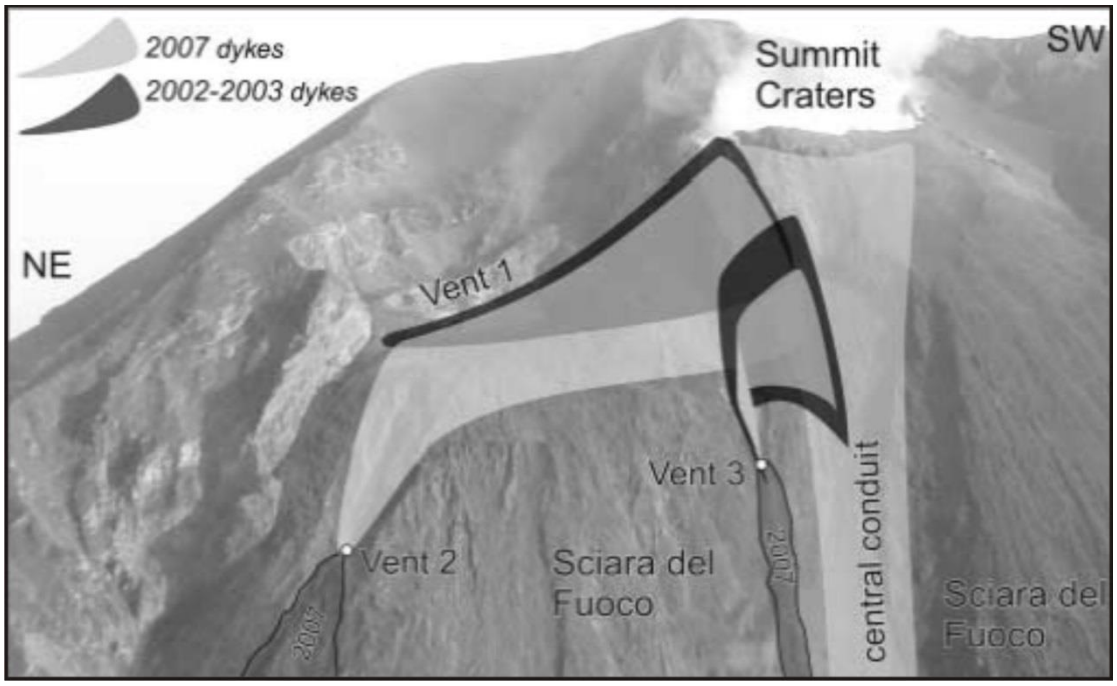

Fig.7. A 3D reconstruction of the dikes feeding the 2002–2003 and 2007 eruptions from [Neri et al., 2008].

During the 2011-2012 El Hierro eruption, magma migrated laterally offshore for nearly 20 km (towards SE) along the upper mantle-oceanic crust boundary (at 14 km depth) [Martì et al., 2013]. After this phase of lateral propagation, magma ascended vertically to the surface, feeding a submarine eruption 5 km from the southern corner of the island [Martì et al., 2013]. This eruption revealed a complex and tortuous dike propagation path, with alternating phases of vertical and lateral migration of magma, attributed to a combination of the effects of rheological contrasts (i.e. layering) in the lithosphere, tectonic stresses and gravitational loading (i.e. topography) [Martì et al., 2013; 2017]. In particular, it has been inferred that the stress field imposed by the island plus the rheological contrast

at the crust–mantle boundary favored the lateral propagation phase, while vertical ascent was promoted by an E-W striking regional fault [Martì et al., 2013; 2017].

Two alternating vertical and lateral propagation phases were also observed during the 2012-2013 Tolbachik eruption: vertical migration under the northern slope of the volcano was followed by shallow (~1 km depth) lateral migration towards a ~6 km long radial fissure on the SW flank of the volcano [Caudron et al., 2015; Lundgren et al., 2015].

All these natural cases reveal that central volcanoes are characterized by a complex dike propagation pattern with alternating lateral and vertical propagation stages (except Miyakejima). In particular, lateral propagation occurs at both deep (as at El Hierro) and shallow (as at Etna, Stromboli and Tolbachik) crustal levels. This reveals that some factors affect dike propagation at shallow depths (such as topography) whereas other factors became dominant at higher depths (such as rheological contrasts of the host rock) increasing the complexity on forecasting the magma path at central volcanoes.

1.2 Lateral vs vertical dike propagation within rift systems

Models on dike propagation within rift systems, provide that fissure eruptions are fed by laterally propagating dikes, injected from a shallow magma chamber, (Fig.8a [Hartley and Thordarson, 2013]) or by vertical dikes rising from a deep reservoir (Fig.8b [Hartley and Thordarson, 2013]). Some natural cases of lateral (described first) and vertical propagation within rift systems will be described following a chronological order.

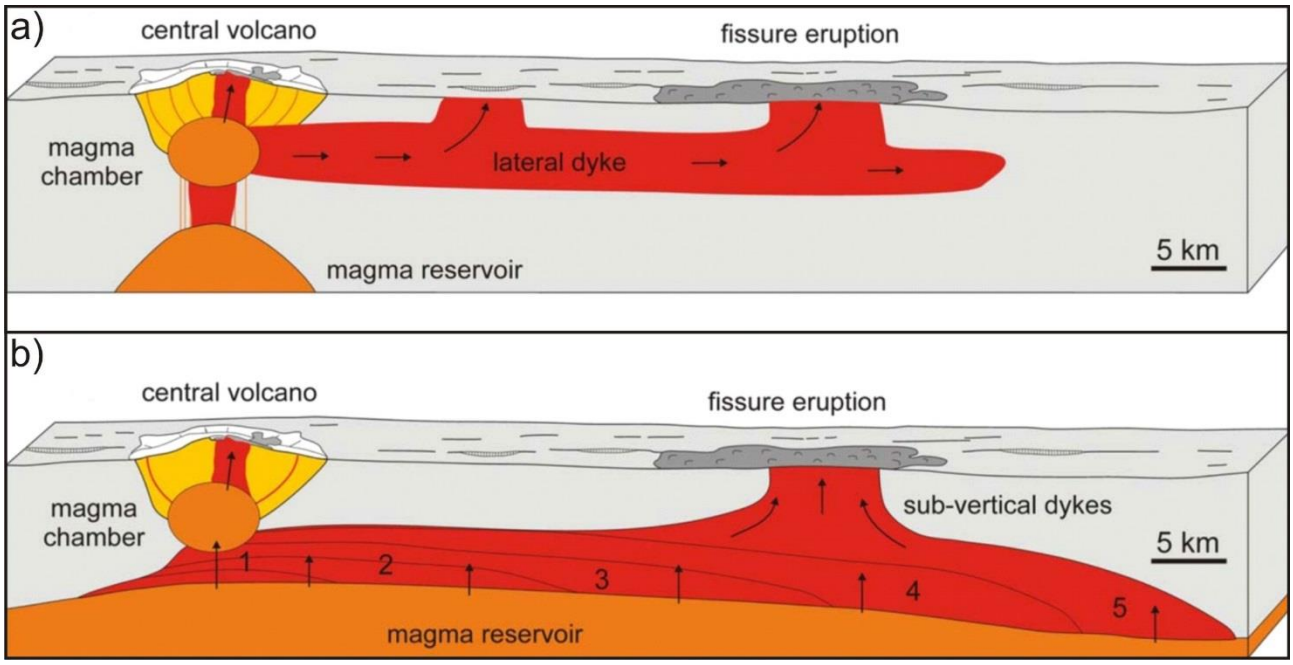

Fig.8. Schematic diagrams illustrating models of lateral (a) versus vertical (b) dike propagation in rift systems. a) Lateral propagation of dikes injected from a shallow magma chamber feeding fissure eruptions. b) Vertically propagating dikes from deep magma reservoirs at the base of the crust. The numbers indicate the growth sequence of the dikes. Modified from [Hartley and Thordarson, 2013].

The 11 km long Inyo dike, located at the edge of the Long Valley caldera in eastern California, shows a shallow en-echelon segmentation due to a change of the rheology (from ductile to brittle) and fracturing mode (from extensional to shear) of the upper crust (about 3 km depth) [Reches and Fink, 1988].

Geodetic and seismic data suggest that during the 1975-1984 Krafla (Iceland) rifting episode 20 dikes intruded laterally from a shallow magma chamber (~3 km depth), the first of which reached a distance of up to 70 km (Fig.9) [Bjornsson et al., 1977; Brandsdottir and Einarsson,1979; Einarsson and Brandsdottir, 1980]. The data from the Krafla episode are consistent with a numerical model suggesting that the propagation distance was influenced by the initial tectonic stresses, the lithosphere thickness and magma chamber size [Buck et al., 2006].

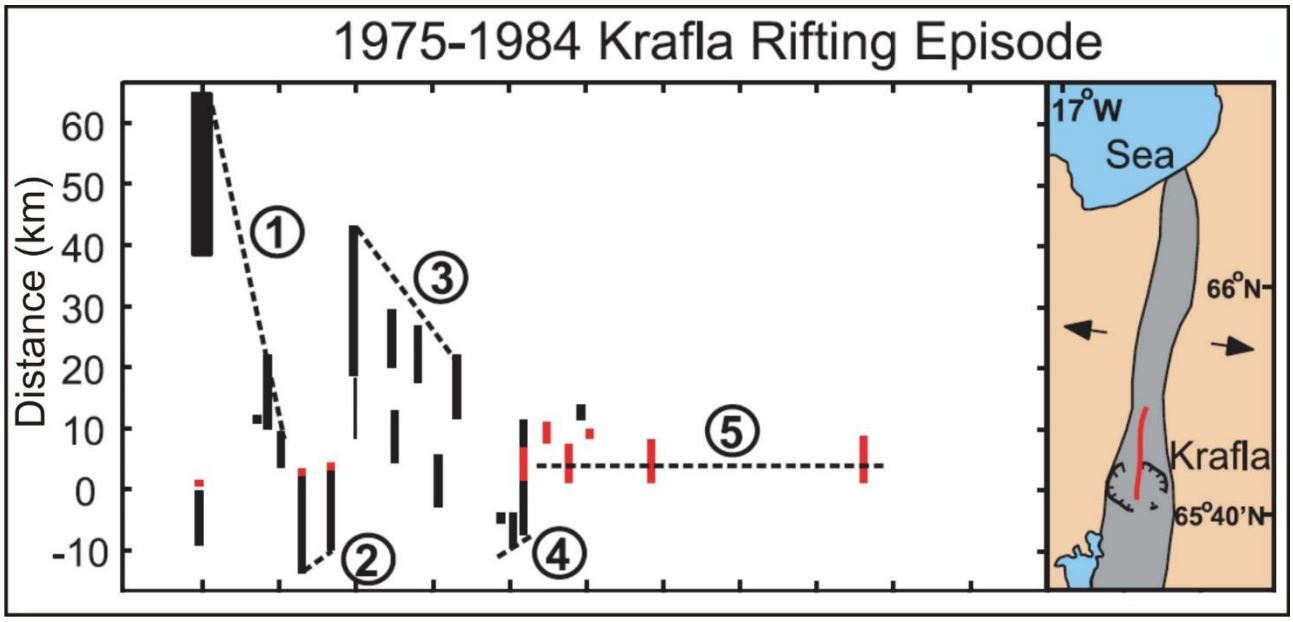

Fig.9. Krafla rifting episode 1974–1989. Distance reached by dikes (black) or eruptive fissures (red) measured from the center of the Krafla inflation (shown on the map, right). Modified from [Buck et al., 2006].

In October 2004 a ~9 km long NNW-SSE trending dike intruded laterally from a shallow magma chamber (2.4 km depth) in the Dallol rift segment (Afar, Ethiopia). The dike intrusion triggered movement on the faults, located on the western flank of the rift, suggesting that magma induced slip can contribute to rift opening [Nobile et al., 2012].

A few months later, during the Dabbahu (Afar, Ethiopia) rifting cycle in 2005-2010, a ~60 kilometers long dike propagated laterally parallel to the rift axis erupting on the NE flank of the eponymous central volcano [Wright et al., 2006; Ayele et al., 2009]. In this case, the final section of the dike propagated upslope before erupting, contrary to what occurred at Bardarbunga, since a lateral thermal gradient may have influenced the crustal stresses overcoming the effect of topography [Grandin et al., 2012]. This intrusion was followed by 13 shorter dikes, the last one in 2010, showing the same path (Fig.10) [Ebinger et al., 2010; Belachew, et al., 2011; Wright et al., 2012].

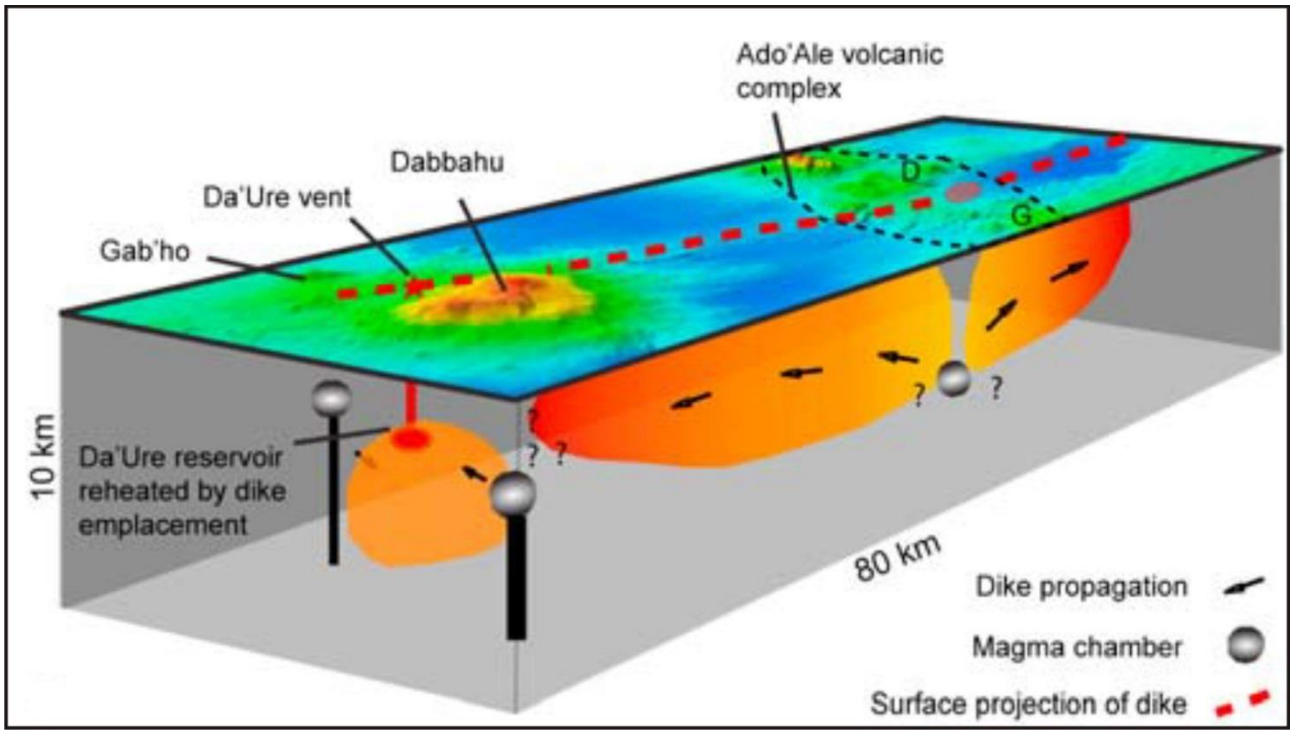

Fig.10. Cartoon interpretation of the Manda-Harraro dike intrusion in September 2005. The dike propagated laterally from Ado' Ale to Dabbahu erupting on its flank (Da'Ure vent). Modified from [Ayele et al., 2009].

Lateral propagation of a ~7 km long dike was also observed during the 2007 Lake Natron (Tanzania) rifting episode [Biggs et al., 2009]. Despite the fact that the Lake Natron and Dabbahu dikes intruded in the same tectonic setting (i.e. a continental rift), they showed an one order of magnitude length difference (7 km versus 60 km in Lake Natron and Dabbahu respectively). This difference may be explained by the fact that the Dabbahu dike intruded in a more mature segment of the East African Rift favoring the formation of larger and shallower magma chambers that in turn promote lateral propagation of longer and shallower dikes [Biggs et al., 2009]. Otherwise, a higher extension rate in the mature segment of the rift favors lateral propagation as suggested by the progressively lower aspect ratio (width/length) of the magmatic systems with increasing extension rate [Acocella, 2014].

Lateral dike propagation has been more recently observed at Bardarbunga (Iceland) in 2014-2015, where a dike propagated laterally for about 45 kilometers under the slope of the Vatnajokull ice-cap before arresting and erupting inside a plain in front of the opposite slope of the Askja volcano [Sigmundsson et al., 2015]. Five different segments of the dike were identified, with a progressive change of the strike from N127° to the N25° of the northernmost one, which is oriented obliquely (11°) with respect to the perpendicular to the regional extension (oriented N104°, Fig.11) [Sigmundsson et al., 2015; Agustsdottir et al., 2016; Ruch et al., 2016]. This suggests that the dike path was first strongly influenced by the local stress induced by topography (i.e. the volcanic edifice) and then, as the dike propagated towards the plain, the tectonic regional extension became dominant in determining the propagation direction [Sigmundsson et al., 2015]. Two arguments against the lateral flow interpretation have been proposed which in turn support a vertical flow model [Gudmundsson et al., 2014; Browning and Gudmundsson, 2015]:

1) The lack of seismicity between some of the dike segments, which suggests that no magma flow occurred between them;

2) Two adjacent pairs of dike segments show a higher depth of seismicity, which requires a vertical downward magma flow for at least 10 km.

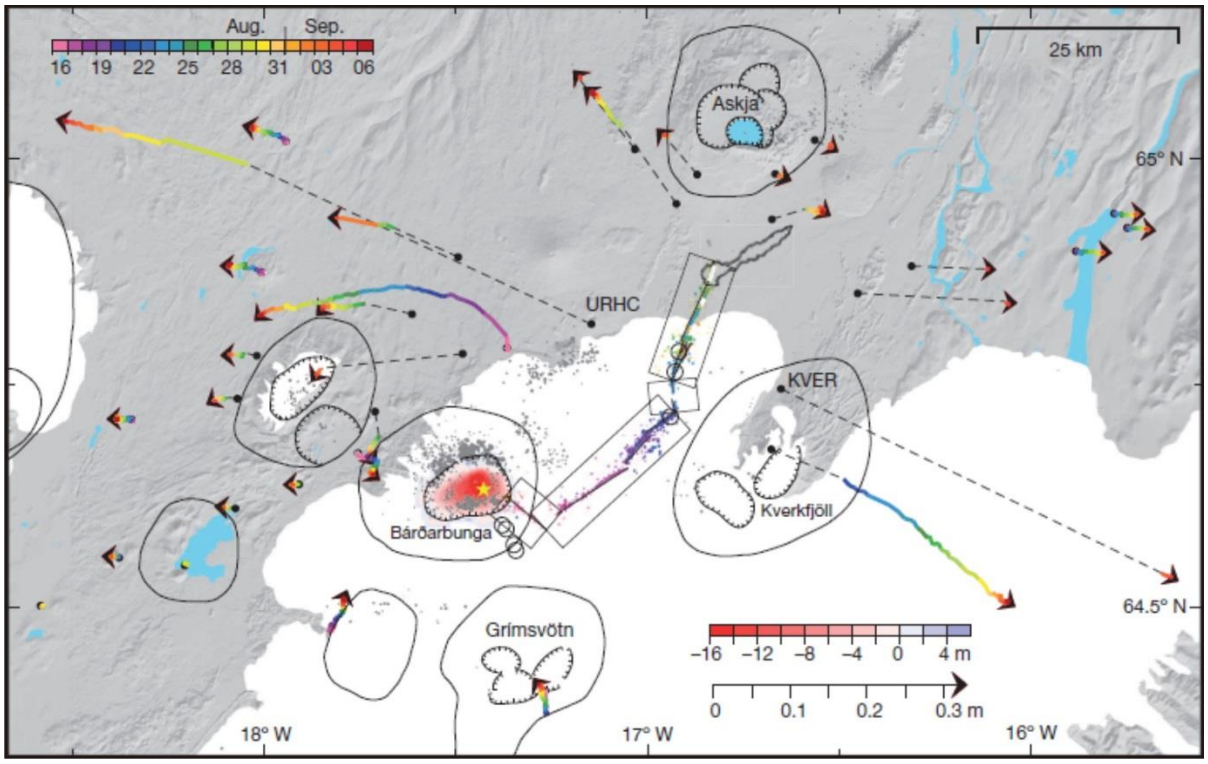

Fig.11. Bardarbunga 2014-2015 diking event. The dots and the arrows indicate the earthquakes from 16 August to 6 September 2014 and the horizontal ground displacements measured by GPS respectively. The thin lines in the rectangles indicate the inferred dike segments. The star marks the location of the magma source inferred from modelling. From [Sigmundsson et al., 2015].

However, lateral dike propagation is not the only mechanism delivering magma along rift zones. In fact, vertical dike propagation has been recently invoked for the 1874-1876 Sveinagja rifting event, based on geochemical data [Hartley and Thordarson, 2012, 2013]. The magmatic sources at Askja (showing explosive activity during the 1875) and Sveinagja may be different and located at ~3 km and ~12 km depth, respectively, suggesting a vertical flow from a deep magma reservoir. This new interpretation of the magma evolution during the 1874-1876 volcanic episode challenges the previous hypothesis of lateral flow from the Askja central volcano to the Sveinagja fissure swarm (45 km away from Askja) [Sigurdsson and Sparks, 1978].

Moreover, vertical dike propagation has been inferred for the 2009 Harrat Lunayyir non-eruptive intrusion, subparallel to the Red sea rift axis [Pallister et al., 2010]. A NW trending surface rupture,

8 km long with 91 cm of offset, was detected following the dike intrusion which arrested at ~ 2 km of depth.

In synthesis, within rift systems, lateral propagation occurs at shallow depth (~3 km) whereas vertical propagation occurs at higher depths (~10 km) supporting the model in Fig.8a-b.

1.3 Review of the models on dike propagation

The natural cases described above suggest that, both at central volcanoes and rift systems, various mechanisms (such as topography, or crustal layering) can drive dike propagation and arrest, highlighting the complexity on considering the effects of each of them separately. Particular interest must be posed to the mechanism favoring lateral dike propagation, which can open eruptive vents far away from the magma chamber below a central volcano, affecting densely populated areas and increasing volcanic hazard [Cappello et al., 2012; Tadini et al., 2017a, 2017b].

To address what drives the propagation direction and arrest of dikes, many factors controlling dike propagation have been identified (summarized in Table 1). These include: crustal layering (i.e. density and/or rigidity layering), buoyancy, topographic reliefs, regional stresses (either compressional or extensional), pre-fractured host rock, effects of gas segregation and cooling of magma, variations of magma influx rate from the chamber (Table 1). Each of these factors has been object of several studies (Table 1).

Controlling factor on dike propagation	**References**
Rigidity layering	[Gudmundsson 2002, 2003, 2005, 2006, 2011]; [Gudmundsson and Loetveit, 2005]; [Rivalta et al., 2005]; [Kavanagh et al., 2006]; [Maccaferri et al., 2010, 2011]; [Ritter et al., 2013].
Density layering	[Lister 1990, 1991]; [Lister and Kerr, 1991]; [Rubin, 1995 and references therein]; [Dahm, 2000]; [Maccaferri et al., 2011]; [Taisne and Jaupart, 2009]; [Taisne et al., 2011]; [Townsend et al., 2017].
Buoyancy	[Takada, 1990]; [Menand and Tait, 2002]; [Taisne and Tait, 2009].
Topography and volcanic edifice load	[Fiske and Jackson, 1972]; [Hyndman and Alt; 1987]; [Rubin and Pollard, 1987]; [Fialko and Rubin, 1999]; [Pinel and Jaupart, 2000, 2004]; [Muller et al., 2001]; [Watanabe et al., 2002]; [Acocella and Tibaldi, 2005]; [Kervyn et al., 2009]; [Roman and Jaupart, 2014]; [Heimisson et al., 2015]; [Pinel et al., 2017].
Regional stresses	[Menand et al., 2010]; [Daniels and Menand, 2015].
Pre-existing structures (faults, fractures, dikes)	[Ziv et al., 2000]; [Ito and Martel, 2002]; [Watanabe et al., 2002]; [Le Corvec et al., 2013].

Volatile exsolution	[Menand and Tait, 2001]; [Taisne and Jaupart, 2011].
Magma cooling	[Taisne and Tait, 2011].
Flow rate form the chamber	[Rivalta, 2010]; [Taisne et al., 2011].

Table 1. List of the identified controlling factors on dike propagation.

In particular, both analogue and numerical models have been representing a useful tool to investigate the processes responsible for dike propagation, as these two approaches are partly complementary.

The lateral propagation of magma has been commonly attributed, by analytical and numerical models, to density contrasts between magma and the host rock, with magma reaching the Level of Neutral Buoyancy (LNB, Fig.12a) [Lister, 1990, 1991; Lister and Kerr, 1991; Ryan, 1994; Rubin, 1995, and references therein; Taisne and Jaupart, 2009; Townsend et al., 2017]. In particular, a dike must penetrate a low density layer for a minimum thickness to reach an equilibrium and start to propagate laterally, since the dike tail is still positively buoyant in the lower, high density layer (Fig.12b) [Taisne and Jaupart, 2009; Taisne et al., 2011].

This suggests that density layering in the crust may strongly influence dike propagation by providing a barrier to magma ascent, thus promoting lateral propagation, dike arrest or sill formation.

However, layers with different density may also reflect different strengths (i.e. rigidity), such as alternating lava and tuff layers (Fig.13a). Therefore, such a rigidity layering, represents a factor that may affect dike propagation, in addition to density layering, by inducing a rotation of σ_1 which leads to dike arrest or sill formation (Fig.13a, [Gudmundsson, 2006]).

The role of both crustal density and rigidity layering has been tested in both analogue [Rivalta et al., 2005; Kavanagh et al., 2006; Ritter et al., 2013] and numerical [Gudmundsson, 2002, 2003, 2005, 2006, 2011; Gudmundsson and Loetveit, 2005; Maccaferri et al., 2010, 2011] models. The analogue

models showed that rigidity layering (i.e. a stiffer layer overlying a soft layer) is the dominant factor on promoting lateral dike propagation, with respect to density layering, since it provides a more efficient barrier to magma ascent (Fig.13b-c).

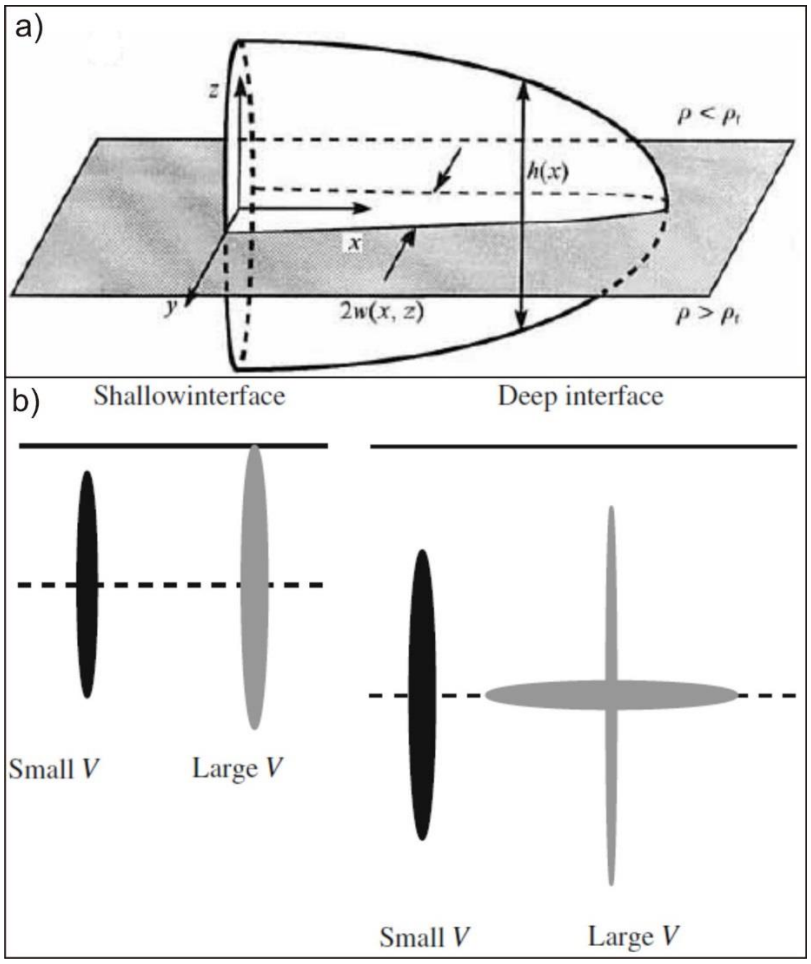

Fig.12. Analytical models showing the effect of the Level of Neutral Buoyancy on dike propagation. a) Analytical model showing a dike propagating laterally at the Level of Neutral buoyancy (at z=0). Modified from [Lister, 1990]. b) Behavior of a dike (with a finite volume of magma) approaching a negative buoyancy layer depending on the depth of the interface (horizontal dashed line). Left hand panel: with a shallow interface, no sill can be generated. If the magma volume is smaller than a critical value, the dike penetrates the low-density layer stalling beneath Earth's surface. Right hand panel: with a deep interface, no eruption is possible regardless of the magma volume. A sill can be generated if the volume of magma is sufficiently large. Modified from [Taisne et al., 2011].

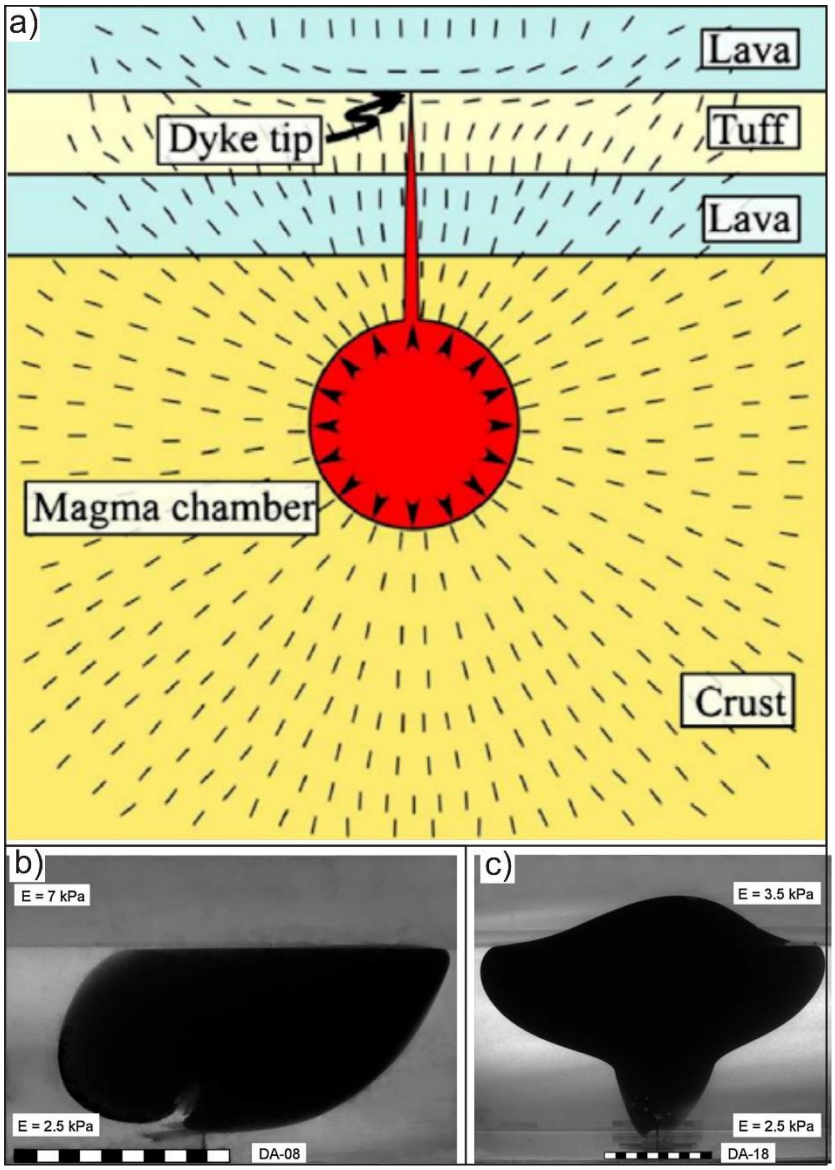

Fig.13. Numerical (a) and analogue (b-c) models showing the effect of rigidity layering on dike propagation. a) Finite-element model of the rotation of the principal compressive stress, σ_1, at the contact between a soft pyroclastic layer and a stiff lava flow. The model indicates that, depending of the magmatic overpressure in the dike, the dike would either become deflected into the contact to form a sill or become arrested. Modified from [Gudmundsson, 2011]. b) and c) Analogue models showing lateral propagation at the interface with a stiff upper layer overlying a soft layer. The rigidity contrast is higher in b) than in c). Modified from [Ritter et al., 2013].

Pioneering analogue models investigated the effect of a ridge-shaped topography, showing that the injected dikes bend parallel to the strike of the ridge-axis, suggesting that the gravitational stress trajectories induced by the ridge topography control dike propagation, favoring lateral flow [Fiske and Jackson, 1972]. Similarly, in volcanoes with sector collapses dikes propagate subparallel to the lateral collapse rim, because of the stress re-orientation induced by the collapse itself, similar to what occurred during the 2002-2003 Stromboli eruption (Fig.14a-b; [Acocella and Tibaldi, 2005]). Flank instability induced by spreading on a weak basal layer may also strongly influence the geometry of the intruded dikes, which may follow a radial pattern in a stable edifice or a curved pattern tangential to the stable/unstable interface [Walter and Troll, 2003].

Many analogue and numerical models investigated the effect of the load of the volcanic edifice on dike propagation [Hyndman and Alt; 1987; Pinel and Jaupart, 2004; Muller et al., 2001; Watanabe et al., 2002; Kervyn et al., 2009; Roman and Jaupart, 2014; Pinel et al., 2017]. All these studies pointed out that the dikes were attracted by the local stress field induced by the load, which prevents vertical propagation favoring magma storage beneath the edifice and/or the injection of a lateral dike (Fig.14c-d). In particular, the local stress field of the edifice, induces the formation of radial dikes which may focus along preferred orientations in case of a superimposing regional stress field [Acocella and Neri, 2009 and references therein]. Conversely, unloading processes such as caldera formation tend to deviate the magma to the collapse rim retarding the eruption [Corbi et al., 2015, 2016]. In this case, the stress pattern resulting from the unloading induces the formation of circumferential dikes parallel to the caldera rim [Corbi et al., 2016]. However, to be affected by the deviatoric stresses induced by both loading and unloading (Fig.15a-b), the internal pressure of the magma (i.e. buoyancy) must be sufficiently low, otherwise the dike will ascend vertically, since it requires longer distances and thus more time to rotate parallel to the σ_1 direction [Pinel et al., 2017]. It is important to note that, in addition to buoyancy, a topographic slope may also change the internal pressure of the dike, without

inducing any deviatoric stress, explaining the observed path of the 2014-2015 Bardarbunga dike with reasonable accuracy [Heimisson et al., 2015].

Therefore, these modeling studies suggest that topography provides a driving pressure for propagation by inducing vertical and lateral stress gradients and additionally it modifies dike trajectories by inducing rotations of the principal stress axes.

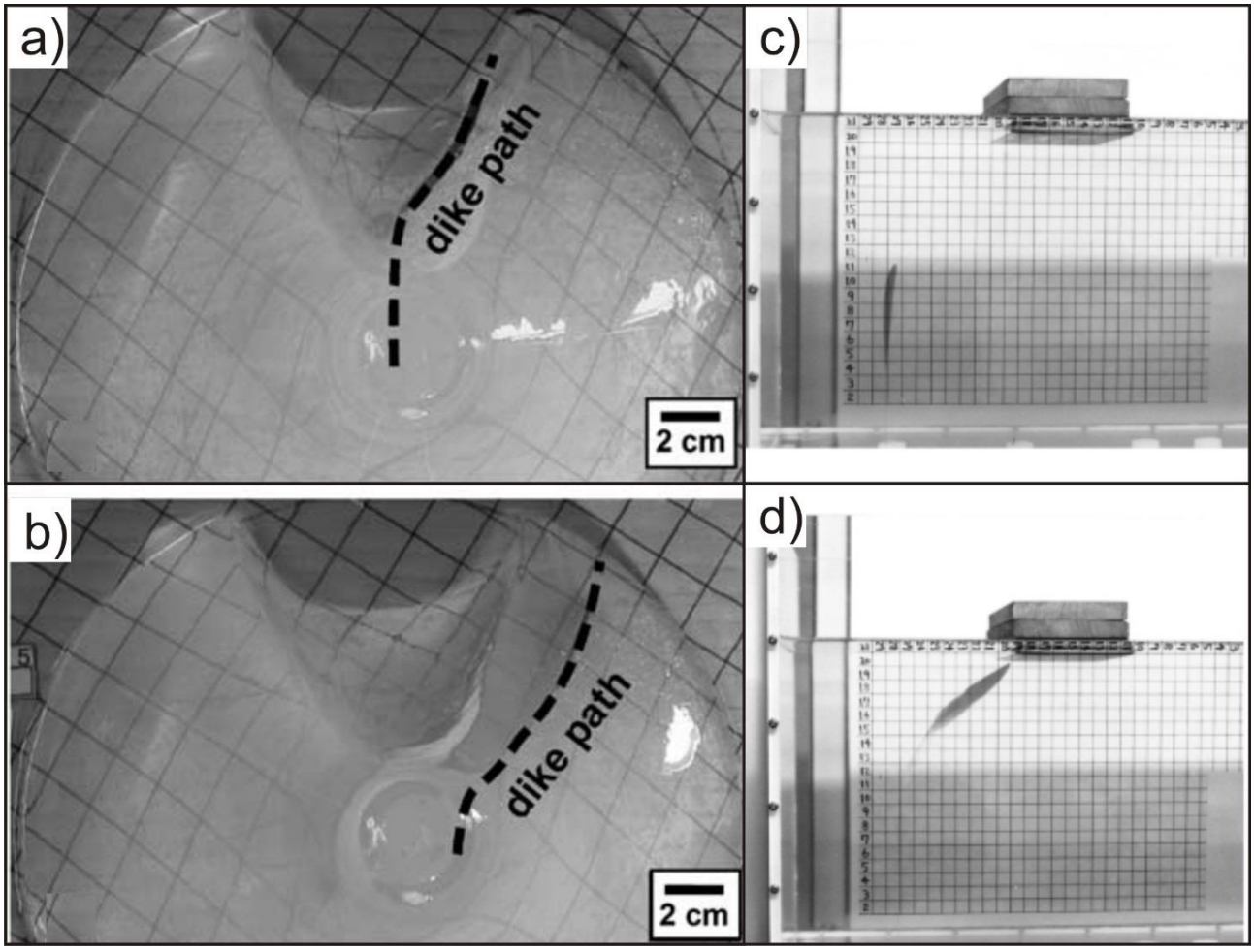

Fig.14. Analogue models showing the effect of topography on dike propagation. (a) and (b): Analogue models on the effects of flank collapse on dike propagation (modified from Acocella and Tibaldi, 2005) showing the evolution of the dike path deflecting from the central area of the cone towards the outer side of the collapse. (c) and (d): photographs showing the progressive deflection of crack orientation under the effect of a surface load (modified from Watanabe et al., 2002).

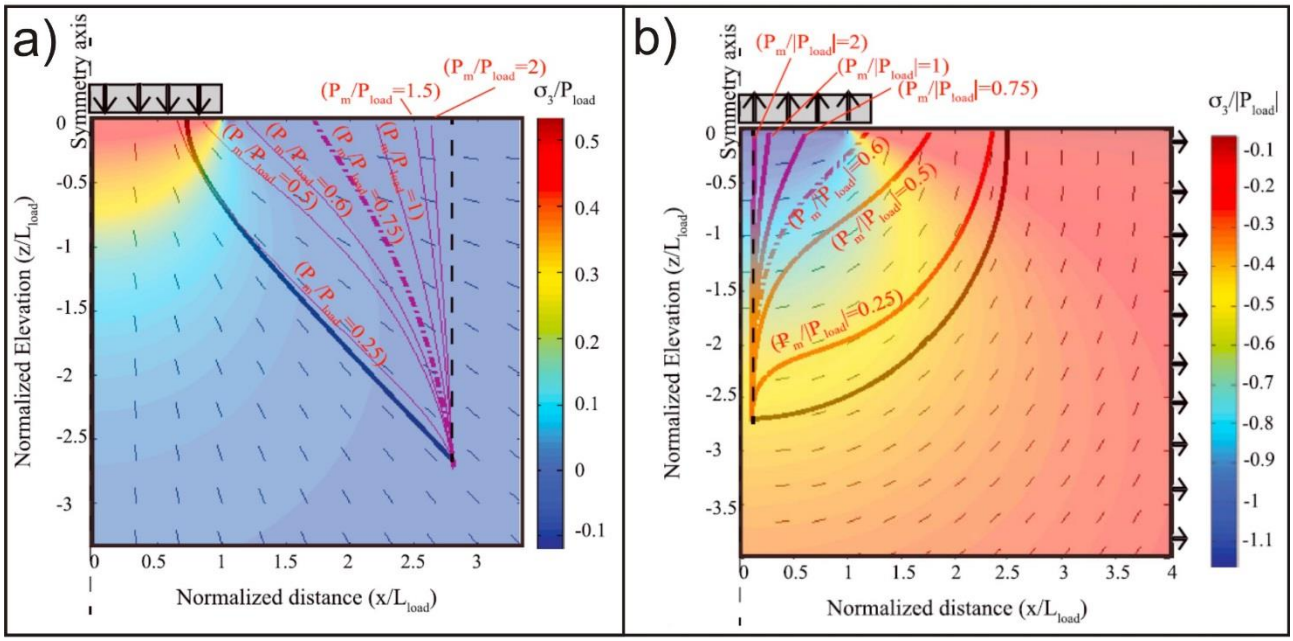

Fig.15. Numerical models (section view) showing dike trajectories in a crust loaded (a) and unloaded (b) at the surface. Black lines indicate the orientation of σ_1. The color scale indicates the amplitude of σ_3. P_m= magma pressure; P_{load}= pressure induced by the load/unload. Modified from [Pinel et al., 2017].

Since natural diking events highlighted the importance of regional stresses on controlling dike propagation, analogue models have also investigated the effects of compressional and extensional stress regimes.

In the case of strong compressive stresses or small effective buoyancy, dikes turn into sills [Menand et al., 2010]. In particular, the balance between the driving effective buoyancy and the deviatoric horizontal compressive stress defines the height over which the dike to sill transition occurs. The length scale of the dike rotation increases exponentially with the ratio between buoyancy and the horizontal compressive stress implying that, if this length-scale is larger than the distance from the surface, the dike will erupt without forming a sill [Menand et al., 2010]. Conversely, if this length-scale is smaller, the dike turns into a sill, despite its buoyancy.

[Daniels and Menand, 2015] addressed the effect of extension and dike- dike interaction of successive repeated intrusions, defining a relationship between the rotation angle of two successive intrusions and their distance under given extensional conditions. They found that the rotation angle depends on two dimensionless ratios: 1) the ratio of fluid overpressure of the first injection and remote tensile stress, 2) the ratio of the spacing between injections and the height of the first intrusion.

For the ascending dikes, it is also common to interact with mechanical heterogeneities (i.e. fractures and or faults) in the upper brittle lithosphere. Models on the influence of pre-existing structures on dike propagation revealed that if they are sufficiently close to each other and the driving pressure inside the dike is low, these structures may deviate the path of dikes channelizing them into pre-weakened zones (Fig.16a) [Watanabe et al., 2002; Le Corvec et al., 2013]. Similarly, depending on the horizontal distance between each other, two ascending dikes may merge or separate (if the horizontal distance is too small, Fig.16b, [Ito and Martel, 2002]).

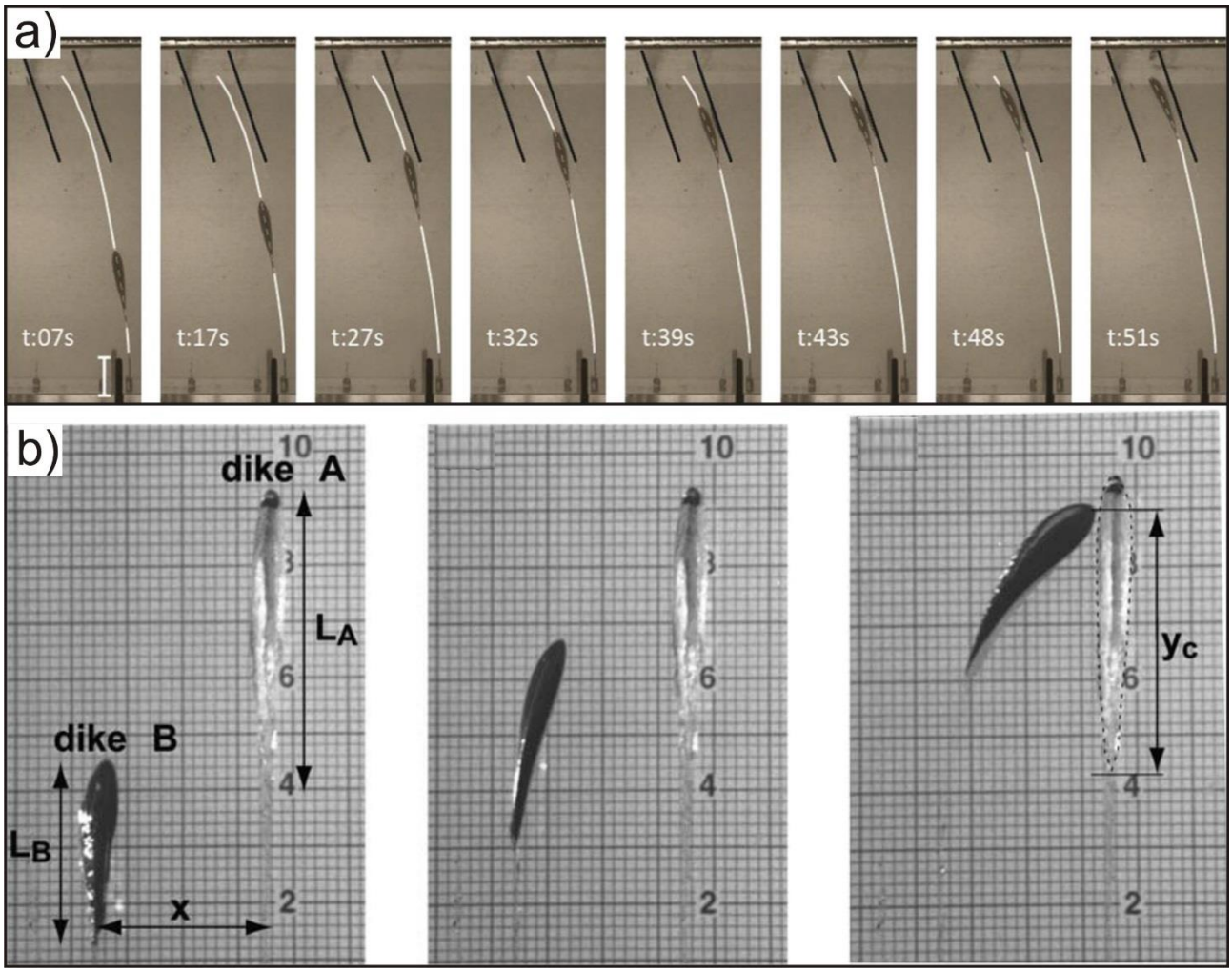

Fig.16. Analogue models showing the effect of pre-existing structures on dike propagation. a) From left to right: example of analogue experiments with two not vertical pre-existing fractures. Modified from [Le Corvec et al., 2013]. b) From left to right: experiments illustrating the interaction between a water filled dike (A) and an air filled dike (B) both injected parallel to each other. Modified from [Ito and Martel, 2002].

All the models discussed above highlighted that small internal pressure (controlled by the buoyancy) is required for the dike to be influenced by the stress changes due to topography, regional tectonics and pre-existing fractures. Consequently, dikes with high buoyancy will rise vertically towards the surface. However, since buoyancy decreases with dike length, a minimum amount of magma is required for the dike to reach the surface [Takada, 1990; Taisne and Tait, 2009]. This

implies that, if the magma input inside the dike from the chamber is not continuous, the dike will stop at a finite distance from its source [Taisne et al., 2011].

Cooling effects on dike propagation are often neglected in the analogue models because of the complexity on controlling the temperature changes of the injected fluid as a magma analogue. However, since magma cooling may change the rheological proprieties of magma (i.e. density and viscosity), the isothermal assumption should miss important effects of magma solidification on dike propagation. To avoid this limitation, analogue models with paraffin wax, which solidifies at contact with the host medium, showed that dike solidification leads to a regime of intermittent propagation, suggesting that this effect may explain the seismicity bursts observed in nature (Fig.17a-b) [Taisne and Tait, 2011].

Similarly, ascending magma may also experience volatile exsolution that, additionally to magma rheology, modifies the balance of pressure within the dike. Analogue models and numerical calculations showed that, in case of magma fragmentation, dikes may decelerate and widen whereas, if no fragmentation occurs, dikes will thin and accelerate towards the surface [Menand and Tait, 2001; Taisne and Jaupart, 2011].

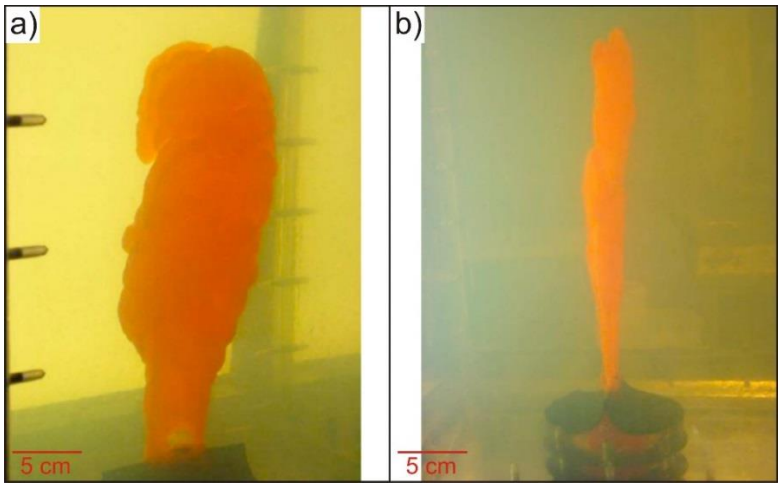

Fig.17. Analogue model showing the effects of magma solidification on dike propagation. Photographs showing discontinuities and irregularities on the dike observed due to the solidification effect a) section view b) side view. Modified from [Taisne and Tait, 2011].

1.4 Scientific problem and aims of the thesis

All the models described above highlighted that the investigated factors may influence dike propagation both directly (i.e. affecting the properties of magma and host rock) and indirectly (i.e. changing the boundary conditions during the ascent, such as the stress state in the crust).

The effects on dike propagation of each of the controlling factors listed above were investigated separately in each study, without considering the possibility that in nature they may occur contemporaneously, overlapping each other. This implies that even if, from both natural observations and models, the list of the factors that control magma ascent may be known, the relative importance of these factors on governing lateral or vertical dike propagation and arrest is still poorly understood. This constitutes a major knowledge gap in understanding dike propagation.

To better address what drives the propagation direction of dikes, the goal of this PhD thesis is to define which are the controlling factors that mostly promote lateral dike propagation and define an hierarchy between them. To this aim, analogue models have been performed varying systematically each of the studied parameters (listed in Table 2), fixing all the other variables, and then comparing quantitatively the observed variations on dike shape and velocity. This approach implies to assume isothermal conditions and gas absence in the fluid, since solidification and volatile exsolution will alter the viscosity and density of the analogue fluid through time making harder to attribute the observed variations of dike velocity and final shape to only one imposed parameter.

This study is particularly focused on how far the dikes propagate laterally in the different imposed conditions.

Chapter 2 of this thesis is based on a paper published on *Geophysical Research Letters* investigating the joint role of topography, density and rigidity layering on lateral dike propagation and arrest. The scope of the paper is to investigate in detail the effect of a topographic slope on dike

propagation along rift zones, comparing analogue and numerical modeling results to the Bardarbunga 2014 event.

Chapter 3 is based on a paper draft ready for submission to *Journal of Geophysical Research*, which is focused on the hierarchy definition among the studied factors (density and rigidity layering, flow rate, topography, buoyancy).

Chapter 4 provides general discussions and conclusions of all the data presented assessing also for future perspectives on dike propagation.

Controlling factor on dike propagation	**References**
Rigidity layering	[Gudmundsson 2002, 2003, 2005, 2006, 2011]; [Gudmundsson and Loetveit, 2005]; [Rivalta et al., 2005]; [Kavanagh et al., 2006]; [Maccaferri et al., 2010, 2011]; [Ritter et al., 2013].
Density layering	[Lister 1990, 1991]; [Lister and Kerr, 1991]; [Rubin, 1995 and references therein]; [Dahm, 2000]; [Maccaferri et al., 2011]; [Taisne and Jaupart, 2009]; [Taisne et al., 2011]; [Townsend et al., 2017].
Buoyancy	[Takada, 1990]; [Menand and Tait, 2002]; [Taisne and Tait, 2009].
Topography and volcanic edifice load	[Fiske and Jackson, 1972]; [Hyndman and Alt; 1987]; [Rubin and Pollard, 1987]; [Fialko and Rubin, 1999]; [Pinel and Jaupart, 2000, 2004]; [Muller et al., 2001]; [Watanabe et al.,

	2002]; [Acocella and Tibaldi, 2005]; [Kervyn et al., 2009]; [Roman and Jaupart, 2014]; [Heimisson et al., 2015]; [Pinel et al., 2017].
Regional stresses	[Menand et al., 2010]; [Daniels and Menand, 2015].
Pre-existing structures (faults, fractures, dikes)	[Ziv et al., 2000]; [Ito and Martel, 2002]; [Watanabe et al., 2002]; [Le Corvec et al., 2013].
Volatile exsolution	[Menand and Tait, 2001]; [Taisne and Jaupart, 2011].
Magma cooling	[Taisne and Tait, 2011].
Flow rate form the chamber	[Rivalta, 2010]; [Taisne et al., 2011].

Table 2. List of the identified controlling factors on dike propagation. The factors considered in this study are indicated in red.

Bibliography

Acocella, V. (2014), Structural control on magmatism along divergent and convergent plate boundaries: overview, model, problems, *Earth Sci. Rev.*, *136*, 226-288, doi:10.1016/j.earscirev.2014.05.006.

Acocella, V., and M. Neri (2003), What makes flank eruptions ? The 2001 Etna eruption and its possible triggering mechanisms, *Bull. Volcanol.*, *65*, 517–529, doi:10.1007/s00445-003-0280-3.

Acocella, V., and A. Tibaldi (2005), Dike propagation driven by volcano collapse: A general model tested at Stromboli, Italy, *Geophys. Res. Lett.*, *32*, L08308, doi:10.1029/2004GL022248.

Acocella, V., M. Porreca, M. Neri, E. Massimi, and M. Mattei (2006a), Propagation of dikes at Vesuvio (Italy) and the effect of Mt. Somma, *Geophys. Res. Lett., 33,* L08301, doi:10.1029/2005GL025590.

Acocella, V., M. Neri, and P. Scarlato (2006b), Understanding shallow magma emplacement at volcanoes: Orthogonal feeder dikes during the 2002–2003 Stromboli (Italy) eruption, *Geophys. Res. Lett.*, 33, L17310, doi:10.1029/2006GL026862.

Acocella, V., and M. Neri (2009), Dike propagation in volcanic edifices: Overview and possible developments, *Tectonophysics, 471,* 67–77, doi:10.1016/j.tecto.2008.10.002.

Ágústsdóttir, T., J. Woods, T. Greenfield, R. G. Green, R. S. White, T. Winder, B. Brandsdóttir, S. Steinthórsson, and H. Soosalu (2016), Strike-slip faulting during the 2014 Bárðarbunga-Holuhraun dike intrusion, central Iceland, *Geophys. Res. Lett., 43*, 1495-1503, doi:10.1002/2015GL067423.

Ayele, A., D. Keir, C. Ebinger, T. J. Wright, G. W. Stuart, W. R. Buck, E. Jacques, G. Ogubazghi, and J. Sholan (2009), September 2005 mega-dike emplacement in the Manda-Harraro nascent oceanic rift (Afar depression), *Geophys. Res. Lett., 36,* L20306, doi:10.1029/2009GL039605.

Bagnardi, M., F. Amelung, and M. P. Poland (2013), A new model for the growth of basaltic shields based on deformation of Fernandina volcano, Galápagos Islands, *Earth Planet. Sci. Lett., 377–378,* 358–366, doi:10.1016/j.epsl.2013.07.016.

Belachew, M., C. Ebinger, D. Coté, D. Keir, J. V Rowland, J. O. S. Hammond, and A. Ayele (2011), Comparison of dike intrusions in an incipient seafloor - spreading segment in Afar, Ethiopia: Seismicity perspectives, *J. Geophys. Res., 116,* B06405, doi:10.1029/2010JB007908.

Biggs, J., F. Amelung, N. Gourmelen, T. H. Dixon, and S. Kim (2009), InSAR observations of 2007 Tanzania rifting episode reveal mixed fault and dyke extension in an immature continental rift, *Geophys. J. Int., 179,* 549–558, doi:10.1111/j.1365-246X.2009.04262.x.

Bjornsson, A., K. Saemundsson, P. Einarsson, E. Tryggvason and K. Gronvold (1977), Current rifting episode in north Iceland, *Nature, 266,* 318-323, doi:10.1038/266318a0.

Brandsdottir, B., & Einarsson, P., (1979). Seismic activity associated with the September 1977 deflation of the Krafia central volcano in NE-Iceland. , *J. Volcanol. Geotherm. Res., 6*,197-212, doi:10.1016/0377-0273(79)90001-5.

Brenguier, F., N. M. Shapiro, M. Campillo, V. A. L. Erie, Z. Duputel, O. Coutant, and A. Nercessian (2008), Towards forecasting volcanic eruptions using seismic noise, Nat Gesoci, *1,* 126-130, doi:10.1038/ngeo104.

Browning J., and A. Gudmundsson (2015), Surface displacements resulting from magma-chamber roof subsidence, with application to the 2014–2015 Bardarbunga–Holuhraun volcanotectonic episode in Iceland, *J. Volcanol. Geotherm. Res., 308,* 82-98, doi:10.1016/j.jvolgeores.2015.10.015.

Buck, W.R., P. Einarsson, and B. Brandsdóttir (2006), Tectonic stress and magma chamber size as controls on dike propagation: constraints from the 1975–1984 Krafla rifting episode, *J. Geophys. Res. Solid. Earth, 111*, B12404, doi:10.1029/2005JB003879.

Cappello, A., M. Neri, V. Acocella, G. Gallo, A. Vicari, and C. Del Negro (2012) Spatial vent opening probability map of Etna volcano (Sicily, Italy), *Bull. Volcanol., 74*, 2083-2094, doi:10.1007/s00445-012-0647-4.

Caudron, C., B. Taisne, Y. Kugaenko, and V. Saltykov (2015), Magma migration at the onset of the 2012–13 Tolbachik eruption revealed by Seismic Amplitude Ratio Analysis, *J. Volcanol. Geotherm. Res., 307,* 60–67, doi:10.1016/j.jvolgeores.2015.09.010.

Chadwick, W. W., and K. A. Howard (1991), The pattern of circumferential and radial eruptive fissures on the volcanoes of Fernandina and Isabela islands, Galapagos, *Bull. Volcanol., 53*, 259-275, doi:10.1007/BF00414523.

Chadwick, W. W., S. Jónsson, D. J. Geist, M. Poland, D. J. Johnson, S. Batt, K. S. Harpp, and A. Ruiz (2011), The May 2005 eruption of Fernandina volcano, Galápagos: The first circumferential dike intrusion observed by GPS and InSAR, *Bull. Volcanol., 73,* 679–697, doi:10.1007/s00445-010-0433-0.

Corbi, F., E. Rivalta, V. Pinel, F. Maccaferri, M. Bagnardi, and V. Acocella (2015), How caldera collapse shapes the shallow emplacement and transfer of magma in active volcanoes, *Earth Planet. Sci. Lett., 431*, 287–293, doi:10.1016/j.epsl.2015.09.028.

Corbi, F., E. Rivalta, V. Pinel, F. Maccaferri, and V. Acocella (2016), Understanding the link between circumferential dikes and eruptive fissures around calderas based on numerical and analog models, *Geophys. Res. Lett., 43*, 6212–6219, doi:10.1002/2016GL068721.

Dahm, T. (2000), Numerical simulations of the propagation path and arrest of fluid-filled fractures in the earth, *Geophys. J. Int., 141,* 623-638, 10.1046/j.1365-246x.2000.00102.x.

Daniels, K. A., and T. Menand (2015), An experimental investigation of dyke injection under regional extensional stress, *J. Geophys. Res. Solid Earth, 120*, 2014–2035, doi:10.1002/2014JB011627.

Ebinger, C. J., A. Ayele, D. Keir, J. Rowland, G. Yirgu, T. Wright, M. Belachew, and I. Hamling (2010), Length and timescales of rift faulting and magma intrusion: The Afar rifting cycle from 2005 to present, *Annu. Rev. Earth Planet. Sci., 38(1),* 439–466, doi:10.1146/annurev-earth-040809-152333.

Einarsson, P., and B. Brandsdóttir (1980), Seismological evidence for Lateral magma intrusion during the July 1978 deflation of the Krafla volcano in NE-Iceland, *J. Geophys.,47,* 160-165, doi:10.2172/890964.

Fialko, Y. A., and A. M. Rubin (1999), What controls the along-strike slopes of volcanic rift zones?, *J. Geophys. Res., 104(B9),* 20007–20020, doi:10.1029/1999JB900143.

Fiske, R. S., and E. D. Jackson (1972), Orientation and Growth of Hawaiian Volcanic Rifts: The Effect of Regional Structure and Gravitational Stresses, *Proc. R. Soc. Lond. A, 329,* 299-326, doi:10.1098/rspa.1972.0115.

Geshi, N. (2008), Vertical and lateral propagation of radial dikes inferred from the flow-direction analysis of the radial dike swarm in Komochi Volcano, Central Japan, *J. Volcanol. Geotherm. Res., 173,* 122–134, doi:10.1016/j.jvolgeores.2008.01.001.

Grandin, R., A. Socquet, C. Doubre, E. Jacques, and G. C. P. King (2012), Elastic thickness control of lateral dyke intrusion at mid-ocean ridges, *Earth Planet. Sci. Lett., 319–320,* 83–95, doi:10.1016/j.epsl.2011.12.011.

Gudmundsson, A. (2002), Emplacement and arrest of sheets and dykes in central volcanoes, J. *Volcanol. Geotherm. Res., 116,* 279–29, doi:10.1016/S0377-0273(02)00226-3.

Gudmundsson, A. (2003), Surface stresses associated with arrested dykes in rift zones, *Bull. Volcanol., 65,* 606–619, doi:10.1007/s00445-003-0289-7.

Gudmundsson, A. (2005), The effects of layering and local stresses in composite volcanoes on dyke emplacement and volcanic hazards, *Geodynamics, 337,* 1216–1222, doi:10.1016/j.crte.2005.07.001.

Gudmundsson, A. (2006), How local stresses control magma-chamber ruptures, dyke injections, and eruptions in composite volcanoes, *Earth Sci. Rev., 79,* 1–31, doi:10.1016/j.earscirev.2006.06.006.

Gudmundsson, A. (2011), Deflection of dykes into sills at discontinuities and magma-chamber formation, *Tectonophysics, 500*, 50–64, doi:10.1016/j.tecto.2009.10.015.

Gudmundsson, A., and I.F. Loetveit (2005), Dyke emplacement in a layered and faulted rift zone, *J. Volcanol. Geotherm. Res., 144*, 311-327, doi:10.1016/j.jvolgeores.2004.11.027.

Gudmundsson, A., N. Lecoeur, and N. Mohajeri (2014), Dike emplacement at Bardarbunga, Iceland, induces unusual stress changes, caldera deformation, and earthquakes, *Bull. Volcanol., 76*, 869, doi:10.1007/s00445-014-0869-8.

Hartley, M. E., and T. Thordarson (2012), Formation of Öskjuvatn caldera at Askja, North Iceland : Mechanism of caldera collapse and implications for the lateral flow hypothesis, *J. Volcanol. Geotherm. Res., 227–228*, 85–101, doi:10.1016/j.jvolgeores.2012.02.009.

Hartley, M. E., and T. Thordarson (2013), The 1874 – 1876 volcano-tectonic episode at Askja, North Iceland: Lateral flow revisited, *Geochem. Geophys. Geosyst., 14*, 2286–2309, doi:10.1002/ggge.20151.

Heimisson, E. R., A. Hooper, and F. Sigmundsson (2015), Forecasting the path of a laterally propagating dike, *J. Geophys. Res. Solid Earth, 120*, 8774-8792, doi:10.1002/2015JB012402.

Hyndman, D.W., and D. Alt (1987), Radial dikes, laccoliths and gelatin models, *J. Geol., 95*, 763-774, doi:10.1086/629176.

Ito, G., and S. J. Martel (2002), Focusing of magma in the upper mantle through dike interaction, *J. Geophys. Res., 107 (B10)*, 2223, doi:10.1029/2001JB000251.

Kauahikaua, J., and M. Poland (2012), One Hundred Years of Volcano Monitoring in Hawaii, *Eos, 93(3)*, 1–3.

Kavanagh, J. L., T. Menand, and R. S. J. Sparks (2006), An experimental investigation of sill formation and propagation in layered elastic media, *Earth Planet. Sci. Lett., 245,* 799–813, doi:10.1016/j.epsl.2006.03.025.

Kervyn, M., G. G. J. Ernst, B. V. W. De Vries, L. Mathieu, and P. Jacobs (2009), Volcano load control on dyke propagation and vent distribution: Insights from analogue modeling, *J. Geophys. Res., 114,* B03401, doi:10.1029/2008JB005653.

Le Corvec, N., T. Menand, and J. Lindsay (2013), Interaction of ascending magma with pre-existing crustal fractures in monogenetic basaltic volcanism: an experimental approach, *J. Geophys. Res. Solid Earth, 118,* 968-984, doi:10.1002/jgrb.50142.

Lister, J. R. (1990), Buoyancy-driven fluid fracture: similarity solutions for the horizontal and vertical propagation of fluid-filled cracks, *J. Fluid Mech., 217,* 213-239, doi:10.1017/S0022112090000696.

Lister, J. R. (1991), Steady solutions for feeder dykes in a density-stratified lithosphere, *Earth Planet. Sci. Lett., 107,* 233–242, doi:10.1016/0012-821X(91)90073-Q.

Lister, J. R., and R. C. Kerr (1991), Fluid-Mechanical Models of Crack Propagation and Their Application to Magma Transport in Dykes, *J. Geophys. Res., 96(B6),* 1049–1077, doi:10.1029/91JB00600.

Lundgren, P., A. Kiryukhin, P. Milillo, and S. Samsonov (2015), Dike model for the 2012–2013 Tolbachik eruption constrained by satellite radar interferometry observations, *J. Volcanol. Geotherm. Res., 307,* 79–88, doi:10.1016/j.jvolgeores.2015.05.011.

Maccaferri, F., M. Bonafede, and E. Rivalta (2010), A numerical model of dyke propagation in layered elastic media, *Geophys. J. Int., 180,* 1107–1123, doi:10.1111/j.1365-246X.2009.04495.x.

Maccaferri, F., M. Bonafede, and E. Rivalta (2011), A quantitative study of the mechanisms governing dike propagation, dike arrest and sill formation, *J. Volcanol. Geotherm. Res., 208(1–2)*, 39–50, doi:10.1016/j.jvolgeores.2011.09.001.

Maccaferri, F., E. Rivalta, L. Passarelli, and Y. Aoki (2016), On the mechanisms governing dike arrest: Insight from the 2000 Miyakejima dike injection, *Earth Planet. Sci. Lett., 434*, 64–74, doi:10.1016/j.epsl.2015.11.024.

Martí, J., V. Pinel, C. López, A. Geyer, R. Abella, M. Tárraga, M. J. Blanco, A. Castro, and C. Rodríguez (2013), Causes and mechanisms of the 2011–2012 El Hierro (Canary Islands) submarine eruption, *J. Geophys. Res. Solid Earth*, *118*, 823–839, doi:10.1002/jgrb.50087.

Martí, J., A. Villaseñor, A. Geyer, C. López, and A. Tryggvason (2017), Stress barriers controlling lateral migration of magma revealed by seismic tomography, *Sci. Rep., 7*, 1–10, doi:10.1038/srep40757.

Menand, T., K. A. Daniels, and P. Benghiat (2010), Dyke propagation and sill formation in a compressive tectonic environment, *J. Geophys. Res., 115*, B08201, doi:10.1029/2009JB006791.

Menand, T., and S. R. Tait (2001), A phenomenological model for precursor volcanic eruptions, *Nature, 411*, 678–680, doi:10.1038/35079552.

Menand, T., and S. R. Tait (2002), The propagation of a buoyant liquid-filled fissure from a source under constant pressure: An experimental approach, *J. Geophys. Res., 107(B11)*, 2306, doi:10.1029/2001JB000589.

Muller, J. R., G. Ito, and S. J. Martel (2001), Effects of volcano loading on dike propagation in an elastic half-space, *J. Geophys. Res., 106(B6)*, 11101–11113, doi:10.1029/2000JB900461.

Neri, M., G. Lanzafame and V. Acocella (2008) Dyke emplacement and related hazard in volcanoes with sector collapse: the 2007 Stromboli (Italy) eruption, *J. Geol. Soc. London.*,165, 883–886, doi:10.1144/0016-76492008-002.

Nobile, A., C. Pagli, D. Keir, T. J. Wright, A. Ayele, J. Ruch, and V. Acocella (2012), Dike-fault interaction during the 2004 Dallol intrusion at the northern edge of the Erta Ale Ridge (Afar , Ethiopia), *Geophys. Res. Lett.*, *39*, L19305, doi:10.1029/2012GL053152.

Pallister, J. S. et al. (2010), Broad accommodation of rift-related extension recorded by dyke intrusion in Saudi Arabia, *Nat. Geosci., 3(10)*, 705–712, doi:10.1038/ngeo966.

Peltier, A., V. Ferrazzini, T. Staudacher, and P. Bache (2005), Imaging the dynamics of dyke propagation prior to the 2000–2003 flank eruptions at Piton de La Fournaise, Reunion Island, *Geophys. Res. Lett.*, *32*, L22302, doi:10.1029/2005GL023720.

Peltier, A., P. Bachèlery, and T. Staudacher (2009), Magma transport and storage at Piton de La Fournaise (La Réunion) between 1972 and 2007: A review of geophysical and geochemical data, *J. Volcanol. Geotherm. Res.*, *184*, 93–108, doi:10.1016/j.jvolgeores.2008.12.008.

Pinel, V., and C. Jaupart (2000), The effect of edifice load on magma ascent beneath a volcano, *Phil. Trans. R. Soc. Lond. A,* 1515-1532, doi:10.1098/rsta.2000.0601

Pinel, V., and C. Jaupart (2004), Magma storage and horizontal dyke injection beneath a volcanic edifice, *Earth Planet. Sci. Lett., 221*, 245–262, doi:10.1016/S0012-821X(04)00076-7.

Pinel, V., A. Carrara, F. Maccaferri, E. Rivalta, and F. Corbi (2017), A two-step model for dynamical dike propagation in two dimensions: Application to the July 2001 Etna eruption, *J. Geophys. Res. Solid Earth*, *122*, 1107–1125, doi:10.1002/2016JB013630.

Reches, Z., and E. Fink (1988), The mechanism of intrusion of the Inyo dike, Long Valley Caldera, California, *J. Geophys. Res., 93*, 4321-4334, 10.1029/JB093iB05p04321.

Ritter, M. C., V. Acocella, J. Ruch, and S. L. Philipp (2013), Conditions and threshold for magma transfer in the layered upper crust: Insights from experimental models, *Geophys. Res. Lett., 40*, 1–5, doi:10.1002/2013GL058199.

Rivalta, E., M. Bottinger, and T. Dahm (2005), Buoyancy-driven fracture ascent: Experiments in layered gelatine, *J. Volcanol. Geotherm. Res., 144*, 273–285, doi:10.1016/j.jvolgeores.2004.11.030.

Rivalta, E. (2010), Evidence that coupling to magma chambers controls the volume history and velocity of laterally propagating intrusions, *J. Geophys. Res., 115*, B07203, doi:10.1029/2009JB006922.

Roman, A., and C. Jaupart (2014), The impact of a volcanic edifice on intrusive and eruptive activity, *Earth Planet. Sci. Lett., 408*, 1–8, doi:10.1016/j.epsl.2014.09.016.

Rubin, A.M., and D. Pollard (1987), Origins of blade like dikes in volcanic rift zones, *in Volcanism in Hawaii*, edited by R. W. Decker, T. L. Wright, and P. H. Stauffer, pp. 1449-1470, United States Geological Survey, Reston, VA.

Rubin, A. M. (1995), Propagation of magma-filled cracks, *Annu. Rev. Earth Planet. Sci., 23(1)*, 439–466, 287–336, doi:10.1146/annurev.ea.23.050195.001443.

Ruch, J., T. Wang, W. Xu, M. Hensch, and S. Jonsson (2016), Oblique rift opening revealed by reoccurring magma injection in central Iceland, *Nature Communications, 7*, 1–7, doi:10.1038/ncomms12352.

Ryan, M. P., (1994) Neutral-buoyancy controlled magma transport and storage in mid-ocean ridge magma reservoirs and their sheeted-dike complex: A summary of basic relationships, in *Magmatic Systems*, edited by M. P. Ryan, pp. 97-135, Academic Press, San Diego, Calif.

Sigmundsson, F. et al., (2015), Segmented lateral dyke growth in a rifting event at Bárðarbunga volcanic system, Iceland, *Nature, 517,* 191-195, doi:10.1038/nature14111.

Sparks, R. S. J., and H. Sigurdsson (1978), Rifting Episode in North Iceland in 1874-1875 and the Eruptions of Askja and Sveinagja, *Bull. Volcanol., 41,* 149–167, doi:10.1007/BF02597219

Smets, B., M. Kervyn, N. Oreye, and F. Kervyn (2015), Spatio-temporal dynamics of eruptions in a youthful extensional setting: Insights from Nyamulagira Volcano (D.R. Congo), in the western branch of the East African Rift, *Earth Sci. Rev., 150,* 305–328, doi:10.1016/j.earscirev.2015.08.008.

Sparks, R. S. J. (2003), Forecasting volcanic eruptions, *Earth Planet. Sci. Lett. , 210,* 1–15, doi:10.1016/S0012-821X(03)00124-9.

Sparks, R. S. J., J. Biggs, and J.W. Neuberg (2012), Monitoring Volcanoes, *Science, 335*, 1310-1311 doi:10.1126/science.1219485.

Taisne, B., and C. Jaupart (2009), Dike propagation through layered rocks, *J. Geophys. Res., 114*, B09203, doi:10.1029/2008JB006228.

Taisne, B., and S. Tait (2009), Eruption versus intrusion? Arrest of propagation of constant volume, buoyant, liquid-filled cracks in an elastic, brittle host, *J. Geophys. Res., 114*, B06202, doi:10.1029/2009JB006297.

Taisne, B., and S. Tait (2011), Effect of solidification on a propagating dike, *J. Geophys. Res., 116*, B01206, doi:10.1029/2009JB007058.

Taisne, B., and C. Jaupart (2011), Magma expansion and fragmentation in a propagating dyke, *Earth Planet. Sci. Lett., 301,* 146–152, doi:10.1016/j.epsl.2010.10.038.

Taisne, B., S. Tait, and C. Jaupart (2011), Conditions for the arrest of a vertical propagating dyke, Bull. Volcanol. 73, 191–204, doi:10.1007/s00445-010-0440-1.

Tadini, A., M. Bisson, A. Neri, R. Cioni, A. Bevilacqua, and W.P. Aspinall (2017a), Assessing future vent opening locations at the Somma-Vesuvio volcanic complex: 1. A new information geodatabase with uncertainty characterizations *J. Geophys. Res. Solid Earth, 122*, 4336–4356, doi:10.1002/2016JB013858.

Tadini, A., et al. (2017b), Assessing future vent opening locations at the Somma-Vesuvio volcanic complex: 2. Probability maps of the caldera for a future Plinian/sub-Plinian event with uncertainty quantification *J. Geophys. Res. Solid Earth, 122*, 4357–4376, doi:10.1002/2016JB013860.

Takada, A. (1990), Experimental Study on Propagation of Liquid-Filled Crack in Gelatin: Shape and Velocity in Hydrostatic Stress Condition, *J. Geophys. Res., 95*, 8471–8481, doi: 10.1029/JB095iB06p08471.

Townsend, M. R., D. D. Pollard, and R. P. Smith (2017), Mechanical models for dikes: A third school of thought, *Tectonophysics, 703–704*, 98–118,doi:10.1016/j.tecto.2017.03.008

Ueda, H., E. Fujita, M. Ukawa, E. Yamamoto, M. Irwan, and F. Kimata (2005), Magma intrusion and discharge process at the initial stage of the 2000 activity of Miyakejima, Central Japan, inferred from tilt and GPS data, *Geophys. J. Int., 161*, 891–906, doi:10.1111/j.1365-246X.2005.02602.x.

Walter, T. R., and V. R. Troll (2003*), Experiments on rift zone evolution in unstable volcanic edifices, J. Volcanol. Geotherm. Res., 127*, 107–120, doi:10.1016/S0377-0273(03)00181-1.

Watanabe, T., T. Masuyama, K. Nagaoka, and T. Tahara (2002), Analog experiments on magma-filled cracks: Competition between external stresses and internal pressure, *Earth Planet Sp., 54*, 1247–1261, doi:10.1186/BF03352453.

White, R., and W. Mccausland (2016), Volcano-tectonic earthquakes: A new tool for estimating intrusive volumes and forecasting eruptions, *J. Volcanol. Geotherm. Res.*, *309*, 139–155, doi:10.1016/j.jvolgeores.2015.10.020.

Wright, T. J., C. Ebinger, J. Biggs, A. Ayele, G. Yirgu, D. Keir, and A. Stork (2006), Magma-maintained rift segmentation at continental rupture in the 2005 Afar dyking episode, *Nature, 442*, 291-294, doi:10.1038/nature04978.

Wright, T. J. et al. (2012), Geophysical constraints on the dynamics of spreading centres from rifting episodes on land, *Nat. Geosci.*, *5(4)*, 242–250, doi:10.1038/ngeo1428.

Ziv, A., A. M. Rubin, and A. Agnon (2000), Stability of dike intrusion along preexisting fractures, *J. Geophys. Res., 105(B3)*, 5947–5961, doi:10.1029/1999JB900410.

Chapter 2

(published in Geophysical Research Letters doi:10.1002/2017GL073130)

Propagation and arrest of dikes under topography: models applied to the 2014 Bardarbunga (Iceland) rifting event

S. Urbani[1], V. Acocella[1], E. Rivalta[2] and F. Corbi[3]

[1]Dipartimento di Scienze, Università Roma Tre, Rome, Italy,
[2]Deutsches GeoForschungsZentrum GFZ, Section 2.1, Potsdam, Germany,
[3]Géosciences Montpellier Laboratory, University of Montpellier, Montpellier, France
Corresponding author: stefano.urbani@uniroma3.it

Abstract

Dikes along rift zones propagate laterally downslope for tens of kilometers, often becoming arrested before topographic reliefs. We use analogue and numerical models to test the conditions controlling the lateral propagation and arrest of dikes, exploring the presence of a slope in connection with buoyancy and rigidity layering. A gentle downslope assists lateral propagation when combined with an effective barrier to magma ascent, e.g. gelatin stiffness contrasts, while anti-buoyancy alone may be insufficient to prevent upward propagation. We also observe experimental dikes become arrested when reaching a plain before opposite reliefs. Our numerical models show that below the plain the stress field induced by topography hinders further dike propagation. We suggest that lateral dike propagation requires an efficient barrier (rigidity) to upward propagation, assisting anti-buoyancy, and a lateral pressure gradient perpendicular to the least compressive stress axis, while dike arrest may be induced by external reliefs.

1. Introduction

Recent diking events suggest that topography plays a role in both driving and arresting lateral dike propagation. For example, the 2014 Bardarbunga (Iceland) dike propagated for tens of km downslope before arresting below a plain in front of the Askja volcanic edifice [Sigmundsson et al., 2015]. At the volcanic edifice scale, feeder dikes have also propagated downslope and arrested before opposite reliefs, as on Somma-Vesuvio, Italy [Acocella et al., 2006]. The lateral propagation of magma has been commonly attributed to density contrasts with the host rock, with the magma reaching the level of neutral buoyancy [Lister, 1990; Lister, 1991; Lister and Kerr, 1991; Ryan, 1994; Rubin, 1995 and references therein; Taisne and Jaupart, 2009]. A lateral stress gradient, of tectonic [Dahm et al., 2010], rheological [Grandin et al., 2012] or topographic [e.g. Fialko and Rubin, 1999; Buck et al., 2006] origin, may be also necessary to drive dikes laterally. Since many dikes originate from magma chambers below volcanic edifices, the role played by topographic stresses in driving dike propagation and facilitating arrest may often dominate [Fiske and Jackson, 1972; Pinel and Jaupart, 2000, 2004, 2005; Watanabe et al., 2002; Acocella and Tibaldi, 2005; Acocella et al., 2006; Kervyn et al., 2009; Roman and Jaupart, 2014; Maccaferri et al., 2016].

Other factors may discourage magma ascent, indirectly favoring lateral dike propagation. These include dike-induced graben faulting [Xu et al., 2016] and layering [Gudmundsson, 2002, 2011; Maccaferri et al., 2011], or a stiffer upper layer [Rivalta et al., 2005; Kavanagh et al., 2006; Ritter et al., 2013]. A weak upper layer may also arrest dike ascent, as not storing much stress [Gudmundsson, 2003]. These studies considered only the role of a single feature in lateral dike propagation. Here we use experiments to investigate the joint role of topography, layering and density on lateral dike propagation and arrest; we present a representative selection of our dataset of 20 experiments (Table S1). We complement these with numerical models describing quantitatively the stress field affecting the experiments.

2. Experimental set-up and scaling

We injected dyed water in a 33×58×38.5 cm^3 plexiglass box filled with pigskin gelatin [Di Giuseppe et al., 2009] as magma and upper crust analogues, respectively (Figure 1a). In each experiment we imposed a layering using two concentrations of gelatin and/or adding NaCl (2.5-4 wt % and 0-10 wt % respectively; Brizzi et al., 2016). Similarly, we added NaCl to increase water density (ρ_f = 1053.6 Kg m^{-3}), so that ρ_f is comprised between the density of the upper (ρ_u) and lower (ρ_l) layers (i.e. $\rho_l > \rho_f > \rho_u$), being ρ_u/ρ_f constant. We then poured the upper layer's solution gently on top of the bottom one while this was still liquid, so the two layers mixed partially and we obtained, after cooling, a ~4 cm thick, non-sharp interface with a concentration gradient. We refer to density layering when the two layers have the same rigidity but different densities ($E_u/E_l \sim 1$ where E_u and E_l are the rigidity of the upper and lower layer, respectively) and to rigidity layering when $E_u/E_l > 1$, regardless of their densities (Table S1). We fixed the thickness ratio between the upper and lower layer as between 0.7 and 0.8. The temperatures of the gelatin and water were 9° and 20° C, respectively.

We shaped the gelatin surface using a mold with gently inward dipping flanks (2.4° and 3.7°) separated by a 8 cm wide horizontal plain (Figure 1a). This configuration allows investigating the role of two opposite slopes on dike propagation. It roughly simulates the 2D along-strike topography of the 2014 Bardarbunga intrusion (Figure 1c), considered representative of a dike propagating laterally downslope. We avoided any local stress due to the central volcano (see Corbi et al., 2015 and 2016 instead). Hereafter we refer to "topography" models indicating experiments having this profile. In experiment 5 (Table S1), we increased to 7° the dip of the slope, without any opposite slope. We injected dyed water from the box side using a peristaltic pump (Figure 1a) with constant influx rate of 0.079 ml/s. We held the needle tip on the x-z plane (Figure 1a-b and Figure 2a-d), aiming to impose the initial dike strike parallel to the same plane.

We monitored the dike propagation in side and top view at 0.1 frames per second, measuring the final dike length and horizontal distance between the eruption and injection points (S and X, respectively; Figure 1b).

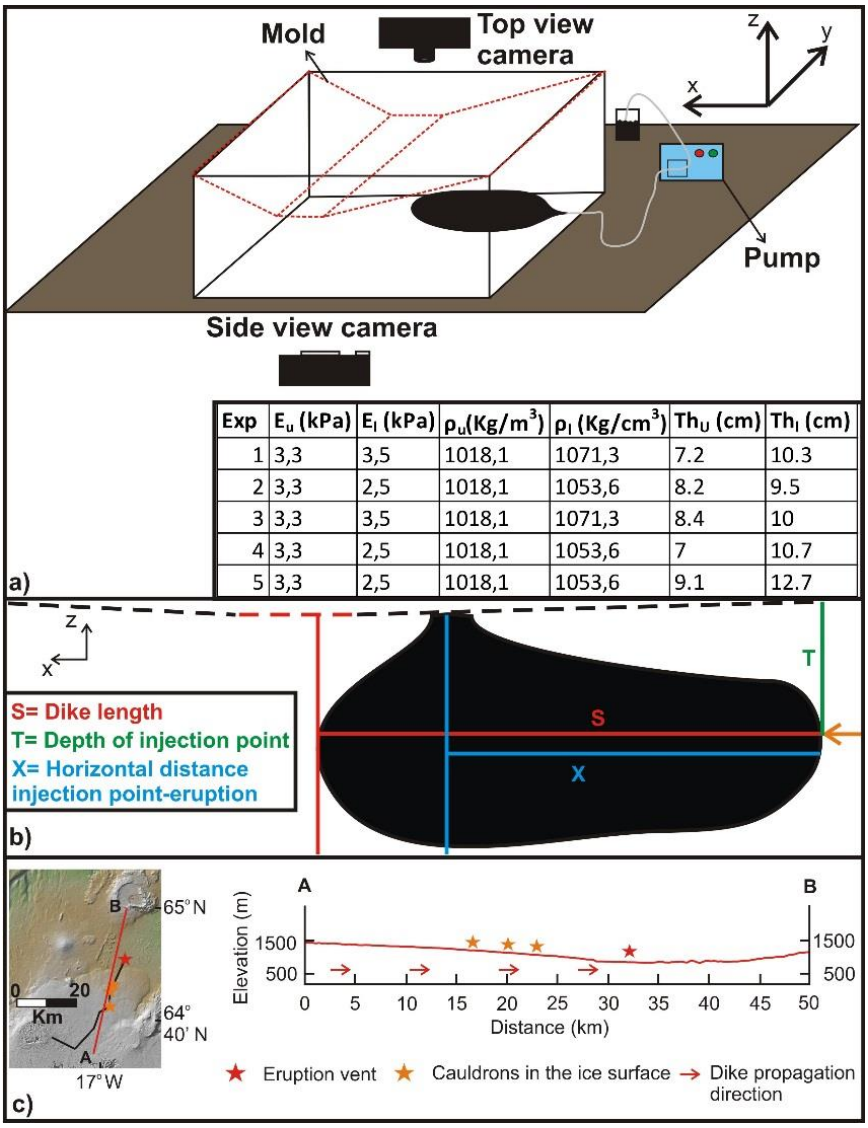

Exp	E_u (kPa)	E_l (kPa)	ρ_u(Kg/m^3)	ρ_l (Kg/cm^3)	Th_U (cm)	Th_l (cm)
1	3,3	3,5	1018,1	1071,3	7.2	10.3
2	3,3	2,5	1018,1	1053,6	8.2	9.5
3	3,3	3,5	1018,1	1071,3	8.4	10
4	3,3	2,5	1018,1	1053,6	7	10.7
5	3,3	2,5	1018,1	1053,6	9.1	12.7

Figure 1. a) Experimental set-up. The reference system in the top right refers to the box sides. Inset in the bottom right shows the values of the young modulus (E), density (ρ) and thickness (Th) of the upper (E_u, ρ_u, Th_u) and lower layers (E_l, ρ_l, Th_l) in the representative experiments. b) Calculations of S, X and T (see inset on the left) in each experiment. Dashed black and red lines indicate the slopes and the plain, respectively. Orange arrow indicates injection point. c) Topography profile along approximate pathway of Bardarbunga dike (Elevation:Distance = 1:2). Black line in map view indicates the surface projection of the dike.

Below are the calculations to scale our models. The difference in density between gelatin and water in the models is ~20 kg m^{-3}. As for nature, we take the density difference between basaltic dikes and host rock as ~20 kg m^{-3}, with ρ_{solid}= 2800 kg m^{-3}, thus $\Delta\rho^*$ is 1 (where * refers to the ratio of the parameter values measured at the laboratory and natural scale). The fracture toughness (K_c) of the gelatin is calculated from Kavanagh et al. [2013]:

$$K_c = (1.4 \pm 0.1)\sqrt{E} \quad (1)$$

where the Young's modulus, E, is 3.5 kPa for pig-skin gelatin [Ritter, 2012] and K_c = 83 Pa $m^{1/2}$. K_c of natural rocks spans from 10^6 to 10^9 Pa $m^{1/2}$, based on laboratory studies or field estimates, respectively [Scholz, 2010; Olson and Schultz, 2011; Rivalta et al., 2015, and references therein]. We assume that K_c in nature is ~10^9 Pa $m^{1/2}$, which is appropriate for tens of km long dikes [Rivalta et al., 2015]; therefore, $K_c^* = 8.3 \times 10^{-8}$. The dimensionless scaling ratios between model and nature for the propagation velocity (V^*), rigidity (E^*) and buoyancy length (L_b^*) are as follows [Kavanagh et al., 2013]:

$$L_b^* = (K_c^* / \Delta\rho^*)^{2/3} = 1.9 \times 10^{-5} \quad (2)$$

$$V^* = (\Delta\rho^*)^{1/6} K_c^{*1/3} \rho^*_{solid}{}^{-1/2} = 7.2 \times 10^{-3} \quad (3)$$

$$E^* = \Delta\rho^* L_b^* (L/\Psi)^* = 1.9 \times 10^{-7} \quad (4)$$

Where Ψ is the dike thickness.

Therefore, the height of our dikes corresponds to ~5.8 and ~7.6 km in nature, similar to the Bardarbunga dike or the main dike of the Dabbahu (Afar) sequence. The thickness of the experimental dikes (≤1 mm) corresponds to a few meters in nature (Eq. 4, Rivalta et al., 2015).

We additionally define the time scaling factor as:

$$t^* = L^*/V^* \quad (5)$$

Observed velocities of laterally propagating dikes in Iceland and Afar are ~7-112 km per day [Wright et al., 2012; Agustsdottir et al., 2016], thus on the upper side of our experimental ones (~6 km per day; section 3.1).

We now compare the ratio *r* between the vertical pressure gradient (buoyancy) and the horizontal pressure gradient (loading) in the model and nature:

r (nature)= $(\Delta\rho\, L)/(\rho\, \Delta h)$= 0.46 (6)

where L=45 km and Δh=700 m, as in the Bardarbunga case;

r (model)= $(\Delta\rho\, L)/(\rho\, \Delta h)$= 0.52 (7)

being L=32 cm and Δh=1.3 cm. Since the ratios are similar, the two gradients play a similar relative role in experiments and nature.

To scale additional pressure contributions, we need more parameters, as follows. Volumetric flux into the dike (Q) is 7.9×10^{-8} m^3 s^{-1} in the models and 286 m^3 s^{-1} for Bardarbunga [Gudmundsson et al., 2016], thus $Q^* = 2.76\times10^{-10}$; shear modulus (μ) is 1.17×10^{3} Pa in the models and 0.3×10^{11} Pa for basalts [Turcotte and Schubert, 2002], thus $\mu^*= 3.89\times10^{-8}$; fluid viscosity (η) is 1.2×10^{-3} Pa s in the models and 10 Pa s for basalts, thus $\eta^* = 1.2\times10^{-4}$; Poisson's ratio ($\nu$) is 0.5 for pig-skin gelatin and 0.25 in nature, thus $(1-\nu)^*= 0.67$. We now calculate the:

1) topographic (loading) pressure scale ratio:

$$p_L^* = (\rho^*g^*\Delta h^*)= 0.6\times10^{-5} \quad (8)$$

where $\rho^*= 1000$ kg m^{-3}/ 2800 kg $m^{-3}= 0.36$ and $\Delta h^*= 1.3\times10^{-2}$ m / 700 m $= 1.9\times10^{-5}$

2) fracture pressure scale ratio (Eq. 28 in Rivalta et al., 2015):

$$p_f^*= (\Delta\rho^*g^*Kc^{*2})^{1/3} = 1.9\times10^{-5} \quad (9)$$

3) viscous pressure scale ratio (Eq. 25 in Rivalta et al., 2015):

$$p_v^*=((\mu^{*3}Q^*\eta^*\Delta\rho^{*2})/(1-\nu)^{*3})^{1/6}= 1.1\times10^{-6} \quad (10)$$

For the range of parameters considered, while the viscous pressure drop is slightly higher in nature than experiments, we find that p_L^* and p_f^* are similar: this ensures, together with eq. 6-7, that the loading gradient and fracturing play a similar proportional role in nature and experiments.

We assume: 1) no phase change (vesiculation or solidification) in the magma; this assumption is not excessively restrictive for the mafic lateral dike intrusions that we aim to study; 2) steady magma inflow into the dike; in reality, inflow decreased with time changing the ratio between fracture and viscous pressure. A possible limitation is the finite size of the box and of the gelatin layers, as addressed with additional numerical models. 3) We neglect any effect of regional extension or of pre-existing tectonic discontinuities.

3. Results

3.1 Experiments

We first describe two experiments with flat topography (experiments 1 and 2, respectively; Figure 2a-b) and then compare these with two experiments representative of the general influence of topography on dike propagation with density and rigidity layering (experiments 3 and 4 respectively; Figure 2c-d and Table S1). We describe the shape of the dike in each experiment (breadth/height, B/H) to evaluate any change due to the imposed factors.

In Experiment 1 (density layering; Figure 2a), the dike propagated vertically penetrating the upper medium and elongating laterally close to the surface prior to erupting after 300 s (1.3 days in nature). This resulted in final aspect ratio (B/H) and length (S) of 0.84 and 8.55 cm, respectively. The mean lateral and vertical propagation velocities were 0.48 and 0.61 mm/s, respectively.

In Experiment 2 (rigidity layering; Figure 2b) the dike propagated laterally at the interface with the stiff upper layer, erupting after 1320 s (~6 days in nature). The final aspect ratio and length were 1.45 and 21.3 cm, respectively. The mean lateral and vertical propagation velocities were 0.28 and 0.24 mm/s, respectively.

In Experiment 3 (topography and density layering; Figure 2c) the dike propagated vertically, showing a similar shape to experiment 1 and erupting after 330 s (~1.5 days in nature). The final aspect ratio and length were 0.90 and 9.1 cm, respectively. The mean lateral and vertical propagation velocities were 0.46 and 0.56 mm/s, respectively.

In experiment 4 (topography and rigidity layering; Figure 2d) the dike propagated laterally at the interface between the upper and lower layer, stopping below the plain and erupting after 1960 s (~9 days in nature). The final shape was elliptical (B/H= 2.28), though “inflated” towards the plain, 33.8 cm long. The mean lateral and vertical propagation velocities were 0.24 and 0.17 mm/s, respectively. Moreover, as the dike approached the plain before erupting, it bent toward the y-axis reaching an angle $\alpha = 70°$ between the slope direction and the dike strike (Figure S1c).

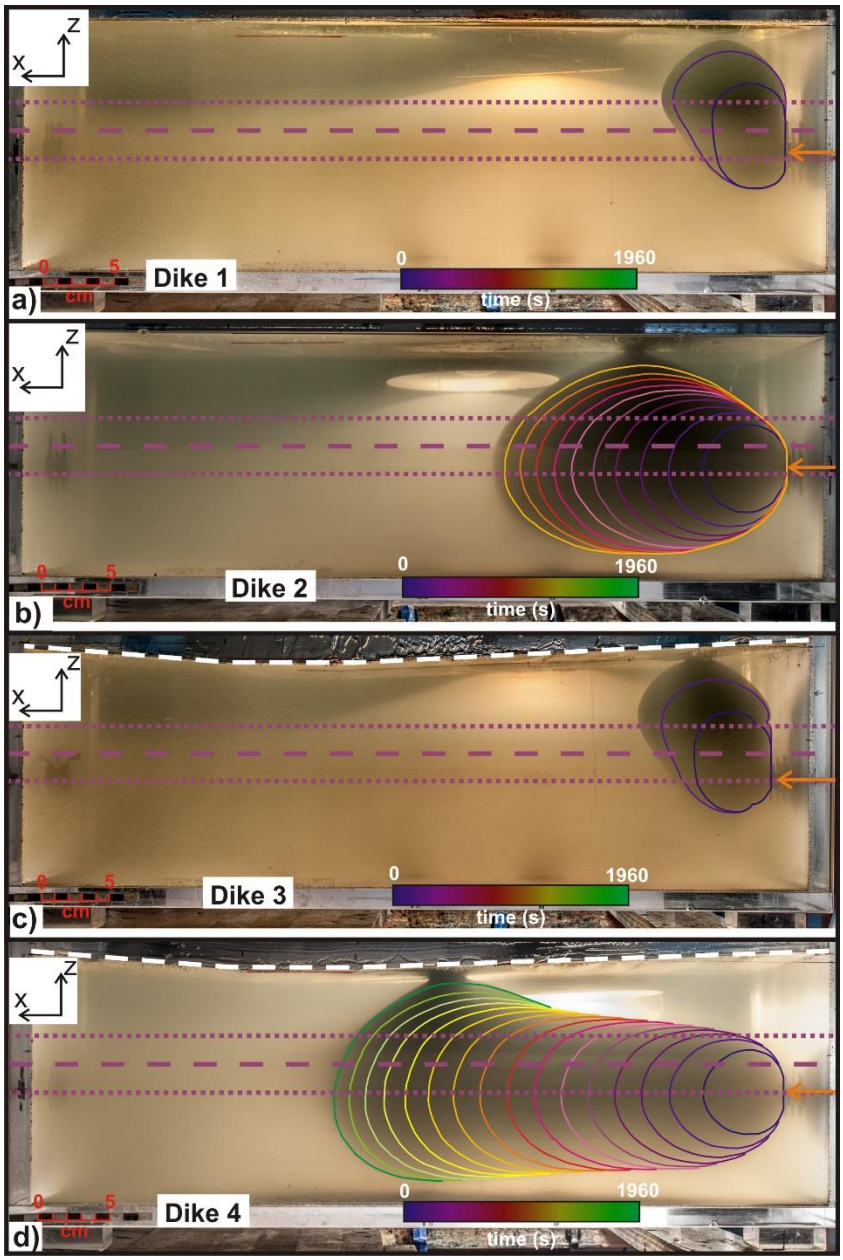

Figure 2. Experiments with flat topography, density (a, experiment 1) and rigidity layering (b, experiment 2). Experiments with topography, density (c, experiment 3) and rigidity layering (d, experiment 4). The dashed white and purple lines indicate the surface and the center of the interface respectively. Dotted purple lines indicate the limits of the interface. The orange arrows indicate the injection points. The colored lines indicate the dike edge contour every 120 seconds.

In experiment 5 (enhanced topography and rigidity layering) we increased the downslope dip (from 2.4° to 7°) and plain (from 0° to 4°), letting the upslope become flat (from 3.7° to 0°, Figure

S1a-b). The dike, after the injection below the slope on the right (Figure S1a), propagated laterally bending towards the y-axis, reaching α= 20° (Figure S1b).

We find that rigidity layering, particularly when combined to a slope, leads to longer dikes: higher rigidity ratios, E_u/E_l, result in higher S/T (Figure 3a) with maximum S/T (ratio between dike length and injection depth) obtained in experiment 4, with high rigidity contrast and load gradient (Figure 3a). Experiments 1 and 3 (only density layering) have similar S/T (0.86 and 0.91, respectively), while experiments 2 and 4, with density and rigidity layering, show a much higher S/T (3.38 and 2.14, respectively). The S/X ratio appears more uniform, although experiments 1 and 3 show a smaller difference (ΔS/X= 0.12) with respect to experiments 2 and 4 (ΔS/X= 0.47). Experiments 1 and 3 show low S/T values with respect to experiments 2 and 4 (equal to 0.86, 0.91, 2.14 and 3.38, respectively; figure 3a), indicating that density layering has minor influence on dike shape.

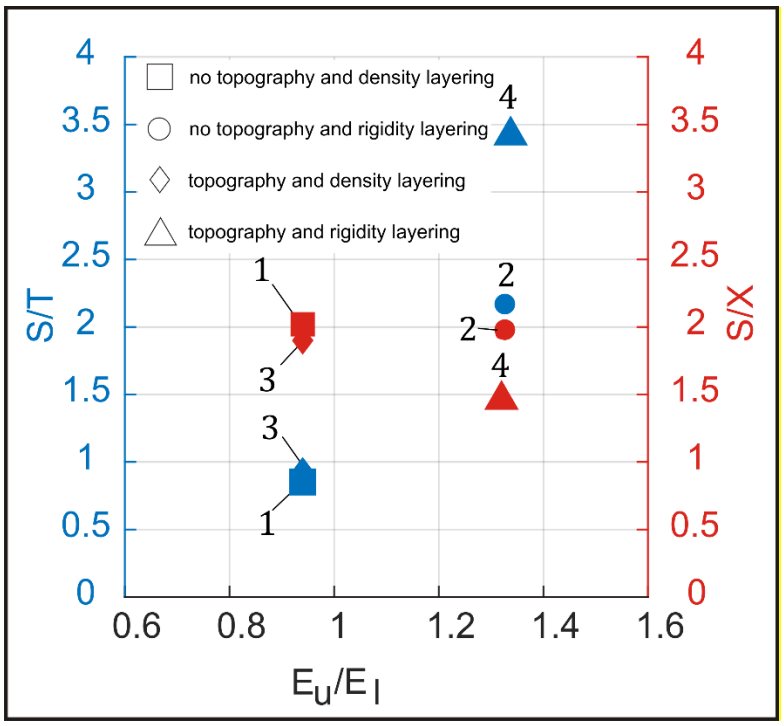

Figure 3. Rigidity ratio (E_u/E_l) against the ratio between dike length and depth of the injection point (S/T, blue) and the ratio between dike length and the distance between the injection and eruption points (S/X, red).

3.2 Numerical models

To better understand dike propagation and arrest, we evaluate the stress pattern within the gelatin. We generate a Finite Element model with COMSOL Multiphysics®. We assume 2D plane strain, on the x-z plane. We set zero displacement both for the lateral and bottom boundaries; the surface, shaped as in the experiments, is stress-free. The properties of the subdomains are: density ρ=1000 kg m^{-3}, Young's modulus E= 3500 Pa and Poisson's ratio ν = 0.4999. Gravity mimics the laboratory conditions, so that the stresses include the gelatin load [e.g. Corbi et al., 2016].

The model shows that the minimum compressive stress σ_3 is sub-horizontal beneath the slopes and rotates progressively to sub-vertical beneath the plain (Figure 4a). Such a configuration where σ_3 is lying on the x-z plane favors in general dike strikes along the y-axis (perpendicular to the figure plane), explaining the bending toward the y-axis observed in experiments 4 (Fig. S1c). This effect is enhanced if the slope dip is increased (experiment 5, Fig. S1b). The dike in experiment 4 did not reorient, probably because $(\sigma_2 - \sigma_3)/\sigma_2$ was very small, indicating that σ_2 is similar to σ_3 (Figure 4b). Such stress configuration is not particularly affected by the rigidity layering (Figure S2).

Since σ_1 and σ_3 lie on the propagation plane, the stress normal to the dike plane is σ_2, plotted in Figure 4c. The gradient of σ_2 is ~170 Pa m^{-1}. Revising the ratio of buoyancy to loading gradient estimated in Eq. 7 we obtain 1.1. The lateral gradient in our experiments may be too low to correctly simulate the 2014 Bardarbunga dike. However, we observe that the propagating tip of our dikes becomes arrested where σ_2 is minimum before increasing again (Figure 4c). This observation highlights that a non-zero driving gradient is essential for lateral propagation. Since σ_2 is large below the "mountain" and decreases downslope, it compresses the dike tail and squeezes its front towards the plain, further promoting lateral propagation. Conversely, below the upslope, the increase of σ_2 compresses the dike tip, arresting the dike where σ_2 is minimum (Figure 4c).

4. Discussion and conclusions

Our models suggest that lateral dike propagation is promoted by several factors: 1) vertical dike ascent needs to be prevented; 2) the dike must be pushed laterally by a pressure gradient; 3) for highest efficiency, this pressure gradient should be maximum in the direction perpendicular to σ_3. Below we discuss these factors and their relevance for dike propagation in nature, recalling that in our experiments σ_3 was in the plane of the dike. Even though we cannot properly evaluate what would have changed if σ_3 was dike-perpendicular, available evidence from magmatic systems along divergent plate boundaries suggests that this promotes further lateral propagation [Acocella, 2014].

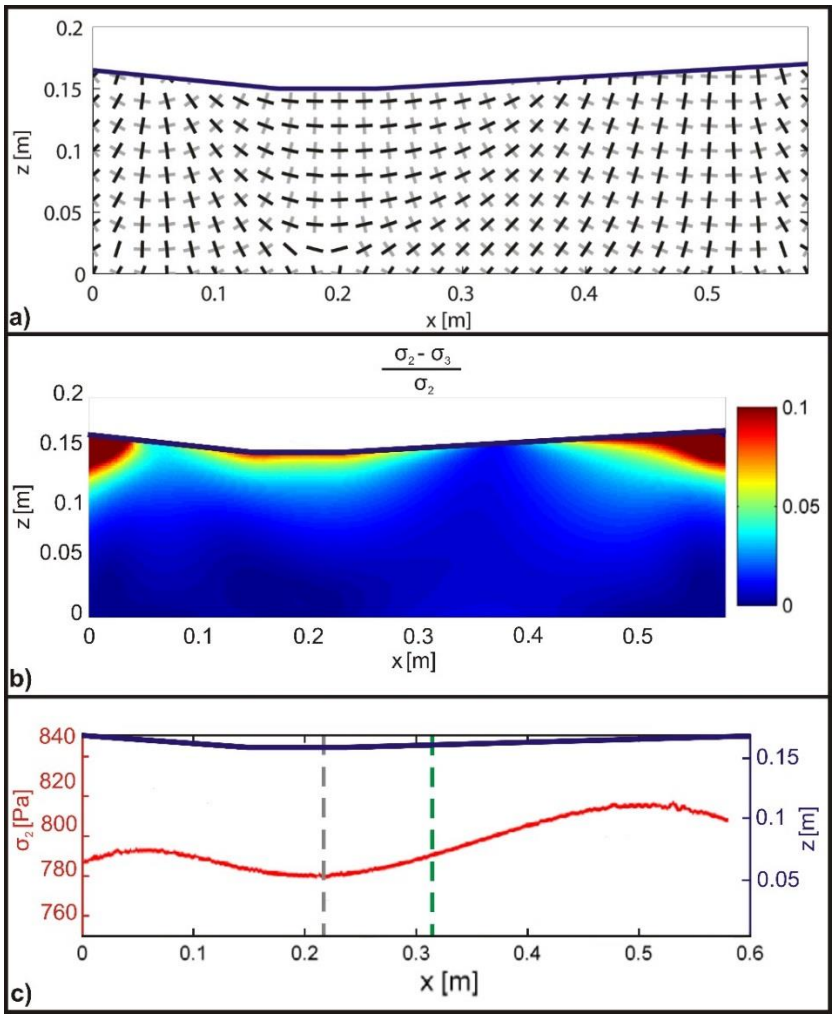

Figure 4. Stresses in the gelatin experiments. a) Direction of the principal stress components σ_1 (black lines) and σ_3 (gray lines). b) $(\sigma_2 - \sigma_3)/\sigma_2$ variations due to the imposed topography. c) σ_2 profile (red line). The blue line indicates the topography profile; the dashed green and grey lines indicate the eruption point and the final position of the dike tip in experiment 4, respectively.

Regarding point 1), in experiments 2 and 4 we prevented vertical dike ascent and obtained lateral propagation through rigidity layering. These experiments suggest that rigidity layering is more efficient than anti-buoyancy in driving lateral dike propagation, as it acts as a barrier to ascent, while anti-buoyancy determines only the vertical equilibrium position of the dike [Rivalta et al., 2015]. However, models of dike injection at the base of a box with soft layers above stiff ones suggest that vertical propagation is promoted [Rivalta et al., 2005]. In volcanic areas, stiff layers often overlie softer layers, as soft scoria and/or pyroclastic deposits may be capped by km-thick stiffer lava piles, as in Central Afar [Abbate et al., 2015]. This decrease in rigidity with depth affecting dike propagation is exemplified by the 2004 eruption at Asama (Japan), where part of the feeder dike propagated laterally below a stiffer zone [Aoki et al., 2009]. Thermal weakening of the upper crust, due to the presence of partial melt or to chemical reactions triggered by heat advection, may also decrease the rigidity of the rock, so that this becomes more compliant at depth [Heap et al., 2013]. These wide-scale rigidity inversions are geophysically detected below rifts, as Kilauea's East Rift Zone (Hawaii), Krafla (Iceland) and Afar (Ethiopia) [Brandsdottir et al., 1997; Haslinger et al., 2001; Desissa et al., 2013] and, possibly, at Bardarbunga, with the vent located within a basin with alternating sediments and lavas.

Other processes may inhibit vertical dike propagation. Magma may be more anti-buoyant in the shallowest layers than what modelled here. Additionally, graben faulting may arrest an ascending dike by compressing its upper tip, as suggested for the 2009 dike at Harrat Lunayyir [Saudi Arabia; Xu et al., 2016]. These processes may be more important than previously thought for lateral propagation.

As for points 2) and 3), a lateral pressure gradient is necessary to drive dikes to larger distances. We imposed a lateral gradient by shaping the topography of our gelatin similar to a volcanic slope, even though other factors may induce lateral stress gradients. Here we have shown that a lateral pressure gradient is not very efficient in driving dike propagation if σ_3 is not perpendicular to the dike. This was already demonstrated by Dahm [2000], who compared with a numerical model dike trajectories for three cases: a) pressure gradient with $\sigma_1=\sigma_3$, b) pressure gradient aligned with σ_3, c)

pressure gradient perpendicular to σ_3. In case c), where the two factors (pressure gradient and σ_3) reinforced each other, the dike deviated toward the maximum gradient direction over a short distance. In case a), a larger distance was needed for the dike to bend and align with the maximum gradient direction. In case b), where the two factors played against each other, the dike bent towards an intermediate direction.

The pathway of the Bardarbunga dike resulted from a combination of tectonic and loading stresses [Sigmundsson et al., 2015]. The final strike of the dike deviated from that perpendicular to the maximum tectonic extension by 10°, as shown by deformation models and focal mechanisms of earthquakes [Ruch et al., 2016; Agustdottir et al., 2016]. Here we confirm that any inconsistency between the direction of the maximum topographic gradient and that perpendicular to σ_3 leads to dike bending and shearing on the dike plane. In nature, surface loads may have more complex 3D distributions. Indeed, at stratovolcanoes, σ_3 is horizontal and circumferential around the volcanic cone; thus, as the dike propagates downslope, the bending observed in the experiments would not take place, unless other factors contribute to the stress field, such as pre-existing fractures [Le Corvec et al., 2013; Ruch et al., 2016] or regional tectonics [Sigmundsson et al., 2015], both not modeled here.

As for the factors causing dike arrest below the plain in our experiments, we speculate that the lithostatic load of the opposite slope acts as a "pressure barrier", compressing the propagating tip and thus hindering dike propagation, as suggested for Somma-Vesuvio [Acocella et al., 2006] or Miyakejima [Maccaferri et al., 2016]. This is also supported by the model of the σ_2 profile with single slope compared to that of a double slope (Figure S3): with two opposite slopes σ_2 increases upslope, while with a single slope σ_2 keeps decreasing. Therefore, the dike would propagate farther without any upslope.

An important role may be also played by the stress induced in the gelatin by the specific distribution of loads, which involves a sub-vertical σ_3 beneath the plain and a sub-horizontal σ_3 moving towards the slopes, as in Figure 4a and previous studies [e.g., Maccaferri et al., 2014]. This

stress pattern causes the experimental dike to bend sideways and stop, as the more it bends the smaller the topographic gradient it experiences.

Our results help interpreting some features of recent lateral diking events (such as Bardarbunga in 2014). In experiment 4, we observe dike arrest in a region of flat and low topography, similar to the southern flank of Askja volcano, encountered by the 2014 Bardarbunga dike on its pathway. We note a discrepancy in the position of the eruption point, which is before the plain in the models and inside the plain in Bardarbunga, and in the final position of the dike tip, which is at ~ 10 km from the plain edge in Bardarbunga and 3.3 cm (corresponding to ~2 km in nature) in experiment 4. Experiments 15 and 16 (replicating experiment 4, except for the layer thicknesses, Table S1) also erupted before the plain (X= 15.1 cm and 20.1 cm, respectively), confirming reproducibility. However, the Bardarbunga dike intersected the surface in three more locations beside the plain (where two major vents opened). In fact, three cauldrons formed on the Vatnajökull ice cap [Sigmundsson et al., 2015]. The longest dike in our models (experiment 4 = 33.8 cm corresponding to ~ 18 km in nature) has the same order of magnitude of the dike segment that propagated laterally under the ice cap at Bardarbunga (~ 30 km).

Concerning the 2005 Dabbahu diking episode, the southern portion arrested just before a region of minor relief (height difference of 300 meters compared to 400 and 300 meters for Bardarbunga and Somma-Vesuvio, respectively); conversely, the northern part of the dike propagated up-slope erupting on the NE flank of the edifice [Wright et al. 2006; Ebinger et al., 2010]. In this case, the effect on crustal stresses of a lateral thermal gradient of the crust may have dominated over the effect of topography [Grandin et al., 2012] and allowed the dike propagating upslope for some distance, possibly explaining the discrepancy with our models that suggest a difficulty in propagating along an opposite slope. This confirms, as mentioned, that other processes in addition to topography may drive lateral propagation and arrest.

Concluding, lateral dike propagation downslope is particularly efficient when the topographic pressure gradient is accompanied with crustal rigidity layering (i.e. stiffer layers above weak ones).

Conversely, dikes may arrest if an external relief produces an opposite topographic pressure gradient.

Authors contributions

S.U. performed and interpreted the analogue models. E.R. provided the equations and managed the scaling calculations. V.A. supervised the project and provided suggestions for the analogue modelling. F.C. performed the numerical model. All authors discussed the results and contributed to writing the manuscript.

Acknowledgements

Giulia Sili provided technical support during the experiments. Matteo Trolese provided useful suggestions for the image processing. Malte C. Ritter shared his data about gelatin rigidity. Janine Kavanagh provided helpful advices for the setting of the analogue models. Laurent Michon provided helpful suggestions. Nicolas Le Corvec, Robert White and Joel Ruch provided constructive reviews. This work was financed by the Italian government. Any user can access the data of this work by contacting the corresponding author.

References

Abbate, E., P. Bruni, and M. Sagri (2015), Geology of Ethiopia: A Review and Geomorphological Perspectives, in Landscapes and Landforms of Ethiopia, World Geomorphological Landscapes, edited by P. Billi, pp. 33-64, Springer Science + Business Media, Dordrecht, Netherlands, doi: 10.1007/978-94-017-8026-1_2.

Acocella, V. (2014), Structural control on magmatism along divergent and convergent plate boundaries: overview, model, problems, *Earth Sci. Rev.*, *136*, 226-288, doi:10.1016/j.earscirev.2014.05.006.

Acocella, V., and A. Tibaldi (2005), Dike propagation driven by volcano collapse: A general model tested at Stromboli, Italy, *Geophys. Res. Lett.*, *32*, L08308, doi:10.1029/2004GL022248.

Acocella, V., M. Porreca, M. Neri, E. Massimi, and M. Mattei (2006), Propagation of dikes at Vesuvio (Italy) and the effect of Mt. Somma, *Geophys. Res. Lett.*, *33*, L08301, doi:10.1029/2005GL025590.

Ágústsdóttir, T., J. Woods, T. Greenfield, R. G. Green, R. S. White, T. Winder, B. Brandsdóttir, S. Steinthórsson, and H. Soosalu (2016), Strike-slip faulting during the 2014 Bárðarbunga-Holuhraun dike intrusion, central Iceland, *Geophys. Res. Lett., 43*, 1495-1503, doi:10.1002/2015GL067423.

Aoki, Y., et al. (2009), P-wave velocity structure beneath Asama Volcano, Japan, inferred from active source seismic experiment, *J. Volcanol. Geotherm. Res., 187*, 272–277, doi:10.1016/j.jvolgeores.2009.09.004.

Brandsdottir, B., W. Menke, P. Einarsson, R.S. White, and R.K. Staples (1997), Faroe-Iceland Ridge Experiment: 2.Crustal structure of the Krafla central volcano, *J. Geophys. Res.*, *102*, 7867–7886, doi:10.1029/96JB03799.

Brizzi, S., F. Funiciello, F. Corbi, E. Di Giuseppe, and G. Mojoli (2016), Salt matters: How salt affects the rheological and physical properties of gelatine for analogue modelling. *Tectonophysics, 679*, 88-101, doi:10.1016/j.tecto.2016.04.021.

Buck, W.R., P. Einarsson, and B. Brandsdóttir (2006), Tectonic stress and magma chamber size as controls on dike propagation: constraints from the 1975–1984 Krafla rifting episode, *J. Geophys. Res. Solid. Earth, 111*, B12404, doi:10.1029/2005JB003879.

Corbi, F., E. Rivalta, V. Pinel, F. Maccaferri, M. Bagnardi, and V. Acocella (2015), How caldera collapse shapes the shallow emplacement and transfer of magma in active volcanoes, *Earth Planet. Sci. Lett., 431*, 287–293, doi:10.1016/j.epsl.2015.09.028.

Corbi, F., E. Rivalta, V. Pinel, F. Maccaferri, and V. Acocella (2016), Understanding the link between circumferential dikes and eruptive fissures around calderas based on numerical and analog models, *Geophys. Res. Lett., 43*, 6212–6219, doi:10.1002/2016GL068721.

Dahm, T. (2000), Numerical simulations of the propagation path and arrest of fluid-filled fractures in the earth, *Geophys. J. Int., 141,* 623-638, 10.1046/j.1365-246x.2000.00102.x.

Dahm, T., S. Hainzl, and T. Fischer (2010), Bidirectional and unidirectional fracture growth during hydrofracturing : Role of driving stress gradients, *J. Geophys. Res.*, *115*, B12322, doi:10.1029/2009JB006817.

Desissa, M., N. E. Johnson, K. A. Whaler, S. Hautot, S. Fisseha, and G. J. K. Dawes (2013), A mantle magma reservoir beneath an incipient mid-ocean ridge in Afar , Ethiopia, *Nat. Geosci.*, *6*(10), 861–865, doi:10.1038/ngeo1925.

Di Giuseppe, E., F. Funiciello, F. Corbi, G. Ranalli, and G. Mojoli (2009), Gelatins as rock analogs: A systematic study of their rheological and physical properties, *Tectonophysics*, *473(3–4)*, 391–403, doi:10.1016/j.tecto.2009.03.012.

Ebinger, C. J., A. Ayele, D. Keir, J. Rowland, G. Yirgu, T. Wright, M. Belachew, and I. Hamling (2010), Length and timescales of rift faulting and magma intrusion: The Afar rifting cycle from 2005 to present, *Annu. Rev. Earth Planet. Sci.*, *38(1)*, 439–466, doi:10.1146/annurev-earth-040809-152333.

Fialko, Y. A., and A. M. Rubin (1999), What controls the along-strike slopes of volcanic rift zones?, *J. Geophys. Res.*, *104(B9)*, 20007–20020, doi:10.1029/1999JB900143.

Fiske, R. S., and E. D. Jackson (1972), Orientation and Growth of Hawaiian Volcanic Rifts: The Effect of Regional Structure and Gravitational Stresses, *Proc. R. Soc. Lond. A*, *329*, 299-326, doi:10.1098/rspa.1972.0115.

Grandin, R., A. Socquet, C. Doubre, E. Jacques, and G. C. P. King (2012), Elastic thickness control of lateral dyke intrusion at mid-ocean ridges, *Earth Planet. Sci. Lett.*, *319–320*, 83–95, doi:10.1016/j.epsl.2011.12.011.

Gudmundsson, A. (2002), Emplacement and arrest of sheets and dykes in central volcanoes, *J. Volcanol. Geotherm. Res.*, *116*, 279–298, doi:10.1016/S0377-0273(02)00226-3.

Gudmundsson, A. (2003), Surface stresses associated with arrested dykes in rift zones, *Bull. Volcanol., 65*, 606–619, doi:10.1007/s00445-003-0289-7.

Gudmundsson, A. (2011), Deflection of dykes into sills at discontinuities and magma-chamber formation, *Tectonophysics, 500(1–4)*, 50–64, doi:10.1016/j.tecto.2009.10.015.

Gudmundsson, M.T., et al. (2016), Gradual caldera collapse at Bárdarbunga volcano, Iceland, regulated by lateral magma outflow, *Science, 353*, aaf8988, doi:10.1126/science.aaf8988.

Haslinger, F., C. Thurber, M. Mandernach, and P. Okubo (2001), Tomographic image of P-velocity structure beneath Kilauea's East Rift Zone and South Flank: seismic evidence for a deep magma body, *Geophys. Res. Lett., 28(2)*, 375–378, doi:10.1029/2000GL012018.

Heap, M. J., S. Mollo, S. Vinciguerra, Y. Lavallée, K.-U. Hess, D. B. Dingwell, P. Baud, and G. Iezzi (2013), Thermal weakening of the carbonate basement under Mt. Etna volcano (Italy): Implications for volcano instability, *J. Volcanol. Geotherm. Res.*, *250*, 42–60, doi:10.1016/j.jvolgeores.2012.10.004.

Kavanagh, J. L., T. Menand, and R. S. J. Sparks (2006), An experimental investigation of sill formation and propagation in layered elastic media, *Earth Planet. Sci. Lett., 245*, 799–813, doi:10.1016/j.epsl.2006.03.025.

Kavanagh, J. L., T. Menand, and K.A. Daniels (2013), Gelatine as a crustal analogue: Determining elastic properties for modelling magmatic intrusions. *Tectonophysics, 582*, 101-111, doi:10.1016/j.tecto.2012.09.032.

Kervyn, M., G. G. J. Ernst, B. V. W. De Vries, L. Mathieu, and P. Jacobs (2009), Volcano load control on dyke propagation and vent distribution: Insights from analogue modeling, *J. Geophys. Res., 114*, B03401, doi:10.1029/2008JB005653.

Le Corvec, N., T. Menand, and J. Lindsay (2013), Interaction of ascending magma with pre-existing crustal fractures in monogenetic basaltic volcanism: an experimental approach, *J. Geophys. Res. Solid Earth, 118,* 968-984, doi:10.1002/jgrb.50142.

Lister, J. R. (1990), Buoyancy-driven fluid fracture: similarity solutions for the horizontal and vertical propagation of fluid-filled cracks, *J. Fluid Mech., 217,* 213-239, doi:10.1017/S0022112090000696.

Lister, J. R. (1991), Steady solutions for feeder dykes in a density-stratified lithosphere, *Earth Planet. Sci. Lett., 107,* 233–242, doi:10.1016/0012-821X(91)90073-Q.

Lister, J. R., and R. C. Kerr (1991), Fluid-Mechanical Models of Crack Propagation and Their Application to Magma Transport in Dykes, *J. Geophys. Res., 96(B6),* 1049–1077, doi:10.1029/91JB00600.

Maccaferri, F., M. Bonafede, and E. Rivalta (2011), A quantitative study of the mechanisms governing dike propagation, dike arrest and sill formation, *J. Volcanol. Geotherm. Res., 208(1–2),* 39–50, doi:10.1016/j.jvolgeores.2011.09.001.

Maccaferri, F., E. Rivalta, D. Keir, and V. Acocella (2014), Off-rift volcanism in rift zones determined by crustal unloading, *Nat. Geosci., 7,* 297–300, doi:10.1038/NGEO2110.

Maccaferri, F., E. Rivalta, L. Passarelli, and Y. Aoki (2016), On the mechanisms governing dike arrest: Insight from the 2000 Miyakejima dike injection, *Earth Planet. Sci. Lett., 434,* 64–74, doi:10.1016/j.epsl.2015.11.024.

Olson, J. E., and R. A. Schultz (2011), Comment on "A note on the scaling relations for opening mode fractures in rock" by C.H. Scholz, *J. Struct. Geol., 33(10),* 1523–1524, doi:10.1016/j.jsg.2011.07.004.

Pinel, V., and C. Jaupart (2000), The effect of edifice load on magma ascent beneath a volcano, *Phil. Trans. R. Soc. Lond. A, 1515-1532,* doi:10.1098/rsta.2000.0601

Pinel, V., and C. Jaupart (2004), Magma storage and horizontal dyke injection beneath a volcanic edifice, *Earth Planet. Sci. Lett., 221*, 245–262, doi:10.1016/S0012-821X(04)00076-7.

Pinel, V., and C. Jaupart (2005), Some consequences of volcanic edifice destruction for eruption conditions, *J. Volcanol. Geotherm. Res., 145*, 68–80, doi:10.1016/j.jvolgeores.2005.01.012.

Ritter, M. C. (2012), Analogue and numerical modelling of dyke propagation in stratovolcanoes effects of rock mechanical properties and layer thicknesses, M.S. thesis, Department of Structural Geology and Geodynamics, University of Göttingen, Göttingen, Germany.

Ritter, M. C., V. Acocella, J. Ruch, and S. L. Philipp (2013), Conditions and threshold for magma transfer in the layered upper crust: Insights from experimental models, *Geophys. Res. Lett., 40*, 1–5, doi:10.1002/2013GL058199.

Rivalta, E., M. Bottinger, and T. Dahm (2005), Buoyancy-driven fracture ascent: Experiments in layered gelatine, *J. Volcanol. Geotherm. Res., 144*, 273–285, doi:10.1016/j.jvolgeores.2004.11.030.

Rivalta, E., B. Taisne, A. P. Bunger, and R. F. Katz (2015), A review of mechanical models of dike propagation: Schools of thought, results and future directions, *Tectonophysics*, *638*, 1–42, doi:10.1016/j.tecto.2014.10.003.

Roman, A., and C. Jaupart (2014), The impact of a volcanic edifice on intrusive and eruptive activity, *Earth Planet. Sci. Lett.*, *408*, 1–8, doi:10.1016/j.epsl.2014.09.016.

Rubin, A. M. (1995), Propagation of magma-filled cracks, *Annu. Rev. Earth Planet. Sci., 23(1),* 439–466, 287–336, doi:10.1146/annurev.ea.23.050195.001443.

Ruch, J., T. Wang, W. Xu, M. Hensch, and S. Jonsson (2016), Oblique rift opening revealed by reoccurring magma injection in central Iceland, *Nature Communications, 7*, 1–7, doi:10.1038/ncomms12352.

Ryan, M. P., (1994) Neutral-buoyancy controlled magma transport and storage in mid-ocean ridge magma reservoirs and their sheeted-dike complex: A summary of basic relationships, in Magmatic Systems, edited by M. P. Ryan, pp. 97- 135, Academic Press, San Diego, Calif.

Scholz, C. H. (2010), A note on the scaling relations for opening mode fractures in rock, *J. Struct. Geol., 32(10),* 1485–1487, doi:10.1016/j.jsg.2010.09.007.

Sigmundsson, F. et al., (2015), Segmented lateral dyke growth in a rifting event at Bárðarbunga volcanic system, Iceland, *Nature, 517,* 191-195, doi:10.1038/nature14111.

Taisne, B., and C. Jaupart (2009), Dike propagation through layered rocks, *J. Geophys. Res., 114*, B09203, doi:10.1029/2008JB006228.

Turcotte, D. L., and G. Schubert (2002), Geodynamics, Cambridge University Press, Cambridge, England.

Watanabe, T., T. Masuyama, K. Nagaoka, and T. Tahara (2002), Analog experiments on magma-filled cracks: Competition between external stresses and internal pressure, *Earth Planet Sp., 54*, 1247–1261, doi:10.1186/BF03352453.

Wright, T. J., C. Ebinger, J. Biggs, A. Ayele, G. Yirgu, D. Keir, and A. Stork (2006), Magma-maintained rift segmentation at continental rupture in the 2005 Afar dyking episode, *Nature, 442*, 291-294, doi:10.1038/nature04978.

Wright, T. J. et al. (2012), Geophysical constraints on the dynamics of spreading centres from rifting episodes on land, *Nat. Geosci., 5(4)*, 242–250, doi:10.1038/ngeo1428.

Xu, W., S. Jónsson, F. Corbi, and E. Rivalta (2016), Graben formation and dike arrest during the 2009 Harrat Lunayyir dike intrusion in Saudi Arabia: Insights from InSAR, stress calculations and analog experiments, *J. Geophys. Res. Solid. Earth, 121*, 2837–2851, doi:10.1002/2015JB012505.

[Geophysical Research Letters]

Supporting Information for

[Propagation and arrest of dikes under topography: models applied to the 2014 Bardarbunga (Iceland) rifting event]

[S. Urbani[1], V. Acocella[1], E. Rivalta[2] and F. Corbi[3]]

[[1]Dipartimento di Scienze, Università Roma Tre, Rome, Italy, [2]Deutsches GeoForschungsZentrum GFZ, Section 2.1, Potsdam, Germany, [3]Géosciences Montpellier Laboratory, University of Montpellier, Montpellier, France]

Contents of this file

Introduction

[Supplementary material on the analogue and numerical models]

Text S1.

Here we describe the experiments not presented in the main article (experiments 6-20, listed in Table S1). In Experiments 6-11, we injected water from the bottom of the box, to test the influence of the intrusion depth on dike propagation. In experiments 12-20 we injected laterally, as experiments 1-5 varying systematically the imposed parameters presented here, plus the layer thickness (experiments 15-16), water density (experiments 12, 13, 18 and 20) and flow rate (experiment 17). In addition, experiment 4 is replicated by experiment 14 and by experiments 15-16 (excepting for layers thicknesses), while experiment 19 duplicates experiment 5.

Experiment	E_u (kPa)	E_l (kPa)	ρ_u (kg/m^3)	ρ_l (kg/m^3)	E_u/E_l	ρ_u/ρ_l	S (cm)	X (cm)
1	3.3	3.5	1018.1	1071.3	0.94	0.9503	8.55	4.23
2	3.3	2.5	1018.1	1053.6	1.32	0.9663	21.35	10.96
3	3.3	3.5	1018.1	1071.3	0.94	0.9503	9.10	4.79
4	3.3	2.5	1018.1	1053.6	1.32	0.9663	33.83	22.82
5	3.3	2.5	1018.1	1053.6	1.32	0.9663	13.2	7.6
6	3.3	/	1018.1	/	/	/	27.69	4.7
7	3.3	/	1018.1	/	/	/	13.77	0
8	3.3	**/**	1018.1	**/**	/	**/**	24	/
9	3.3	3.5	1018.1	1071.3	0.94	0.9503	13.07	3.07
10	3.3	2.5	1018.1	1053.6	1.32	0.9663	23.14	9.03
11	3.3	/	1018.1	/	/	/	20.75	5.72
12	3.3	/	1018.1	/	/	/	9	/
13	3.3	/	1018.1	/	/	/	16.59	9.48
14	3.3	2.5	1018.1	1053.6	1.32	0.9663	25.5	/
15	3.3	2.5	1018.1	1053.6	1.32	0.9663	24.28	15.1
16	3.3	2.5	1018.1	1053.6	1.32	0.9663	28.66	20.10
17	3.3	/	1018.1	/	/	/	12.37	/
18	3.3	3.5	1018.1	1071.3	0.94	0.9503	10.38	5.69
19	3.3	2.5	1018.1	1053.6	1.32	0.9663	12.78	/
20	3.3	/	1018.1	/	/	/	15.88	8.92

Table S1. List of the imposed and measured parameters in all the performed experiments (in bold are the representative ones presented in the main text).

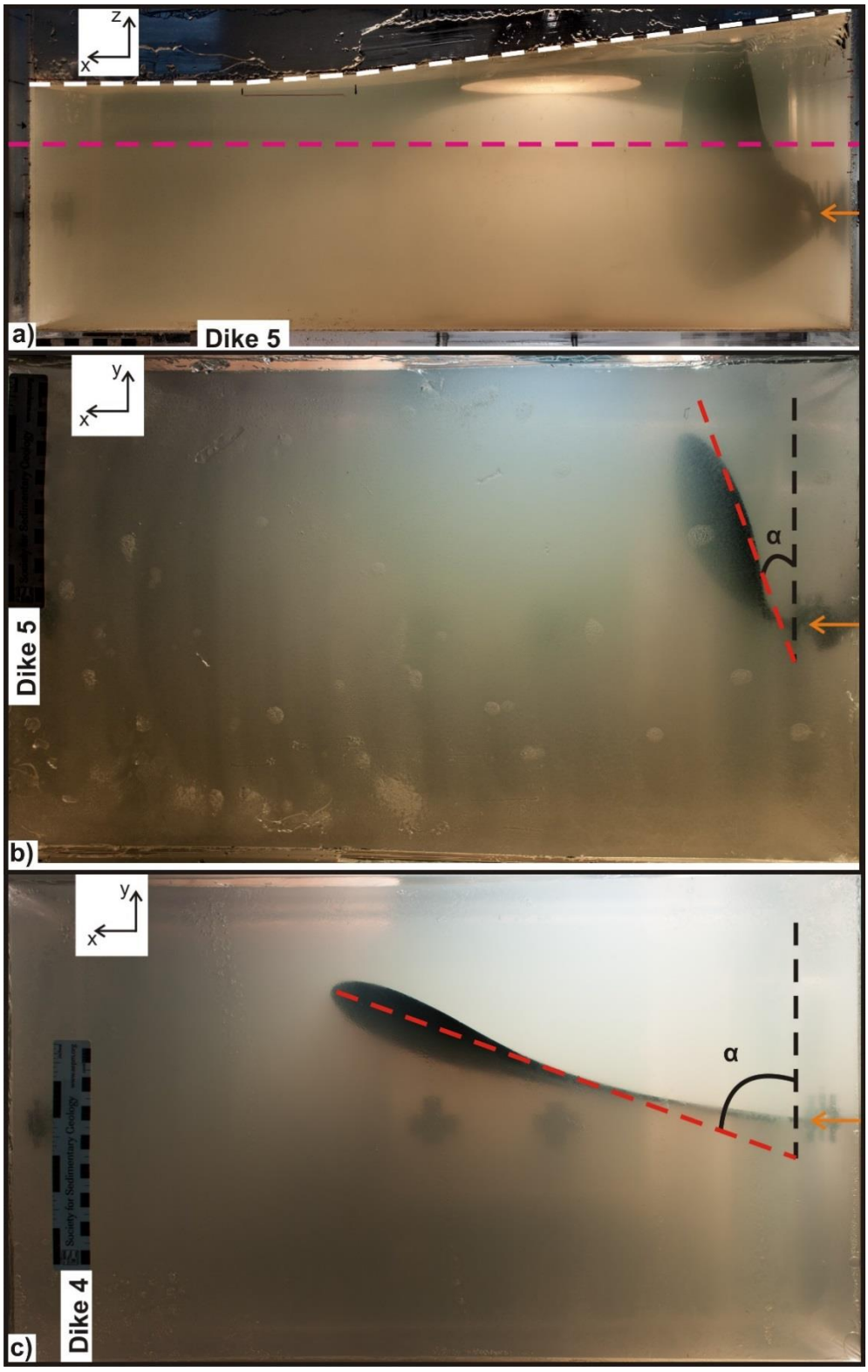

Figure S1. a) Side view of Experiment 5 with a right slope dip decreasing from 7° to 4° and a plain on the left (white dashed line). The dashed purple line indicates the interface between the stiff (upper) and soft layer (lower). The orange arrow indicates the injection point. Top view of experiments 5 (b) and 4 (c), showing how the dike tends to be parallel to the imposed topography more efficiently in (b) than in (a). The red and black dashed lines indicate the dike strike and the slope strike, respectively.

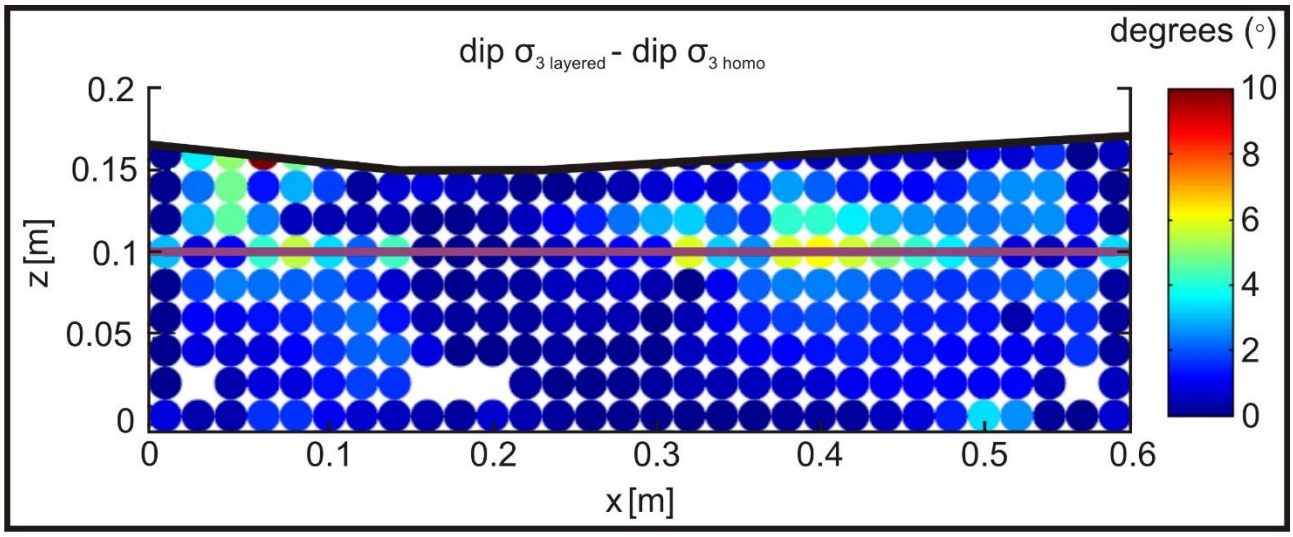

Figure S2. Numerical model showing the dip difference (see Figure 4a of the main article) between σ_3 in a layered and homogeneous gelatin. The purple line indicates the interface. Note that the dip difference is always less than 10°.

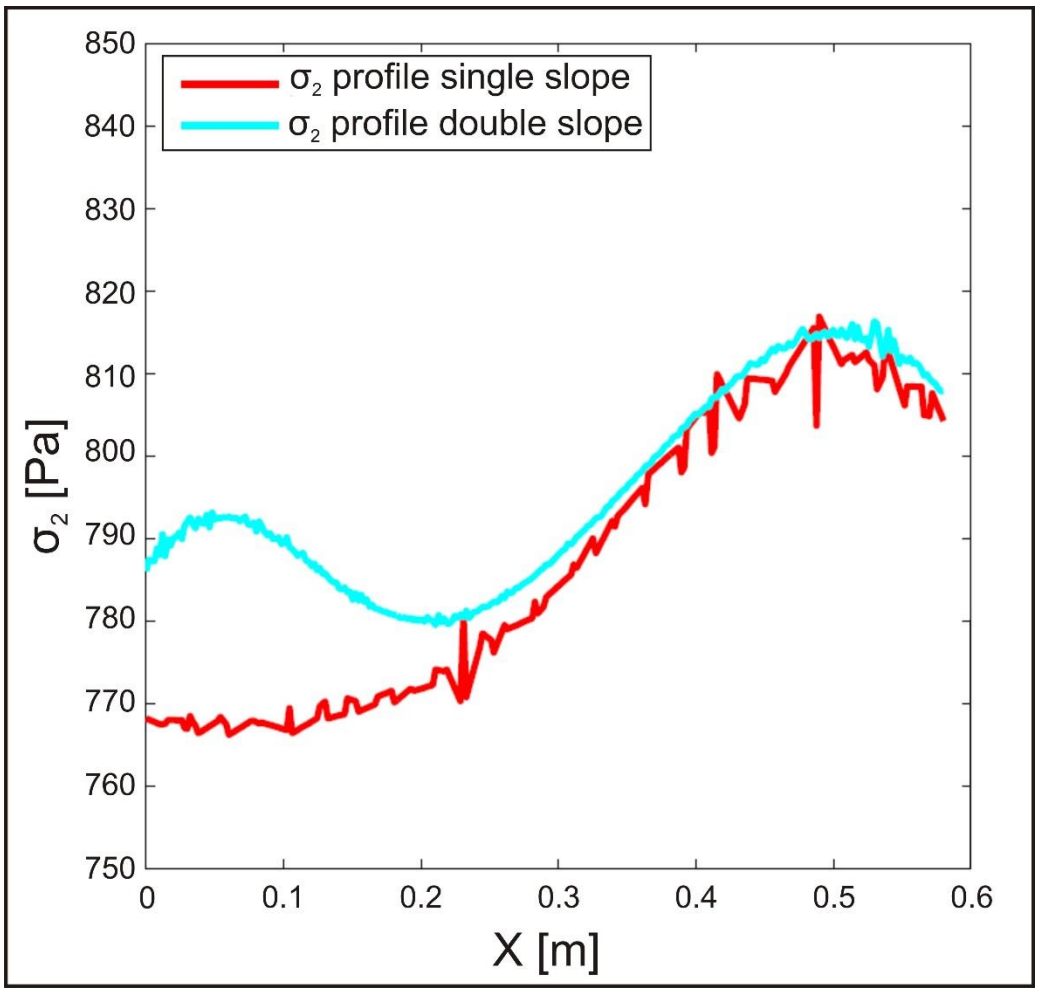

Figure S3. Comparison between profiles of σ_2 with a double slope (light blue line) and single slope (red line).

Chapter 3

(to be submitted to Journal of Geophysical Research Solid Earth)

What drives the lateral vs. vertical propagation of dikes? Insights from analogue models

S. Urbani[1], V. Acocella[1] and E. Rivalta[2]

[1]Dipartimento di Scienze, Università Roma Tre, Rome, Italy, [2]Deutsches GeoForschungsZentrum GFZ, Section 2.1, Potsdam, Germany.

Corresponding author: stefano.urbani@uniroma3.it

Abstract

Understanding dike propagation and emplacement is crucial to define how magma is transferred and extruded. Geological and geophysical data reveal that dikes may propagate laterally and vertically, at both the volcano and regional scale. Many factors, including buoyancy, crustal layering and topography may dictate whether a dike will propagate vertically or laterally, but the relative weight of these contributions has never been investigated in detail. In order to define a hierarchy between the various factors, we have conducted analogue modelling, injecting water (magma analogue) within gelatin (crust analogue). Here we present results from 32 experiments, with vertical (Set 1, 17 experiments) and lateral (Set 2, 15 experiments) injection, investigating the effect of crustal layering (both rigidity and density layering), topography, magma inflow rate and the density ratio between host rock and magma. By comparing the experimental observations and based on scaling considerations we propose a hierarchy of the investigated factors suggesting that rigidity layering (i.e. a stiff layer overlying a weak one) and topography favor predominantly lateral dike propagation while inflow rate, density layering and density ratio play a subordinate role. Our results highlight the higher efficiency of the presence of a stiff layer in preventing magma ascent, with respect to the Level of

Neutral Buoyancy (LNB) proposed by previous studies, which should explain the lateral propagation of recent diking events.

1. Introduction

Understanding dike propagation and emplacement is crucial to define how magma is transferred and extruded within the crust. Geological and geophysical data at volcanoes and rift zones reveal that dikes may propagate both laterally and vertically. Laterally propagating dikes have been recognized at many volcanic edifices such as Etna, Vesuvius, Stromboli, Kilauea, Miyakejima, Piton de La Fournaise and El Hierro [Peltier et al., 2009; Acocella and Neri, 2009, Martì et al., 2013; Rivalta et al., 2015]. Rifting episodes along divergent plate boundaries in Afar and Iceland also highlight a predominant lateral transfer of magma in rifts [Einarsson and Brandsdottir, 1980; Biggs et al., 2009; Ayele et al., 2009; Ebinger et al., 2010; Nobile et al., 2012; Wright et al., 2012; Sigmundsson et al., 2015]. However, magma is also transported vertically by diking, both in volcanic edifices, such as Vesuvius and Etna [Acocella and Neri, 2003; Acocella et al., 2006] and along rift zones, as at Harrat Lunayyr [Pallister et al.; 2010] and Iceland [Hartley and Thordarson, 2012, 2013].

Many factors may dictate whether a dike will propagate vertically or laterally. Among all, buoyancy has often been proposed as dominant in controlling whether a dike propagates vertically or laterally [Takada, 1990; Menand and Tait, 2002; Taisne and Tait, 2009; Townsend et al., 2017]; according to Lister and Kerr [1991], a neutrally buoyant dike is expected to become arrested and expand laterally at the level of neutral buoyancy (LNB). Moreover, stiff layers overlying more compliant ones may provide effective barriers to magma ascent [Rivalta et al., 2005, Gudmundsson, 2006, Kavanagh et al., 2006; Maccaferri et al., 2011]. Topographic reliefs provide a driving pressure for propagation by inducing vertical and lateral stress gradients [Fiske and Jackson, 1972; Rubin and Pollard, 1987; Fialko and Rubin, 1999; Muller et al., 2001; Pinel and Jaupart, 2004; Acocella and Neri, 2009, Kervyn et al., 2009, Maccaferri et al., 2016; Pinel et al., 2017]; additionally, they modify dike trajectories by inducing rotations of the principal stress axes, that may lead e.g. to transitions

from vertical to horizontal propagation or vice-versa [Dahm, 2000, Watanabe et al., 2002, Maccaferri et al., 2014, Corbi et al., 2015, 2016]. Pre-existing fractures, intrusions and faults in the host rock may channelize the dikes into pre-weakened zones, cause their arrest or deviate their pathways [Ziv et al., 2000; Watanabe et al., 2002; Ito and Martel, 2002; Le Corvec et al., 2013, Maccaferri et al., 2016]. The magma influx rate from the magma reservoir has also been shown to provide a driving pressure for propagation [Rivalta, 2010; Taisne et al., 2011]. Magma cooling [Taisne and Tait, 2011] and volatile exsolution [Menand and Tait, 2001; Taisne and Jaupart, 2011] change the rheological proprieties of magma (i.e. density and viscosity) and modify the balance of pressure within the dike.

The relative weight of the potential contributions described above has never been investigated in detail. Numerical models of dike propagation are formulated in two dimensions so they cannot account for the influence of the third dimension that can affect dike propagation direction and stability [Rivalta et al., 2015, Townsend et al., 2017 and references therein].

In order to define a hierarchy between the various factors in 3D, we have conducted analogue modelling, injecting water (magma analogue) within gelatin (crust analogue). In particular, we have investigated the control on lateral vs. vertical dike propagation by the following factors: rigidity layering, density layering, density ratio between the host rock and magma analogue, the flow rate of the magma analogue, topography, and discussed our results based on scaling the experiments to nature.

2. Methods

2.1 Analogue models: experimental Set-up

We performed 32 analogue models, in a 33 × 58 × 38.5 cm^3 plexiglass box, by injecting dyed water in pig-skin gelatin as magma and crustal analogues respectively [Di Giuseppe et al., 2009] (Figure 1a). In 23 of these experiments, we created two layers of gelatin, pouring gently two solutions of different gelatin and/or NaCl concentration one on top of another while this was still at the liquid state. NaCl decreases gelatin rigidity and increases its density [Brizzi et al., 2016]. This process

generated a partial mixing of the two layers and, after cooling in the refrigerator, the formation of a ~4 cm thick non-sharp interface with a rigidity and density gradient. We refer to rigidity layering when the rigidity ratio between the upper and lower layer (E_u/E_l) is < or > 1 regardless of their densities and to density layering when $E_u/E_l \sim 1$ but the two layers show different densities.

To investigate the role of topography, we imposed a mold on the top of the gelatin surface, producing two inward dipping slopes separated by an 8 cm flat plain [Urbani et al., 2017]. The right and left flanks dip 2.4° and 3.7° respectively simulating the role of two oppositely dipping slopes on dike propagation. Hereafter we refer to "topography" models indicating experiments having this profile.

We finally injected dyed water (density ρ_f ranging from 993.6 kg m^{-3} to 1116.4 kg m^{-3}) alternatively from the bottom ("vertical injection" experiments, Set 1) or the side ("horizontal injection" experiments, Set 2) of the box using a peristaltic pump with an influx rate (Q) between 0.079 ml/s and 0.435 ml/s. In both Set 1 and Set 2 we inserted the needle tip parallel to the x-z plane (Figure 1a-c, Figure 2a-d and Figure 4a-d) to force the dike strike to be parallel to that plane at the onset of each experiment. If the dike strike turned out to be oblique to this plane, the value of the measured parameters (i.e. dike length and breadth as described in detail below) was corrected according to the angle calculated from the top view images (β in Table 2, spanning from 0° to 55°).

Gelatin temperature was kept at 9°C, water at 20°C. The thickness ratio between the upper and lower layer (T_u/T_l, where T_u and T_l are the thickness of the upper and lower layer respectively) ranges from 0.63 to 2.54 (Table 1). We monitored dike propagation alternatively in side and top view, at 0.05 and 0.1 frames per second.

We define a hierarchy among the investigated factors by quantifying how far the dikes propagate laterally in different conditions. With regard to Set 1 with flat topography, we measure the dike breadth of each experiment 3 cm above (b_2) and below (b_1) the center of the interface; this allows us to evaluate any change in the dike shape (Figure 1b). We define b_2/b_1 as the shape ratio of the dike. In the experiments of Set 1 with topography, we measured the maximum distance reached by the dike

along either side from the injection point (d_2 and d_1 in Figure 1c) defining d_2/d_1 as dike "asymmetry". With respect to the experiments with flat topography, we shifted the injection point 9 cm from the center to the right side, below the slope. This allows evaluating any dike propagation caused by the asymmetric topography. The horizontal distance between the eruption and injection points (X) has been also measured (Figure 1b-c).

In Set 2 we measured the dike length (S in figure 1c). Moreover, in order to compare the results from Set 1 and Set 2 for experiments with topography, we measured the horizontal distance between the dike tip and the edge of the plain (W in figure 1c). In this case, we considered the plain edge as a reference axis, thus negative values indicate that the dike tip propagated below the plain (Table 2). Finally, in both Set 1 and Set 2 we measured the dike aspect ratio (Breadth/Height, B/H). Table 1 shows the imposed parameters in each experiment. Figures from S1 to S8 in the supporting information show experiments not presented extensively in the main text and/or excluded from the dataset since they replicate experiments already presented.

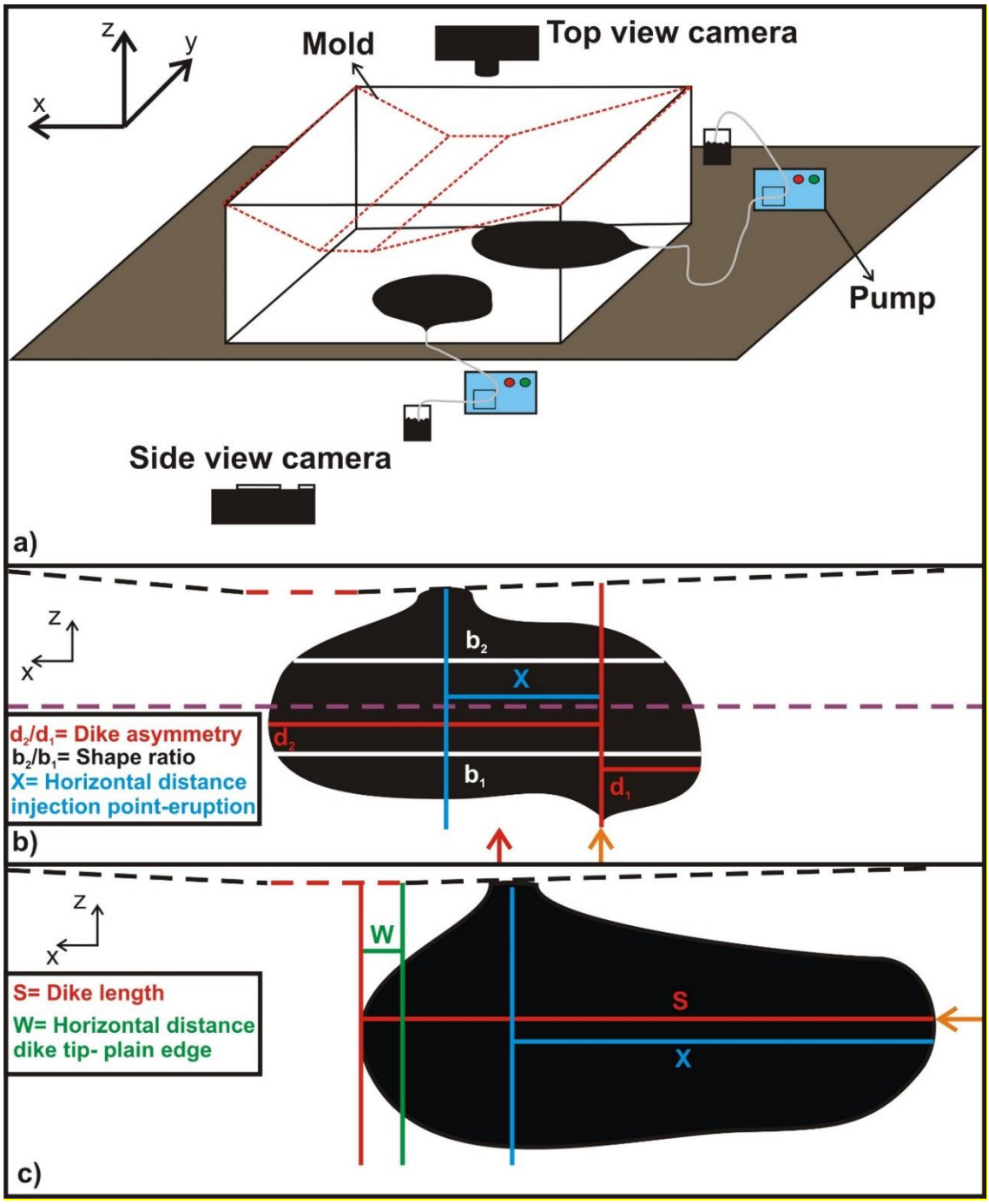

Figure 1. a) Sketch of the experimental set-up. The reference system in the top left refers to the box sides. The red dashed lines in the box represent the topography used in some experiments, while the two black bubbles represent Set 1 and Set 2 experiments where injection was performed from the bottom or the side of the box, respectively. b) Diagram illustrating how the measurements of b_1, b_2, d_1, d_2 and X were carried out for Set 1 experiments (see text for details). The red and orange arrows indicate the injection point with flat and shaped topography, respectively. The dashed black and red lines indicate the slopes and the plain, respectively. c) Measurement procedure for S, W and X, Set 2. The orange arrow indicates the injection point.

Exp	ρ_L (kg/m^3)	ρ_U (kg/m^3)	ρ_f (kg/m^3)	E_l (kPa)	E_U (kPa)	T_l (cm)	T_U (cm)	T_U/T_l	Q (ml/s)
2	1123.2	1018.1	1094.4	1.8	3.3	9.8	7.7	0.79	0.079
5	1053.6	1018.1	1053.6	2.5	3.3	9.1	9.4	1.03	0.079
6	1123.2	1018.1	1073.8	1.8	3.3	8.7	9.5	1.09	0.079
8	1071.3	1018.1	1116.4	3.5	3.3	10.1	7.3	0.72	0.079
10	1071.3	1018.1	993.6	3.5	3.3	10.1	6.6	0.65	0.079
11	1071.3	1018.1	1053.6	3.5	3.3	9.3	8.4	0.90	0.079
12	1071.3	1018.1	993.6	3.5	3.3	8.9	8.1	0.91	0.435
13	1053.6	1018.1	1053.6	2.5	3.3	10	7.1	0.71	0.435
17	/	1018.1	1116.4	/	3.3	/	/	/	0.079
19	/	1018.1	993.6	/	3.3	/	/	/	0.079
20b	/	1018.1	1116.4	/	3.3	/	/	/	0.435
21	1071.3	1018.1	993.6	3.5	3.3	10	8.5	0.85	0.079
23	1053.6	1018.1	1053.6	2.5	3.3	10.5	6.6	0.63	0.079
24	/	1018.1	1053.6	/	3.3	/	/	/	0.079
26	1069.3	1018.1	1053.6	7	3.3	10.3	7.5	0.73	0.079
27	/	1018.1	993.6	/	3.3	/	/	/	0.079
28	1123.2	1018.1	1073.8	1.8	3.3	9.5	8.6	0.91	0.079
29	/	1018.1	1116.4	/	3.3	/	/	/	0.079
30	/	1088	1008.8	/	3.3	/	/	/	0.079
32	1053.6	1018.1	1053.6	2.5	3.3	10.3	8.2	0.80	0.079
33	1071.3	1018.1	1053.6	3.5	3.3	10	7.5	0.75	0.079
33b	1071.3	1018.1	1116.4	3.5	3.3	10	7.5	0.75	0.079
34	1071.3	1018.1	1053.6	3.5	3.3	10	8.2	0.82	0.079
36	1053.6	1018.1	1053.6	2.5	3.3	/	/	/	0.079
39	/	1018.1	1116.4	/	3.3	/	/	/	0.435
51	1053.6	1018.1	1053.6	2.5	3.3	9.5	7.9	0.83	0.079
51b	1053.6	1018.1	1053.6	2.5	3.3	9.5	7.9	0.83	0.435
52	1071.3	1018.1	993.6	3.5	3.3	9.8	7.5	0.77	0.079
52b	1071.3	1018.1	993.6	3.5	3.3	9.8	7.5	0.77	0.435
53	1071.3	1018.1	993.6	3.5	3.3	9.8	9.7	0.99	0.079
57	/	1018.1	993.6	/	3.3	/	/	/	0.079
60	1010	1003	993.6	13	2.5	10	6.6	0.66	0.079
61	1071.3	1018.1	1053.6	3.5	3.3	6.1	15.5	2.54	0.079

Table 1. List of the imposed parameters in each experiment. ρ_U= upper layer density; ρ_L= lower layer density; ρ_f= water density; E_l= lower layer rigidity; E_u= upper layer rigidity; T_l= lower layer thickness; T_u= upper layer thickness; Q= flow rate.

2.2 Scaling

We scaled our models according to [Urbani et al., 2017] and [Kavanagh et al., 2013]. The scale parameters calculated in [Urbani et al., 2017] are listed in Table S1. Here we additionally describe the scaling calculation of the thickness of the experimental dikes according to equation 4 in [Rivalta et al., 2015] as follows:

$$H(z) = (1-\nu) \times \frac{Kc}{2\mu} \times \sqrt{\frac{a}{\pi}} \times \sqrt{[1-\left(\frac{z}{a}\right)^2 \times \left(1+\frac{z}{a}\right)]} \quad (1)$$

Where H(z) is the dike thickness, ν is the Poisson's ratio, K_c is the fracture toughness, μ is the shear modulus, z is the vertical coordinate and a is the half height of the dike. Therefore if we set the following values:

z= 0 (at the dike center)

a^*= 2 × 10-6 (with a= 7.3 cm and 3.6 km in models and nature, respectively)

K_c^*= 8.3 × 10^{-8}

μ^*= 3.89 × 10^{-8} (1.17×10^3 Pa in the models and 0.3×10^{11} Pa for basalts [Turcotte and Schubert, 2002], respectively)

$(1-\nu)^*$= 0.67 (with ν= 0.5 for pig-skin gelatin and 0.25 in nature, respectively)

We obtain:

$H(z)^*$= 0.57 × 10^{-3}

Thus, a typical thickness of 1 mm in our models corresponds to ~ 2 meters in nature, which matches with the order of magnitude of geodetically determined dike openings.

2.3 Experimental limitations

In our experiments, we neglect the contribution of regional stresses (both compressional and extensional) on dike propagation, which has been addressed by Menand et al. [2010] and Daniels and Menand [2015]. In nature, a crust with layered rocks (i.e. with different rigidity) can store different

amounts of stresses thus, for example, a weak upper layer may arrest dike ascent transferring low amounts of the dike tip tensile stresses [Gudmundsson, 2003].

Another limitation of the experimental set-up is the finite size of the gelatin layers (both horizontally and vertically) and the rigidity of the plexiglass box. Indeed, the rigid box sides force an upward propagation even in case of negative buoyancy (experiment 8). However, the rigid box does not affect the stress field induced by the imposed topography (i.e. σ_3 is subhorizontal beneath the slopes and subvertical beneath the plain) [Urbani et al., 2017].

A second factor, discussed in detail in Corbi et al. [2016], is the "gravitationally loaded" state of stress of the gelatin in the models with topography. Such "gravitationally loaded" state of stress arises from the relaxation of the gelatin mass under its own weight when the mold is removed. This may not correspond to the state of stress of volcanoes and rifts in nature, due to the layer-by-layer way volcanic topography develops, and to the many processes acting on volcanoes and rifts that tend to homogenize the state of stress (seismicity, viscoelasticity, plasticity, repeating dike intrusions) [Chadwick and Dieterich, 1995; Corbi et al., 2016].

Moreover, several simplifications were made in the experiments presented in this study. First, we assume isothermal state, neglecting solidification effects that may influence magma ascent. This aspect has been studied by Taisne and Tait [2011] and Chanceaux and Menand [2014, 2016].

Second, we injected water without gas thus neglecting magma expansion due to volatile exsolution that may markedly affects dike behavior [Taisne and Jaupart, 2011].

Third, we assume unlimited magma availability considering a continuous magma input inside the dike. In nature, inflow from the magma chamber into the dike decreases with time changing the ratio between fracture and viscous pressure.

Finally, we neglect viscosity changes due to the presence of crystals in magma. This last assumption is not excessively restrictive for mafic lateral dike intrusions recently observed in nature.

3. Results

3.1 Shape variation of dikes

3.1.1 Set 1 (injection from the bottom)

Here we describe six representative experiments of Set 1 starting with two experiments with flat topography and rigidity or density layering (experiments 5 and 11 respectively; Figure 2a-b), before comparing them with two similar experiments (i.e. showing rigidity and density layering) with topography (experiments 23 and 24 respectively; Figure 2c-d and Table 1). We also describe two experiments with rigidity layering but with a soft layer overlying the stiff layer (i.e. $E_u/E_l < 1$, experiments 26 and 60). For each experiment type, we evaluate any change of dike shape (b_2/b_1, d_2/d_1, X) induced by the presence of layering and a slope. Table 2 lists the measured parameters in each experiment.

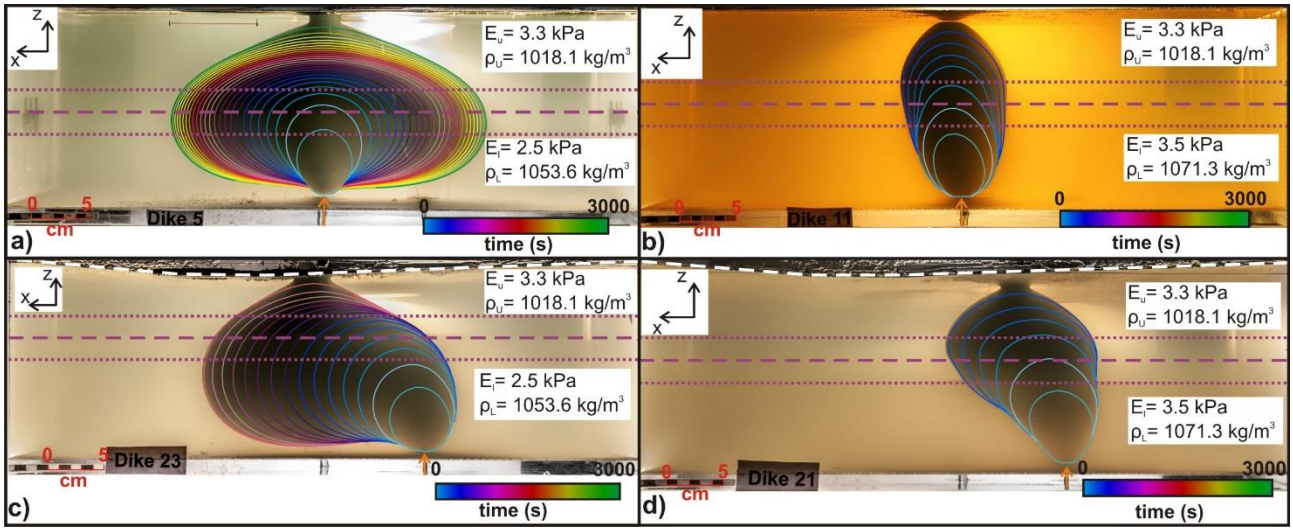

Figure 2. Set 1 experiments showing flat topography, rigidity (a, experiment 5) and density layering (b, experiment 11). Experiments with topography, rigidity (c, experiment 23) and density layering (d, experiment 21). The dashed purple and white lines indicate the interface center and the topography profile respectively. The dotted purple lines indicate the limits of the interface. The reference system in the top left refers to the box sides and figure 1a. The orange arrows indicate the injection points. The colored lines indicate the dike edge contour every 120 seconds.

Exp	ρ_U/ρ_f	E_u/E_l	β	b_2/b_1	d_2/d_1	B/H	X (cm)	S (cm)	W (cm)	Figure
2	0.9303	1.83	52°	0	/	2.73	/	/	/	/
5	0.9663	1.32	17°	0.91	/	1.62	/	/	/	2a
6	0.9481	1.83	27°	0	/	3.20	/	/	/	S4a
8	0.9119	0.94	20°	0.83	/	0.88	/	/	/	S4b
10	1.0247	0.94	16°	1.04	/	0.72	/	/	/	S4c
11	0.9663	0.94	43°	0.86	/	0.79	/	/	/	2b
12	1.0247	0.94	0°	0.86	/	0.72	/	/	/	S7a
13	0.9663	1.32	55°	0.66	/	1.33	/	/	/	S7b
17	0.9119	/	30°	/	2.2	1.45	4.7	/	-4.6	S2a
19	1.0247	/	32°	/	1.93	0.78	0	/	5.2	S2b
20b	0.9119	/	0°	/	1.79	1.78	/	/	-4.3	S2d
21	1.0247	0.94	0°	1.66	4.3	0.78	3.1	/	3.9	2d
23	0.9663	1.32	20°	0.63	6.48	1.25	9	/	-5.3	2c
24	0.9663	/	23°	/	2.31	1.07	5.7	/	-2.6	S2c
26	0.9663	0.47	41°	1.14	/	0.53	/	/	/	S1a
27	1.0247	/	0°	/	/	0.83	5.9	11.7	/	4a
28	0.9481	1.83	10°	0	/	9.27	/	53.3	/	/
29	0.9119	/	15°	/	/	0.86	/	9	21.5	4c
30	1	/	0°	/	/	1.13	9.5	16.6	14.6	4b
32	0.9663	1.32	18°	/	/	2.32	22.8	33.8	-3.3	S6d
33	0.9663	0.94	5°	1.45	/	0.81	4.2	8.5	/	S6a
33b	0.9119	0.94	6°	1.73	/	0.78	4.3	8.4	/	/
34	0.9663	0.94	17°	1.52	/	0.85	4.8	9.1	20.7	S6c
36	0.9663	1.32	26°	/	/	1.75	20.1	28.7	2.5	4d and S3a
39	0.9119	/	19°	/	/	1.06	/	12.4	17.5	S5a
51	0.9663	1.32	0°	/	/	1.45	11	21.3	/	S6b
51b	0.9663	1.32	30°	/	/	1.39	11.3	22	/	/
52	1.0247	0.94	11°	/	/	0.94	4.6	9.3	/	S5b
52b	1.0247	0.94	0°	/	/	0.86	3.9	8.9	/	S5b
53	1.0247	0.94	10°	/	/	0.93	5.7	10.4	23.5	S5c
57	1.0247	/	20°	/	/	0.99	/	/	/	S4d
60	1.0095	0.19	0°	0.78	/	0.60	/	/	/	S1b
61	0.9663	0.94	15°	1.18	/	1	/	/	/	S8

Table 2. List of the measurements for each experiment. ρ_U/ρ_f= density ratio; E_u/E_l= rigidity ratio; β= angle between dike strike and x-z plane; b_2/b_1= shape ratio; d_2/d_1= dike asymmetry; B/H= Dike aspect ratio (Breadth/Height) X= horizontal distance between the eruption and injection points; S= dike length; W= horizontal distance dike tip-plain edge. The experiments with topography are highlighted in bold.

We find that increasing the rigidity ratio from 0.47 to 1.83 leads to a strong decrease of the shape ratio (from 1.14 to 0; Figure 3a). Experiment 60 (E_u/E_l= 0.19) does not fit with this trend, as the dike was wider in the lower layer (b_2/b_1= 0.78, Figure S1b) because of the dike tip narrowing at the interface.

In contrast, keeping constant the rigidity ratio (E_u/E_l= 0.94) and increasing ρ_U/ρ_f (hereafter called density ratio) from 0.91 to 1.02 results in a lower variability: b_2/b_1 ranges from 0.83 to 1.04 (experiments 10, 11 and 8 in Figure 3b).

Increasing the flow rate (from 0.079 ml/s to 0.435 ml/s, see experiment 12 to be compared with experiment 10) when keeping layer thicknesses, density and rigidity ratio unchanged, results in relatively small shape variations so that $\Delta(b_2/b_1)$= 0.18. Conversely, with different layer thicknesses (T_u/T_l= 1.03 and 0.71 in experiments 5 and 13, respectively), the shape variation with an increasing flow rate is higher (from 0.91 in experiment 5 to 0.66 in experiment 13). Therefore, the calculation of b_2/b_1 is affected by the height of the interface (thus by the thickness of the upper and lower layer).

Both density (E_u/E_l= 0.94) and rigidity layering (E_u/E_l= 1.32), keeping density ratio constant, enhance dike asymmetry due to topography (d_2/d_1 ranges from 1.93 and 2.31 to 4.3 and 6.28 in experiments 19, 24, 21 and 23, respectively, Figure 3c); this effect is stronger in the case of rigidity layering (highest asymmetry value in experiment 23 than 21, as shown in figure 3d). On the contrary, only density ratio variations (from 0.91 to 1.02) without any layering have little influence on dike asymmetry, as suggested by the slight variation of d_2/d_1 of experiments 17, 19 and 24 (from 1.93 to 2.31, Figure 3c and Figure S2a-c).

Layering also promotes eruption at larger distance from the injection point (X ranging from 5.7 to 9 cm in experiments 24 and 23 respectively and from 0 to 3.1 cm in experiments 19 and 21 respectively, Figure 3c). The largest distance was observed for E_u/E_l= 1.32 which is the higher rigidity ratio value in the experiments with topography (experiment 23 in figure 3d). In contrast, the density ratio increase in experiments without layering (17, 19 and 24) does not promote a more distant eruption (X = 4.7 cm, 0 cm and 5.7 cm respectively; Figure 3c). Finally, the increased flow rate

(experiment 20b, d_2/d_1= 1.8, Figure S2d) slightly inhibits propagation towards the plain (experiment 17, d_2/d_1= 2.2, figure 3c).

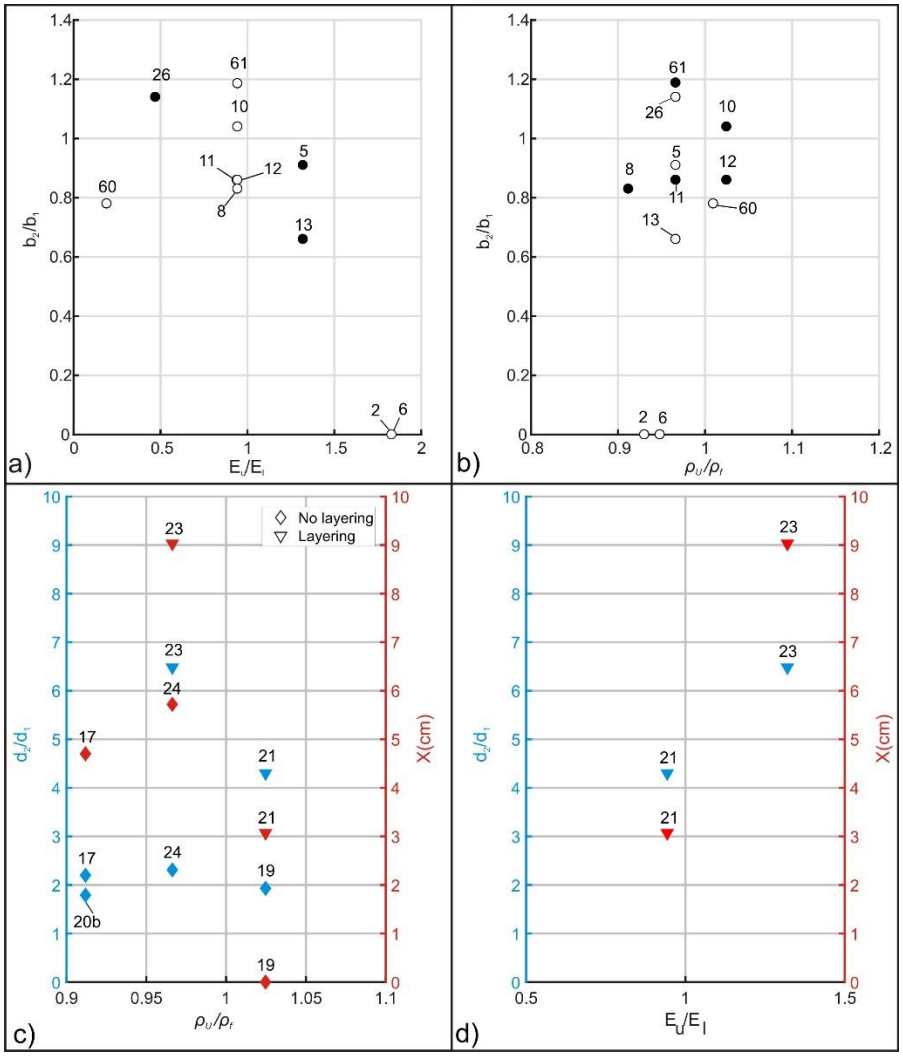

Figure 3. a) Shape ratio (b_2/b_1) vs rigidity ratio (E_u/E_l). b) b_2/b_1 vs. density ratio (ρ_U/ρ_f). Black circles in a) and b) indicate experiments in which the only changing parameter is E_u/E_l and ρ_U/ρ_f, respectively (except for experiments 12 and 13, where also the flow rate changes); the white circles indicate the experiments in which both E_u/E_l and ρ_U/ρ_f change. c) Density ratio (ρ_U/ρ_f) against dike "asymmetry" (d_2/d_1, blue) and X (red). In X vs ρ_U/ρ_f experiment 20b because the dike did not erupt. The blue and red diamonds in c) indicate the experiments in which the only changing parameter is ρ_U/ρ_f (except experiment 20b in which also the flow rate changes). d) E_u/E_l against d_2/d_1 (blue) and X (red). The numbers above each point indicate the experiment number.

3.1.2 Set 2 (injection from the side)

In Set 2 experiments we obtained similar results of Set 1 (i.e. lateral and vertical propagation with rigidity and density layering respectively) except for the effect of flow rate that slightly promotes lateral propagation if combined with topography.

Here we show four representative experiments of Set 2, described in the following order: two experiments showing homogenous gelatin both with and without topography (experiments 27 and 30 respectively; Figure 4a-b); one experiment with homogeneous gelatin, topography and $\rho_U/\rho_f < 1$ (experiment 29; Figure 4c); one experiment with rigidity layering and topography (experiment 36; figure 4d). For each experiment type, we calculate the variations of dike shape (S, W, X) due to the imposed parameters.

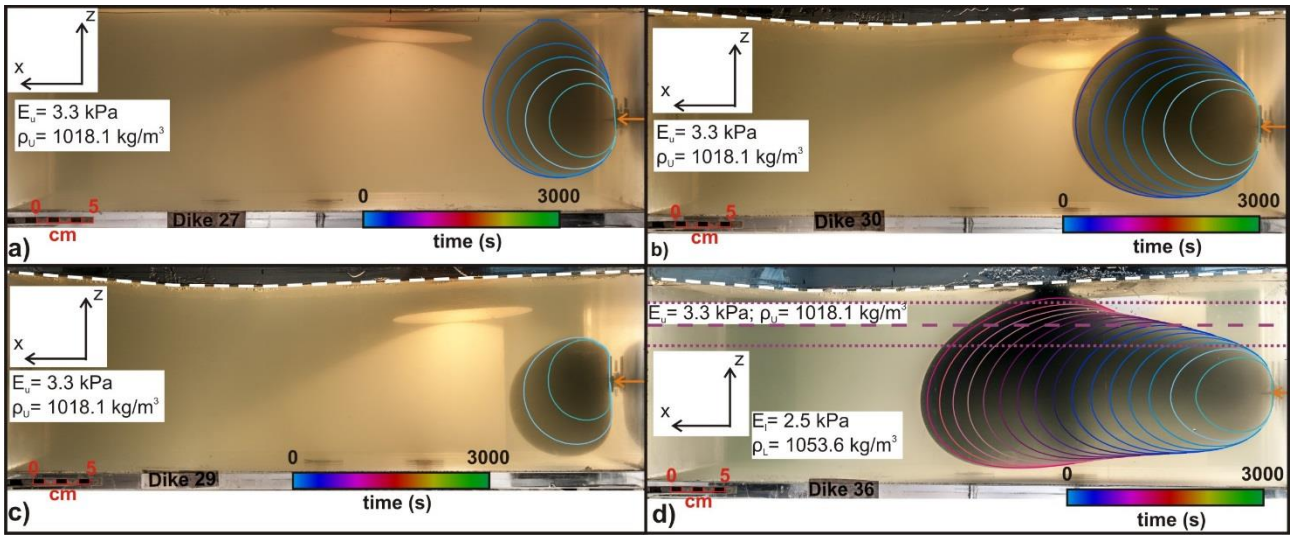

Figure 4. Set 2 experiments showing homogeneous gelatin without (a, experiment 27) and with topography (b, experiment 30). c) Experiment 29 showing topography and negative buoyancy (i.e. density ratio < 1). Experiment 36 showing topography and rigidity layering. The dashed white lines indicate the topography profile. The dashed and dotted purple lines in d) indicate the center and the limits of the interface, respectively. The orange arrows indicate the injection points. The colored lines indicate the dike edge contour every 120 seconds.

Similarly to Set 1, we observed that:

1) A rigid upper layer promotes lateral propagation since the increasing rigidity ratio (from 0.94 to 1.83, Figure 5a), leads to a high increase of S (from 8.4 cm to 53.3 cm).

2) Density ratio variations, with constant E_u/E_l= 0.94, is less effective on lateral propagation leading to very similar values of S and X in experiments 33, 33b and 52 (S equal to 8.5 cm, 8.4 cm, 9.3 cm and X equal to 4.2 cm, 4.3 cm, 4.6 cm respectively, figure 5b and 5d).

3) The increase in flow rate does not affect significantly dike propagation (compare experiments 51 and 52 with 51b and 52b in figure 5a-b), being the difference between the maximum and minimum values of S (henceforth called ΔS) 0.4 cm and 0.6 cm, respectively and X very similar (see table 2 and figure 5d).

However, contrary to Set 1, the increased flow rate favors lateral propagation if combined with topography as the dike length increases from 9 cm in experiment 29 (Q= 0.079 ml/s) to 12.4 cm in experiment 39 (Q= 0.435 ml/s , figure 6b and figure S5a).

Indeed, the imposed topography favors lateral propagation of the dike, as both S and X increase from 11.7 and 5.9 cm (in experiment 27 with no layering and flat topography) to 16.6 and 9.5 cm respectively in experiment 30 (no layering with topography, Figure 5b and figure 5d). Moreover, increasing the density ratio with topography favors lateral propagation, being S equal to 9 cm and 16.6 cm in experiments 29 and 30 respectively (Figure 5b, Table 2 and figure 4b-c).

Decreasing the thickness ratio (T_u/T_l) between the two layers disadvantages lateral propagation, since it decreases the dike length in experiment 36 with respect to 32 (S equal to 28.7 cm and 33.8 cm respectively, figure 5a-b). With vertical injection (Set 1) and topography, decreasing the density ratio (with no layering) promotes lateral propagation towards the plain (W = -4.6 cm, 5.2 cm and -2.6 cm in experiments 17, 19 and 24 respectively, Figure 5c).

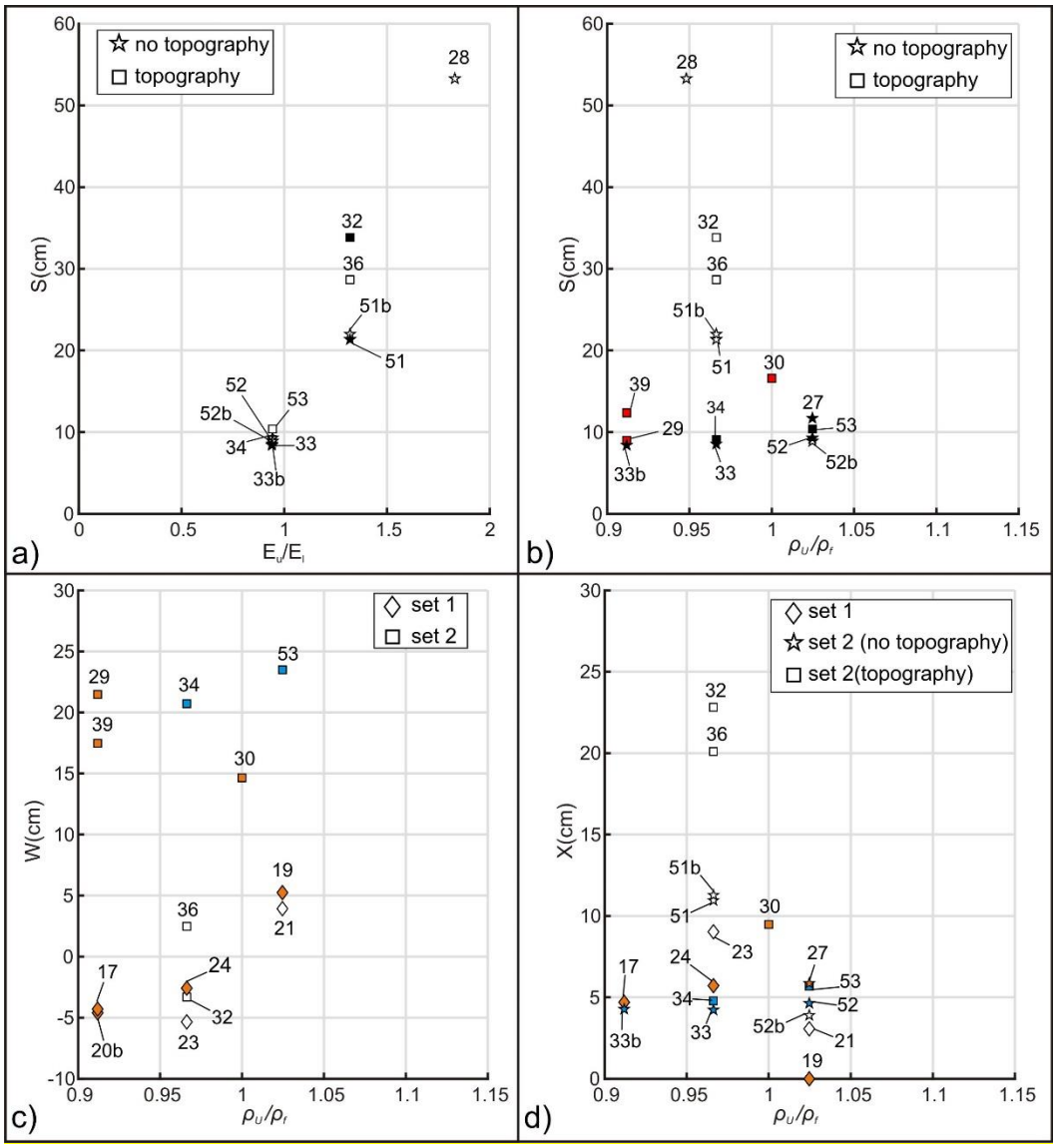

Figure 5. a) S vs. E_u/E_l. b) S vs. ρ_U/ρ_f. The squares and the stars indicate the experiments with and without topography, respectively. Experiments 29, 30 and 39 are excluded in a) as without any layering. The numbers above each point indicate the experiment number. The black and red symbols in a) and b) indicate the experiments in which the only changing parameter is E_u/E_l and ρ_U/ρ_f respectively. The red symbols in b) indicate also the experiments with homogeneous gelatin (no layering). c) W vs. ρ_U/ρ_f of Set 1 (diamonds) and Set 2 experiments (squares). The negative values of W indicate that the dike tip passed below the plain edge. Experiments 28, 33 and 33 b are excluded, as without topography. d) X vs. ρ_U/ρ_f of Set 1 (diamonds) and Set 2 experiments (with and without topography, stars and squares respectively). Experiments 20b, 28, 29 and 39 are excluded because the dike did not erupt. In both c) and d) the blue and orange symbols indicate the experiments whose only changing parameter is ρ_U/ρ_f. The orange symbols indicate also the experiments with homogeneous gelatin (no layering).

3.2 Velocity variations

Both the horizontal (v_h) and vertical (v_v) velocities decrease rapidly with time (except for experiments 26 and 60) because a constant flux of water is injected into a crack with an increasing area (figure 6a-b). In experiment 26 v_h increases in the first 30 seconds, while in experiment 60 v_v increases abruptly when the dike reached the interface with the softer upper layer.

$\langle v_v \rangle$ (v_v averaged in 30s long intervals) ranges from 0.17 mm/s (experiment 32) to 0.61 mm/s (experiment 33b). $\langle v_h \rangle$ ranges from 0.17 mm/s (experiment 11) to 0.60 mm/s (experiment 60), thus the smaller dikes (i.e. with less surface) propagate faster vertically.

Vertically propagating dikes ($B/H < 1$) developed with density layering (experiments,11, 21, 33, 33b and 34), regardless of the position of the injection point and the presence or absence of topography, and in case of rigidity layering with $E_u/E_l < 1$ (experiments 26 and 60, Figure 7).

Lateral propagating dikes ($B/H > 1$) occur only in case of rigidity layering with $E_u/E_l > 1$ (experiments 5, 6, 23, 32 and 51, except for experiment 24 without layering), both with and without topography and vertical or lateral injection (Figure 7).

Concentrically expanding dikes (mean $B/H \sim 1$ i.e. comprised between 0.9 and 1.1) occur in case of density layering and strong anti-buoyancy (experiment 8) and with homogeneous gelatin (i.e. no layering), both with (experiments 19 and 30) and without topography (experiments 27 and 57).

Vertical dikes show a first stage of favored vertical propagation (B/H decrease), followed by a second stage in which lateral propagation is promoted (B/H increase, except experiment 19). In particular, the smaller dikes (i.e. with less surface, experiments 33, 33b and 34) show that the lateral propagation becomes dominant after dike penetration in the upper layer (90-150 s), and not upon the dike arrival at the density interface (approximately 40 s).

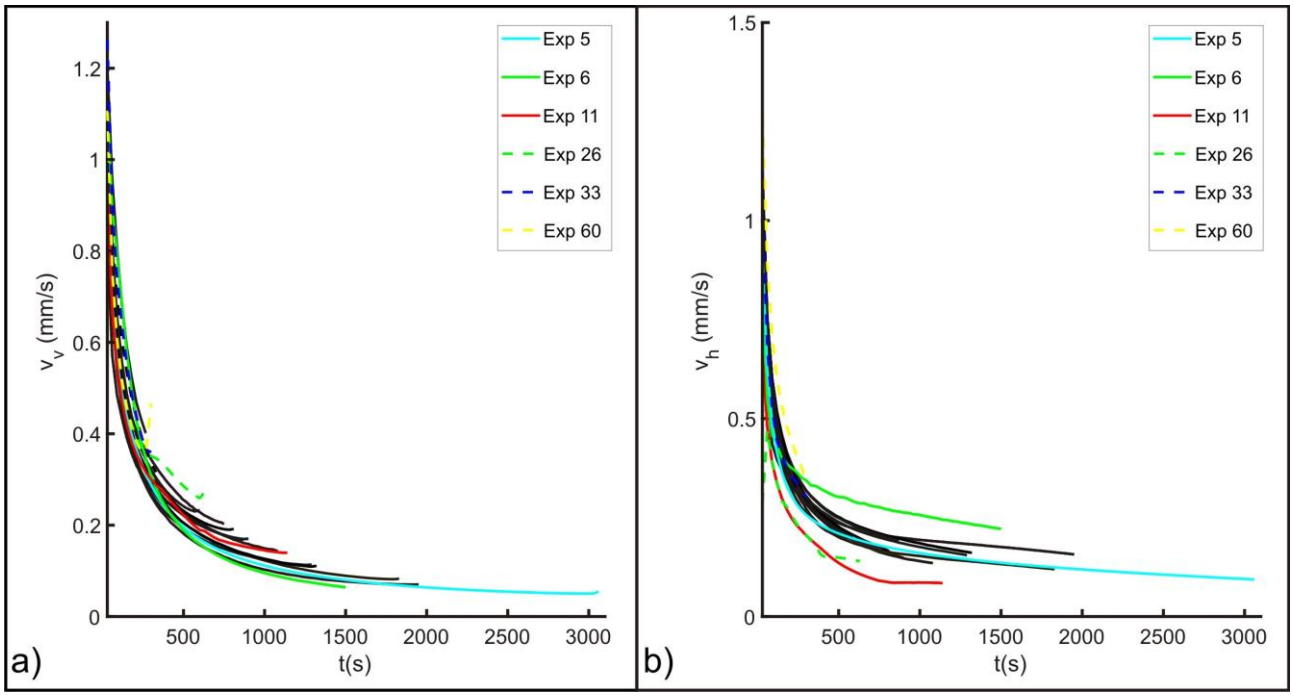

Figure 6. a) Vertical dike velocity (v_v) vs. time. b) Horizontal dike velocity (v_h) vs. time. Only the most representative experiments (5, 6, 11, 26, 33, 60) are highlighted in color otherwise they are in black.

V_h shows higher variations than v_v because the lateral velocity is more sensitive to the studied factors (i.e. gelatin layering and topography). Moreover, the vertical velocity is strongly influenced by the dike height, meaning that shorter dikes are faster than taller ones. As an example experiments 11 (only density layering) and 6 (rigidity layering), which represent two end members of vertical and lateral propagation respectively, show highly different v_h (0.30 mm/s in experiment 6 compared to 0.17 mm/s in experiment 11) despite a lower difference of v_v (0.22 mm/s in experiment 6 and 0.26 mm/s in experiment 11). This happens because in experiment 6 the dike propagates only in the lower layer (spreading laterally at the interface) being shorter than experiment 11 (which reaches the surface) so v_v in experiment 6 is only apparently close to that of experiment 11.

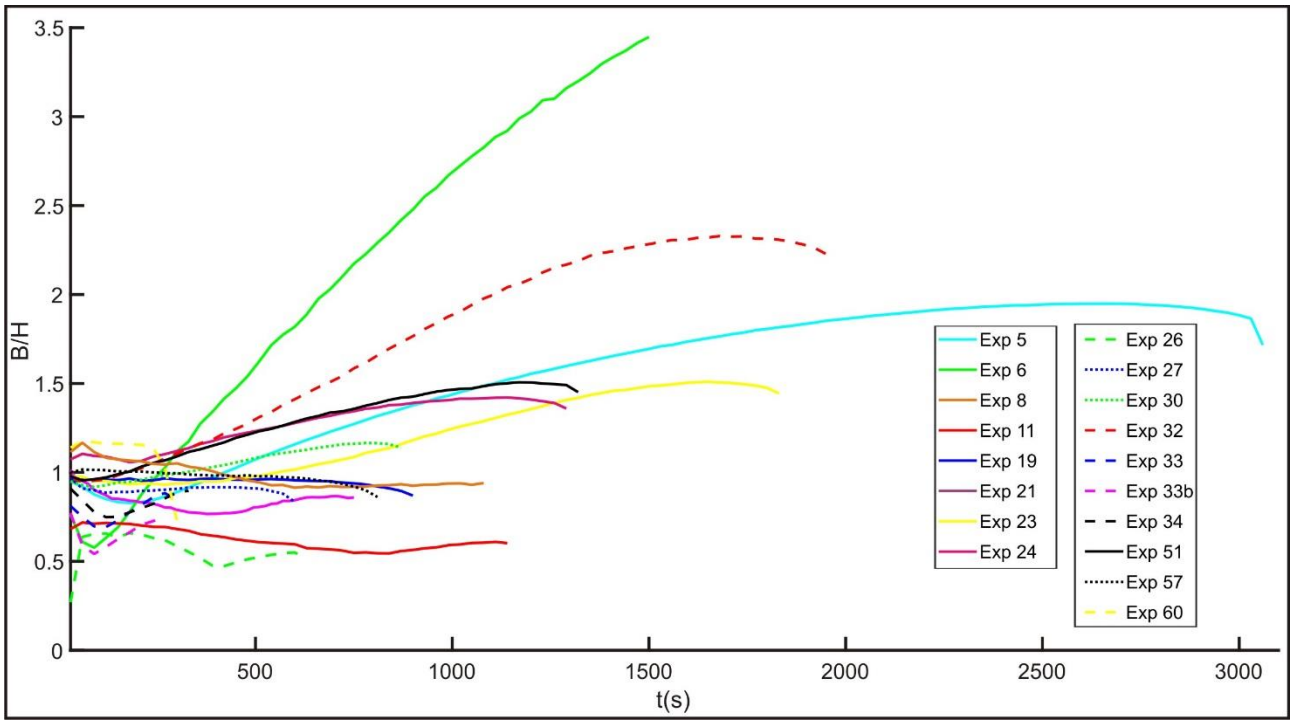

Figure 7. Dike aspect ratio (B/H) vs. time.

In experiments 11 and 21, B/H decreases both in the lower and upper layer then showing an increase due to different causes: in experiment 21 the B/H increase (at t= 400 s) is due to the dike deflection caused by topography, whereas in experiment 11 (at t= 900 s) it is probably due to the effect of the free-surface [Rivalta and Dahm, 2006]. Moreover, the switch between the decrease and the increase of B/H in experiments 11 and 21 is less abrupt than experiments 33, 33b and 34.

Laterally propagating dikes tend to first elongate (increase of the aspect ratio) and then to expand vertically before erupting (except for experiments 6 and 24). Experiments 23, 32 and 51 follow this trend, due to the rigidity layering (with $E_u/E_l > 1$). Otherwise, in experiment 5 the B/H increases in two different stages of dike propagation: 1) the initial water injection in the lower layer; 2) the dike arrival at the interface (350 s, rigidity layering). However, in both the lower and the upper layers the dike shows a similar (and constant) aspect ratio increase rate.

Experiments 6 and 24 show two stages of favored vertical and lateral propagation similarly to the vertical propagating dikes. In particular, experiment 24 isolates the effect of topography (favoring lateral propagation) on dike kinematics: B/H increases after an initial stage of favored vertical propagation but, because there is no layering, the aspect ratio increase is due only to the effect of

topography (which promotes downslope propagation of the dike). In experiment 6, the high B/H decrease is due to the strong positive buoyancy in the lower layer that favors vertical propagation. The abrupt switch to the high B/H increase (t= 90 s) is due to dike approaching the interface with $E_u/E_l = 1.83$.

In experiments with $E_u/E_l < 1$ the interface with the softer layer leads to an abrupt vertical acceleration of the dike. In particular, experiments 26 and 60 show a different trend with respect to the other experiments: in experiment 26 ($E_u/E_l = 0.47$), the aspect ratio is almost constant with time (except for an abrupt increase in the first 60 seconds), showing a slight decrease as the dike approaches the interface (from 60 s to 400 s) and a slight increase as the dike approaches the surface propagating in the upper layer (from 400 s to 630 s). In experiment 60, ($E_u/E_l = 0.19$) the aspect ratio was nearly constant as the dike propagated in the lower layer (until 240 s), then it accelerated vertically (abrupt B/H decrease) as it penetrated the interface with the softer upper layer.

4. Discussion

4.1 Interpretation of the experiments

Our results show that, both in Set 1 and 2, lateral dike propagation is promoted most efficiently in case in case of rigidity layering (with $E_u/E_l > 1$) with respect to density layering and density ratio. This is supported, in set 1, by the large shape variations that occurred by increasing the rigidity ratio whereas in case of density layering and density ratio changes, the shape variability is quite small ($\Delta b_2/b_1 = 0.21$), as most dikes were vertical. In Set 2, experiments with higher rigidity ratio results in longer dikes (up to 53.3 cm), whereas the dike length variations are small in case of density layering (ΔS ranging from 0.9 cm to 1.3 cm, figure 5a-b).

Concerning the effect of topography, in Set 1 all the dikes were elongated towards the plain and in Set 2 lateral propagation is promoted. This is due to the stress component normal to the dike plane (i.e. σ_2, see Urbani et al., [2017]) that decreases downslope, squeezing the dike towards the plain, and increases upslope, hindering further dike propagation as explained in detail in [Urbani et al., 2017].

In order to understand the different behavior of the flow rate combined with topography between Set 1 and Set 2, it is crucial to take into account for the different implications exerted by the position of the injection point. As a matter of fact, experiments 17, 20b, 29 and 39 show a negative buoyancy which drives the dike downward, but only in set 2 with topography (experiments 29 and 39) the dike is free to propagate in that direction (because of the lateral injection), whereas in set 1 (experiments 17 and 20b) the floor of the box prevents any negative buoyant dike propagating downward. Therefore, in case of flow rate variation, if lateral injection (in set 2 with topography) promotes lateral propagation (higher W and lower S in experiment 29 than 39, figure 5c) bottom injection does not.

The analysis of the kinematics of the dikes suggests that rigidity layering favors lateral dike velocity (and thus propagation) and highlights the less effective role of the density layering ($B/H > 1$ in experiments 5, 6, 23, 32 and 51 and $B/H < 1$ in experiments 11, 21, 33, 33b, 34; figure 7). This is similar to what observed in the geometrical analysis. In particular, the abrupt deceleration of the vertical velocity as the dike approaches a stiffer upper layer (experiment 6 in figure 7), suggesting that the vertical propagation is inhibited, is consistent with previous results [Rivalta et al., 2005; Kavanagh et al., 2006; Ritter et al., 2013, Urbani et al., 2017]. Conversely, as the dike approaches a softer upper layer (as in exp 60), the dike tip finds less resistance, accelerating abruptly, consistently with Rivalta et al. [2005].

Moreover, the slight decrease of B/H close to the surface (see the final stages of experiments 19, 23, 24, 32 and 51 in figure 7) is consistent with an increasing vertical velocity when the dike approaches the free surface, since it experiences less resistance, as previously noted by [Rivalta and Dahm, 2006]. It is interesting to note that [Rivalta and Dahm, 2006] used different conditions with respect to this study, by injecting air with constant volume in gelatin. This suggests that this acceleration towards the surface, showing a common behavior in different experimental sets, is not influenced by the modelling assumptions.

The role of density ratio is more complex, because experiments 19 and 24 (which differ only in terms of density ratio; Table 1 and Figure 3c) show a different evolution of the aspect ratio (Figure 7), despite their comparable final shape (see d_2/d_1 values in Figure 3c and Table 1). In experiment 19 B/H is close to 1 and approximately constant throughout the experiment, whereas in experiment 24 B/H increases with time, after an initial decrease, until reaching 1 (Figure 7 and table 1). Moreover, a comparison between experiments 33 and 33b shows that the lower is the density ratio (i.e. higher ρ_f in experiment 33b), the faster is the propagating dike (Figure 7) despite the comparable length (S in figure 5a-b and table 1). Therefore, the density ratio variations show a higher influence of the dike kinematics (i.e. the dike shape evolution with time) with respect to their geometry (i.e. the dike final shape), suggesting that any hierarchy based on the dike shape may be revisited if based on dike velocity.

The kinematic analysis showed that in none of the studied experiments the dike propagated following a steady state regime, as it is in case of injection in a homogenous medium [Takada, 1990; Menand and Tait, 2002]. The exception of experiment 19 (approximately constant B/H throughout the entire experiment) is probably related to: 1) the combined effect of the chosen topography profile and density ratio, which is almost 1 ($\rho_U/\rho_f = 1.0247$), that did not influence the dike kinematics but only its final shape; 2) the propagation of an isolated crack (with constant and finite volume) in both Takada, [1990] and Menand and Tait, [2002] conversely to our propagation of a crack continuously fed with water by the pump (thus with increasing volume throughout the entire experiment).

This suggest that to reach the vertical equilibrium, the dike must penetrate the low-density layer before starting to propagate laterally (experiments 33, 33b, 34 and 61), as pointed out by previous analytical and numerical models [Lister, 1990; Taisne and Jaupart, 2009].

4.2 Hierarchy of parameters controlling lateral and vertical propagation

Our results suggest a hierarchy between the investigated factors (rigidity and density layering, density ratio, flow rate, topography) based on the variations of the aspect ratio, Δ(B/H), of selected

pairs of experimental dikes (Figure 8) showing only one variable between E_u/E_l, ρ_U/ρ_f, Q and topography.

Only in case of Set 1 and topography the indicated value is calculated from the dike asymmetry variation, $\Delta(d_2/d_1)$ (right y-axis in figure 8), instead of the aspect ratio.

Considering this, the hierarchy is defined as follows:

Set 1 (Vertical injection)

1) Rigidity layering, Δ (B/H) = 2.41 (experiments 6 and 57);

2) Topography Δ (d_2/d_1) = 0.94 (experiments 19 and 57);

3) Density ratio Δ (B/H) = 0.16 (experiments 8 and 10);

4) Density layering Δ (B/H) = 0.07 (experiments 10 and 57);

5) Flow rate Δ (B/H) = 0 (experiments 10 and 12);

Set 2 (Lateral injection)

1) Rigidity layering Δ (B/H) = 8.44 (experiments 27 and 28);

2) Topography Δ (B/H) = 0.30 (experiments 27 and 30);

3) Flow rate Δ (B/H) = 0.06 (experiments 51 and 51b);

4) Density ratio Δ (B/H) = 0.05 (experiments 27 and 33b);

5) Density layering Δ (B/H) = 0.02 (experiments 27 and 33);

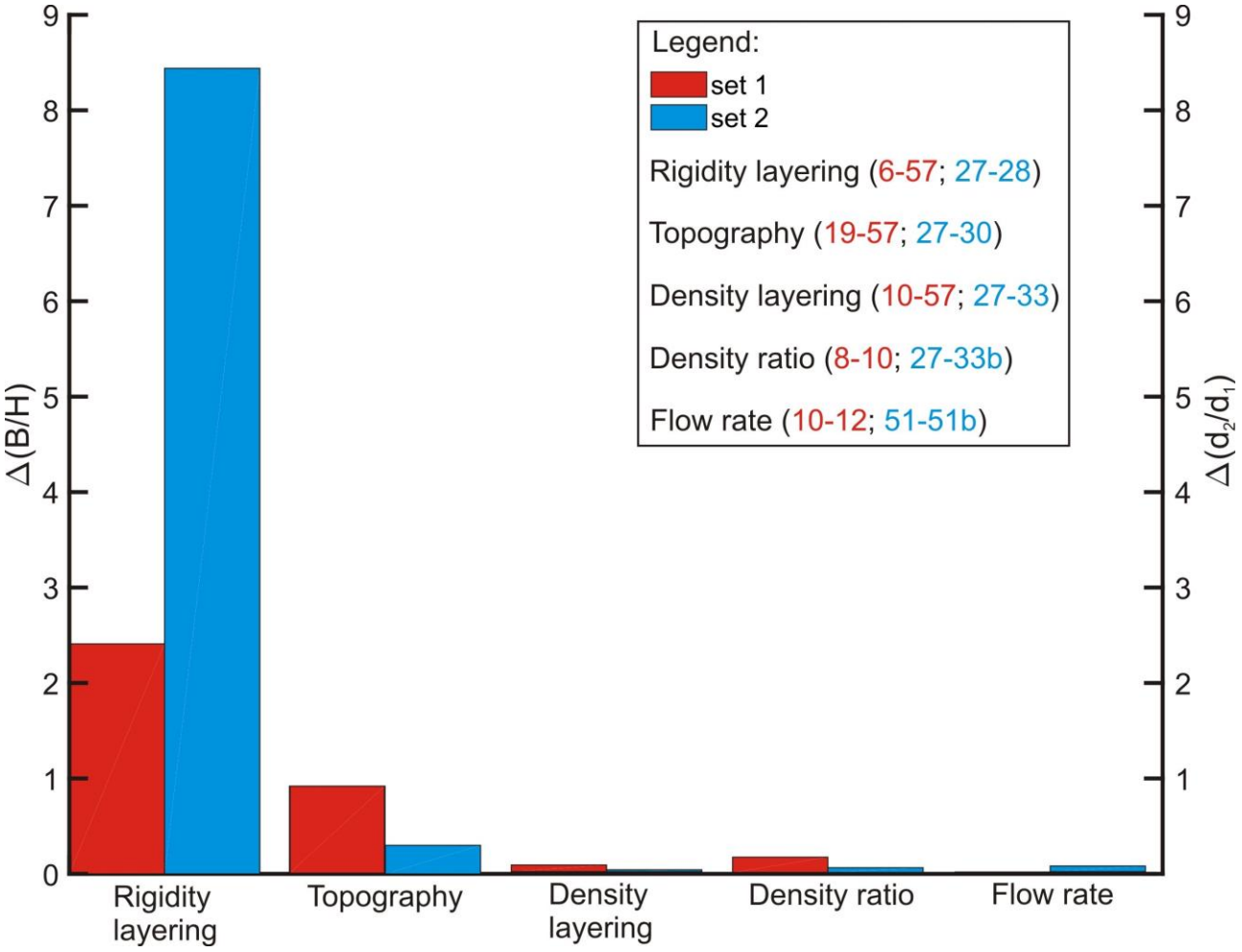

Figure 8. Histogram showing the aspect ratio difference Δ (B/H), left y-axis, for the selected pairs of experiments (indicated in the legend). Exclusively in case of the column referring to set 1 and topography, the indicated value is calculated from the variation of the dike asymmetry (Δ (d_2/d_1), right y-axis) of experiments 19 and 57.

The proposed hierarchy shows that rigidity layering and topography are predominant in promoting lateral propagation regardless the different depth of injection between Set 1 and Set 2. This study highlights that a stiff layer overlying a soft layer (gabbro overlying tuff for example) favors lateral dike propagation (or arrest) more efficiently than the Level of Neutral Buoyancy (LNB) in spite of what previously suggested by analytical [Lister, 1990; Lister, 1991; Lister and Kerr, 1991; Ryan, 1994; Rubin, 1995 and references therein] and numerical models [Taisne and Jaupart, 2009].

The importance of rigidity layering in driving lateral dike propagation or sill inception is also supported by past analogue models, using both air (thus with a buoyancy that is at least one order of

magnitude higher than here) [Rivalta et al., 2005] or water [Kavanagh et al., 2006; Ritter et al., 2013] as magma analogue.

In particular, in [Rivalta et al., 2005], the dike propagated laterally at the interface with the stiffer upper layer and, after the injection of additional volume of air, it inflated penetrating the interface and erupting. This was not observed in our models since the positive buoyancy resulting from injecting water is much less with respect to that injecting air. Therefore, the volume of water injected was insufficient for the dike to break the interface so it propagated laterally up to the box sides.

The formation of lateral dikes (or sills) has never been observed in the case of a neutral buoyancy interface in any of the analogue models cited above. Also in our experiments, we never witnessed lateral propagation or sill formation at the LNB thus confirming previous results.

A model presented in [Lister and Kerr, 1991] is an exception: they obtained lateral dike propagation at the LNB injecting glycerol in agar. The host medium shows a density gradient spanning from 1066 kg m^{-3} to 1310 kg m^{-3} while glycerol density is 1221 kg m^{-3} with the LNB at 18.1 cm from the surface. Two possibilities may explain the discrepancies with our models: 1) The higher anti-buoyancy and thickness of the low-density layer which is - 155 kg m^{-3} and 18.1 cm respectively compared to - 98 kg m^{-3} and 7.3 cm (experiment 8, Table 1); 2) it is possible that the LNB, obtained with the double bucket method resulting in a linear density gradient of the two agar solutions, constitutes also an interface that separates two layers with different rigidity.

The discrepancies (i.e. the lateral propagation at LNB) with analytical and numerical models should be explained by the finite thickness of the layers in our experiments. Indeed, both analytical and numerical models assume an infinite thickness of the regions above and below the interface stating that the dikes, before propagating laterally at the interface, should penetrate the low-density layers over a certain length threshold before reaching the equilibrium [Taisne and Jaupart 2009, Townsend et al., 2017]. Therefore, it is possible that the thickness of the upper layer in our

experiments was below this threshold so that the dikes erupted without showing a consistent lateral propagation which should have shown with a thicker upper layer.

Lastly, numerical models performed by [Maccaferri et al., 2011], suggest that neutral buoyancy by itself cannot induce dikes to turn into sills. Our dataset seem to support that the neutral buoyancy should not induce vertical dikes to turn into lateral dikes as well.

The importance of topography on controlling dike propagation, has been already suggested by analogue [Acocella and Tibaldi, 2005] and numerical models [Maccaferri et al., 2014; Corbi et al., 2015; Heimisson et al., 2015]. In particular, our models show that the stress perpendicular to the dike plane (i.e. σ_2 see [Urbani et al., 2017]) drives lateral propagation especially if is assisted by a stiff upper layer that prevents its ascent. In our experiments, σ_2 decreases downslope, compressing the dike tail and squeezing its front toward the plain, and increases upslope, compressing the dike tip, thus explaining both the asymmetry and the increased length in Set 1 and Set 2 experiments respectively plus the arrest below the plain of all of the experimental dikes (see [Urbani et al., 2017] for further details).

Compared to rigidity layering and topography, it is challenging to define hierarchies between density ratio, density layering and flow rate because the values of the Δ (B/H) are very similar between each other (ranging from 0 to 0.16).

4.3 Comparison to nature

The relevant role of rigidity layering with regard to density is further supported by the fact that the studied range of density ratio variations (ρ_U/ρ_f between 0.9 and 1.03,) is comparable to natural examples. Indeed, if we consider that the density of a basaltic magma ranges from 2600 kg m^{-3} to 2800 kg m^{-3} [Murase and McBirney, 1973] and the density of the crust from 2300 to 2900 kg m^{-3} [Anderson, 1989], we obtain that $\rho_{host\ rock}/\rho_{magma}$ ranges from 0.82 to 1.11.

On the contrary, the rigidity contrasts tested in the experiments represent only a small portion of the natural cases. Indeed, we tested rigidity ratio E_u/E_l ranging from 0.1 to ~ 2 whereas in nature it

spans from 0.09 to 11 (page 435 in [Turcotte and Schubert 2002]) thus up to one order of magnitude higher with respect to our models.

In nature, the decrease in rigidity with depth, leading to rigidity inversions (i.e. stiff layer above a weak one as we modeled here), may be due to soft scoria layers capped by stiff lava flows, as in central Afar [Abbate et al., 2015]. Moreover, in geothermal areas partial melt or superheated steam decreases the rigidity of the host rock by thermal weakening [Heap et al., 2013] so that it becomes more compliant at high depths as it has been geophysically detected at Askja and Krafla (Iceland) [Mitchell et al., 2013; Schuler et al., 2015], Kilauea's East Rift Zone (Hawaii) [Haslinger et al., 2001], Afar [Desissa et al., 2013] and Canary Islands [Martì et al., 2017]. Therefore, these wide scale rigidity inversions, due to thermal and/or chemical alteration of the host rock, may be common in volcanic areas and rift zones and should encourage a dike to propagate laterally at the interface with the stiffer zone as during the 2004 Asama (Japan) and 2011-2012 El Hierro (Canary Islands) eruptions [Aoki et al., 2009; Martì et al., 2013] thus supporting our modeling results.

Recent natural diking events such as Bardarbunga 2014-2015 [Sigmundsson et al., 2015] and Dabbahu 2005-2010 [Ebinger et al., 2010; Belachew et al., 2011] highlighted the relevant role of topography [Urbani et al., 2017] in controlling dike propagation. Indeed, both these two episodes show that the dike stopped before a high relief as observed in our models. Some of our experiments, in case of rigidity layering (experiments 23 and 32, Table 1) or strong negative buoyancy (experiment 17), showed that the dike tip propagated below the plain as during the Bardarbunga eruption [Sigmundsson et al., 2015] but apparently also a discrepancy in the position of the eruption point (which is before and inside the plain in the models and in Bardarbunga respectively). However, during the eruption, were observed three "Ice cauldrons" on the Vatnajökull ice cap right before the plain [Reynolds et al., 2017] suggesting that minor eruptions had occurred but the ice weight forced the main eruption inside it. During the Dabbahu diking episode the northern section of the dike propagated upslope erupting on NE flank of the volcanic edifice in contrast with our experiments which suggest that upslope propagation is inhibited. In this case, the effect on crustal stresses of a

lateral thermal gradient of the crust may have overcome the effect of topography [Grandin et al., 2012] favoring upslope propagation of the dike.

5. Conclusions

In this study, we presented analogue models with the aim to investigate the contribution on dike propagation given by rigidity and density layering, topography, flow rate and the density ratio between magma and host rock. We then the compared the results to evaluate the relative weight of each contribution on lateral dike propagation. Our experimental results suggest that:

1) Rigidity layering (i.e. stiff layers overlying soft layers) and topography (i.e. a slope perpendicular to the dike plane) are the most important factors that promote lateral dike propagation especially if they are combined together. The joint effect of rigidity layering and topography should be considered to explain the lateral propagation observed in recent diking events.

2) Density ratio between magma and host rock, density layering and flow rate show a lower influence on dike propagation. In particular, we did not observed any lateral propagation at the LNB despite what proposed by previous analytical and numerical models.

The proposed hierarchy should be completed adding the processes that influence dike propagation not considered in this study.

Authors contributions

S.U. performed and interpreted the analogue models. E.R. provided the equations and managed the scaling calculations. V.A. supervised the project and provided suggestions for the analogue modelling. All authors discussed the results and contributed to writing the manuscript.

Acknowledgements

Giulia Sili provided technical support during the experiments. Matteo Trolese provided useful suggestions for the image processing. Malte C. Ritter shared his data about gelatin rigidity. Janine Kavanagh provided helpful advices for the setting of the analogue models. This work was financed by the Italian government (MIUR) grants to Roma Tre PhD School in Earth Sciences (XXX doctoral cycle). Any user can access the data of this work by contacting the corresponding author.

References

Abbate, E., P. Bruni, and M. Sagri (2015), Geology of Ethiopia: A Review and Geomorphological Perspectives, in Landscapes and Landforms of Ethiopia, World Geomorphological Landscapes, edited by P. Billi, pp. 33-64, Springer Science + Business Media, Dordrecht, Netherlands, doi: 10.1007/978-94-017-8026-1_2.

Acocella, V., and M. Neri (2003), What makes flank eruptions ? The 2001 Etna eruption and its possible triggering mechanisms, *Bull. Volcanol.*, *65*, 517–529, doi:10.1007/s00445-003-0280-3.

Acocella, V., and A. Tibaldi (2005), Dike propagation driven by volcano collapse: A general model tested at Stromboli, Italy, *Geophys. Res. Lett.*, *32*, L08308, doi:10.1029/2004GL022248.

Acocella, V., M. Porreca, M. Neri, E. Massimi, and M. Mattei (2006), Propagation of dikes at Vesuvio (Italy) and the effect of Mt. Somma, *Geophys. Res. Lett.*, *33*, L08301, doi:10.1029/2005GL025590.

Acocella, V., and M. Neri (2009), Dike propagation in volcanic edifices: Overview and possible developments, *Tectonophysics*, *471*, 67–77, doi:10.1016/j.tecto.2008.10.002.

Anderson, D. L. (1989), Theory of the Earth, Blackwell Scientific Publications, Brookline Village, MA.

Ayele, A., D. Keir, C. Ebinger, T. J. Wright, G. W. Stuart, W. R. Buck, E. Jacques, G. Ogubazghi, and J. Sholan (2009), September 2005 mega-dike emplacement in the Manda-Harraro nascent oceanic rift (Afar depression), *Geophys. Res. Lett.*, *36*, L20306, doi:10.1029/2009GL039605.

Aoki, Y., et al. (2009), P-wave velocity structure beneath Asama Volcano, Japan, inferred from active source seismic experiment, *J. Volcanol. Geotherm. Res.*, *187*, 272–277, doi:10.1016/j.jvolgeores.2009.09.004.

Belachew, M., C. Ebinger, D. Coté, D. Keir, J. V Rowland, J. O. S. Hammond, and A. Ayele (2011), Comparison of dike intrusions in an incipient seafloor - spreading segment in Afar , Ethiopia: Seismicity perspectives, *J. Geophys. Res.*, *116*, B06405, doi:10.1029/2010JB007908.

Biggs, J., F. Amelung, N. Gourmelen, T. H. Dixon, and S. Kim (2009), InSAR observations of 2007 Tanzania rifting episode reveal mixed fault and dyke extension in an immature continental rift, Geophys. J. Int., 179, 549–558, doi:10.1111/j.1365-246X.2009.04262.x.

Brizzi, S., F. Funiciello, F. Corbi, E. Di Giuseppe, and G. Mojoli (2016), Salt matters: How salt affects the rheological and physical properties of gelatine for analogue modelling. *Tectonophysics, 679*, 88-101, doi:10.1016/j.tecto.2016.04.021.

Chadwick, W.W. and J.H. Dieterich (1995), Mechanical modeling of circumferential and radial dike intrusion on Galapagos volcanoes, *J. Volcanol. Geotherm. Res.*, *66*, 37–52, doi:10.1016/0377-0273(94)00060-T.

Chanceaux, L., and T. Menand (2014), Solidification effects on sill formation: An experimental approach, *Earth Planet. Sci. Lett.*, *403*, 79–88, doi:10.1016/j.epsl.2014.06.018.

Chanceaux, L., and T. Menand (2016), The effects of solidification on sill propagation dynamics and morphology, *Earth Planet. Sci. Lett.*, *442*, 39–50, doi:10.1016/j.epsl.2016.02.044.

Corbi, F., E. Rivalta, V. Pinel, F. Maccaferri, M. Bagnardi, and V. Acocella (2015), How caldera collapse shapes the shallow emplacement and transfer of magma in active volcanoes, *Earth Planet. Sci. Lett.*, *431*, 287–293, doi:10.1016/j.epsl.2015.09.028.

Corbi, F., E. Rivalta, V. Pinel, F. Maccaferri, and V. Acocella (2016), Understanding the link between circumferential dikes and eruptive fissures around calderas based on numerical and analog models, *Geophys. Res. Lett.*, *43*, 6212–6219, doi:10.1002/2016GL068721.

Daniels, K. A., and T. Menand (2015), An experimental investigation of dyke injection under regional extensional stress, *J. Geophys. Res. Solid Earth, 120*, 2014–2035, doi:10.1002/2014JB011627.

Desissa, M., N. E. Johnson, K. A. Whaler, S. Hautot, S. Fisseha, and G. J. K. Dawes (2013), A mantle magma reservoir beneath an incipient mid-ocean ridge in Afar , Ethiopia, *Nat. Geosci.*, *6*(10), 861–865, doi:10.1038/ngeo1925.

Di Giuseppe, E., F. Funiciello, F. Corbi, G. Ranalli, and G. Mojoli (2009), Gelatins as rock analogs: A systematic study of their rheological and physical properties, *Tectonophysics, 473(3–4)*, 391–403, doi:10.1016/j.tecto.2009.03.012.

Ebinger, C. J., A. Ayele, D. Keir, J. Rowland, G. Yirgu, T. Wright, M. Belachew, and I. Hamling (2010), Length and timescales of rift faulting and magma intrusion: The Afar rifting cycle from 2005 to present, *Annu. Rev. Earth Planet. Sci., 38(1)*, 439–466, doi:10.1146/annurev-earth-040809-152333.

Einarsson, P., and B. Brandsdóttir (1980), Seismological evidence for Lateral magma intrusion during the July 1978 deflation of the Krafla volcano in NE-Iceland, *J. Geophys., 160-165*, doi:10.2172/890964.

Fialko, Y. A., and A. M. Rubin (1999), What controls the along-strike slopes of volcanic rift zones?, *J. Geophys. Res., 104(B9)*, 20007–20020, doi:10.1029/1999JB900143.

Fiske, R. S., and E. D. Jackson (1972), Orientation and Growth of Hawaiian Volcanic Rifts: The Effect of Regional Structure and Gravitational Stresses, *Proc. R. Soc. Lond. A*, *329*, 299-326, doi:10.1098/rspa.1972.0115.

Fukushima, Y., V. Cayol, and P. Durand (2005), Finding realistic dike models from interferometric synthetic aperture radar data: The February 2000 eruption at Piton de la Fournaise, *J. Geophys. Res., 110*, B03206, doi:10.1029/2004JB003268.

Grandin, R., A. Socquet, C. Doubre, E. Jacques, and G. C. P. King (2012), Elastic thickness control of lateral dyke intrusion at mid-ocean ridges, *Earth Planet. Sci. Lett.*, *319–320*, 83–95, doi:10.1016/j.epsl.2011.12.011.

Gudmundsson, A. (2003), Surface stresses associated with arrested dykes in rift zones, *Bull. Volcanol.*, *65*, 606–619, doi:10.1007/s00445-003-0289-7.

Gudmundsson, A. (2006), How local stresses control magma-chamber ruptures, dyke injections, and eruptions in composite volcanoes, *Earth Sci. Rev.*, *79*, 1–31, doi:10.1016/j.earscirev.2006.06.006.

Hartley, M. E., and T. Thordarson (2012), Formation of Öskjuvatn caldera at Askja, North Iceland : Mechanism of caldera collapse and implications for the lateral flow hypothesis, *J. Volcanol. Geotherm. Res.*, *227–228*, 85–101, doi:10.1016/j.jvolgeores.2012.02.009.

Hartley, M. E., and T. Thordarson (2013), The 1874 – 1876 volcano-tectonic episode at Askja, North Iceland: Lateral flow revisited, *Geochem. Geophys. Geosyst.*, *14*, 2286–2309, doi:10.1002/ggge.20151.

Haslinger, F., C. Thurber, M. Mandernach, and P. Okubo (2001), Tomographic image of P-velocity structure beneath Kilauea's East Rift Zone and South Flank: seismic evidence for a deep magma body, *Geophys. Res. Lett., 28(2)*, 375–378, doi:10.1029/2000GL012018.

Heap, M. J., S. Mollo, S. Vinciguerra, Y. Lavallée, K.-U. Hess, D. B. Dingwell, P. Baud, and G. Iezzi (2013), Thermal weakening of the carbonate basement under Mt. Etna volcano (Italy): Implications for volcano instability, *J. Volcanol. Geotherm. Res.*, *250*, 42–60, doi:10.1016/j.jvolgeores.2012.10.004.

Heimisson, E. R., A. Hooper, and F. Sigmundsson (2015), Forecasting the path of a laterally propagating dike, *J. Geophys. Res. Solid Earth*, *120*, 8774-8792, doi:10.1002/2015JB012402.

Ito, G., and S. J. Martel (2002), Focusing of magma in the upper mantle through dike interaction, *J. Geophys. Res., 107 (B10),* 2223, doi:10.1029/2001JB000251.

Kavanagh, J. L., T. Menand, and R. S. J. Sparks (2006), An experimental investigation of sill formation and propagation in layered elastic media, *Earth Planet. Sci. Lett., 245,* 799–813, doi:10.1016/j.epsl.2006.03.025.

Kavanagh, J. L., T. Menand, and K.A. Daniels (2013), Gelatine as a crustal analogue: Determining elastic properties for modelling magmatic intrusions. *Tectonophysics, 582*, 101-111, doi:10.1016/j.tecto.2012.09.032.

Kervyn, M., G. G. J. Ernst, B. V. W. De Vries, L. Mathieu, and P. Jacobs (2009), Volcano load control on dyke propagation and vent distribution: Insights from analogue modeling, *J. Geophys. Res., 114,* B03401, doi:10.1029/2008JB005653.

Le Corvec, N., T. Menand, and J. Lindsay (2013), Interaction of ascending magma with pre-existing crustal fractures in monogenetic basaltic volcanism: an experimental approach, *J. Geophys. Res. Solid Earth, 118,* 968-984, doi:10.1002/jgrb.50142.

Lister, J. R. (1990), Buoyancy-driven fluid fracture: similarity solutions for the horizontal and vertical propagation of fluid-filled cracks, *J. Fluid Mech., 217,* 213-239, doi:10.1017/S0022112090000696.

Lister, J. R. (1991), Steady solutions for feeder dykes in a density-stratified lithosphere, *Earth Planet. Sci. Lett., 107,* 233–242, doi:10.1016/0012-821X(91)90073-Q.

Lister, J. R., and R. C. Kerr (1991), Fluid-Mechanical Models of Crack Propagation and Their Application to Magma Transport in Dykes, *J. Geophys. Res., 96(B6),* 1049–1077, doi:10.1029/91JB00600.

Maccaferri, F., M. Bonafede, and E. Rivalta (2011), A quantitative study of the mechanisms governing dike propagation, dike arrest and sill formation, *J. Volcanol. Geotherm. Res.*, *208(1–2)*, 39–50, doi:10.1016/j.jvolgeores.2011.09.001.

Maccaferri, F., E. Rivalta, D. Keir, and V. Acocella (2014), Off-rift volcanism in rift zones determined by crustal unloading, *Nat. Geosci.*, *7*, 297–300, doi:10.1038/NGEO2110.

Maccaferri, F., E. Rivalta, L. Passarelli, and Y. Aoki (2016), On the mechanisms governing dike arrest: Insight from the 2000 Miyakejima dike injection, *Earth Planet. Sci. Lett.*, *434*, 64–74, doi:10.1016/j.epsl.2015.11.024.

Martí, J., V. Pinel, C. López, A. Geyer, R. Abella, M. Tárraga, M. J. Blanco, A. Castro, and C. Rodríguez (2013), Causes and mechanisms of the 2011–2012 El Hierro (Canary Islands) submarine eruption, *J. Geophys. Res. Solid Earth*, *118*, 823–839, doi:10.1002/jgrb.50087.

Martí, J., A. Villaseñor, A. Geyer, C. López, and A. Tryggvason (2017), Stress barriers controlling lateral migration of magma revealed by seismic tomography, *Sci. Rep.*, *7*, 1–10, doi:10.1038/srep40757.

Menand, T., K. A. Daniels, and P. Benghiat (2010), Dyke propagation and sill formation in a compressive tectonic environment, *J. Geophys. Res.*, *115*, B08201, doi:10.1029/2009JB006791.

Menand, T., and S. R. Tait (2001), A phenomenological model for precursor volcanic eruptions, *Nature*, *411*, 678–680, doi:10.1038/35079552.

Menand, T., and S. R. Tait (2002), The propagation of a buoyant liquid-filled fissure from a source under constant pressure: An experimental approach, *J. Geophys. Res.*, *107(B11)*, 2306, doi:10.1029/2001JB000589.

Mitchell, M. A., R. S. White, S. Roecker, and T. Greenfield (2013), Tomographic image of melt storage beneath Askja Volcano, Iceland using local microseismicity, *Geophys. Res. Lett., 40*, 5040–5046, doi:10.1002/grl.50899.

Muller, J. R., G. Ito, and S. J. Martel (2001), Effects of volcano loading on dike propagation in an elastic half-space, *J. Geophys. Res., 106(B6)*, 11101–11113, doi:10.1029/2000JB900461.

Murase, T., and A.R. McBirney (1973), Proprieties of some common igneous rocks and their melts at high temperatures, *Geol. Soc. Am. Bull., 84*, 3563-3592, doi:10.1130/0016-7606(1973)84<3563:POSCIR>2.0.CO;2.

Nobile, A., C. Pagli, D. Keir, T. J. Wright, A. Ayele, J. Ruch, and V. Acocella (2012), Dike-fault interaction during the 2004 Dallol intrusion at the northern edge of the Erta Ale Ridge (Afar, Ethiopia), *Geophys. Res. Lett., 39*, L19305, doi:10.1029/2012GL053152.

Pallister, J. S. et al. (2010), Broad accommodation of rift-related extension recorded by dyke intrusion in Saudi Arabia, *Nat. Geosci., 3(10)*, 705–712, doi:10.1038/ngeo966.

Peltier, A., P. Bachèlery, and T. Staudacher (2009), Magma transport and storage at Piton de La Fournaise (La Réunion) between 1972 and 2007: A review of geophysical and geochemical data, *J. Volcanol. Geotherm. Res., 184*, 93–108, doi:10.1016/j.jvolgeores.2008.12.008.

Pinel, V., and C. Jaupart (2004), Magma storage and horizontal dyke injection beneath a volcanic edifice, *Earth Planet. Sci. Lett., 221*, 245–262, doi:10.1016/S0012-821X(04)00076-7.

Pinel, V., A. Carrara, F. Maccaferri, E. Rivalta, and F. Corbi (2017), A two-step model for dynamical dike propagation in two dimensions: Application to the July 2001 Etna eruption, *J. Geophys. Res. Solid Earth*, *122*, 1107–1125, doi:10.1002/2016JB013630.

Ritter, M. C., V. Acocella, J. Ruch, and S. L. Philipp (2013), Conditions and threshold for magma transfer in the layered upper crust: Insights from experimental models, *Geophys. Res. Lett., 40,* 1–5, doi:10.1002/2013GL058199.

Rivalta, E., M. Bottinger, and T. Dahm (2005), Buoyancy-driven fracture ascent: Experiments in layered gelatine, *J. Volcanol. Geotherm. Res., 144*, 273–285, doi:10.1016/j.jvolgeores.2004.11.030.

Rivalta, E., and T. Dahm (2006), Acceleration of buoyancy-driven fractures and magmatic dikes beneath the free surface, *Geophys. J. Int., 166*, 1424-1439, doi:10.1111/j.1365-246X.2006.02962.x.

Rivalta, E. (2010), Evidence that coupling to magma chambers controls the volume history and velocity of laterally propagating intrusions, *J. Geophys. Res., 115*, B07203, doi:10.1029/2009JB006922.

Rivalta, E., B. Taisne, A. P. Bunger, and R. F. Katz (2015), A review of mechanical models of dike propagation: Schools of thought, results and future directions, *Tectonophysics*, *638*, 1–42, doi:10.1016/j.tecto.2014.10.003.

Reynolds, H. I., M. T. Gudmundsson, T. Högnadóttir, E. Magnússon, and F. Pálsson (2017), Subglacial volcanic activity above a lateral dyke path during the 2014–2015 Bárdarbunga-Holuhraun rifting episode, Iceland, *Bull. Volcanol., 79,* 38, doi:10.1007/s00445-017-1122-z.

Rubin, A.M., and D. Pollard (1987), Origins of blade like dikes in volcanic rift zones, in Volcanism in Hawaii, edited by R. W. Decker, T. L. Wright, and P. H. Stauffer, pp. 1449-1470, United States Geological Survey, Reston, VA.

Rubin, A. M. (1995), Propagation of magma-filled cracks, *Annu. Rev. Earth Planet. Sci., 23(1),* 439–466, 287–336, doi:10.1146/annurev.ea.23.050195.001443.

Ryan, M. P., (1994) Neutral-buoyancy controlled magma transport and storage in mid-ocean ridge magma reservoirs and their sheeted-dike complex: A summary of basic relationships, in Magmatic Systems, edited by M. P. Ryan, pp. 97- 135, Academic Press, San Diego, Calif.

Schuler, J., T. Greenfield, R. S. White, S. W. Roecker, B. Brandsdóttir, J. M. Stock, J. Tarasewicz, H. R. Martens, and D. Pugh (2015), Seismic imaging of the shallow crust beneath the Krafla central volcano, NE Iceland, *J. Geophys. Res. Solid Earth*, *120*, 7156-7173, doi:10.1002/2015JB012350.1.

Sigmundsson, F. et al., (2015), Segmented lateral dyke growth in a rifting event at Bárðarbunga volcanic system, Iceland, *Nature*, *517*, 191-195, doi:10.1038/nature14111.

Taisne, B., and C. Jaupart (2009), Dike propagation through layered rocks, *J. Geophys. Res.*, *114*, B09203, doi:10.1029/2008JB006228.

Taisne, B., and S. Tait (2009), Eruption versus intrusion? Arrest of propagation of constant volume, buoyant, liquid-filled cracks in an elastic, brittle host, *J. Geophys. Res.*, *114*, B06202, doi:10.1029/2009JB006297.

Taisne, B., and S. Tait (2011), Effect of solidification on a propagating dike, *J. Geophys. Res.*, *116*, B01206, doi:10.1029/2009JB007058.

Taisne, B., and C. Jaupart (2011), Magma expansion and fragmentation in a propagating dyke, *Earth Planet. Sci. Lett.*, *301(1–2)*, 146–152, doi:10.1016/j.epsl.2010.10.038.

Taisne, B., S. Tait, and C. Jaupart (2011), Conditions for the arrest of a vertical propagating dyke, *Bull. Volcanol. 73*, 191–204, doi:10.1007/s00445-010-0440-1.

Takada, A. (1990), Experimental Study on Propagation of Liquid-Filled Crack in Gelatin: Shape and Velocity in Hydrostatic Stress Condition, *J. Geophys. Res.*, *95*, 8471–8481, doi: 10.1029/JB095iB06p08471.

Townsend, M. R., D. D. Pollard, and R. P. Smith (2017), Mechanical models for dikes: A third school of thought, *Tectonophysics, 703–704*, 98–118, doi:10.1016/j.tecto.2017.03.008.

Turcotte, D. L., and G. Schubert (2002), Geodynamics, Cambridge University Press, Cambridge, England.

Urbani, S., V. Acocella, E. Rivalta, and F. Corbi (2017), Propagation and arrest of dikes under topography: Models applied to the 2014 Bardarbunga (Iceland) rifting event, *Geophys. Res. Lett., 44*, 6692–6701, doi:10.1002/2017GL073130.

Watanabe, T., T. Masuyama, K. Nagaoka, and T. Tahara (2002), Analog experiments on magma-filled cracks: Competition between external stresses and internal pressure, *Earth Planet Sp., 54*, 1247–1261, doi:10.1186/BF03352453.

Wright, T. J. et al. (2012), Geophysical constraints on the dynamics of spreading centres from rifting episodes on land, *Nat. Geosci., 5(4)*, 242–250, doi:10.1038/ngeo1428.

Ziv, A., A. M. Rubin, and A. Agnon (2000), Stability of dike intrusion along preexisting fractures, *J. Geophys. Res., 105(B3)*, 5947–5961, doi:10.1029/1999JB900410.

[Journal of Geophysical Research Solid Earth]

Supporting Information for

[What drives the lateral vs. vertical propagation of dikes? Insights from analogue models]

[S. Urbani[1], V. Acocella[1], E. Rivalta[2]]

[[1]Dipartimento di Scienze, Università Roma Tre, Rome, Italy, [2]Deutsches GeoForschungsZentrum GFZ, Section 2.1, Potsdam, Germany]

Contents of this file

Introduction

[Supplementary material on the analogue models]

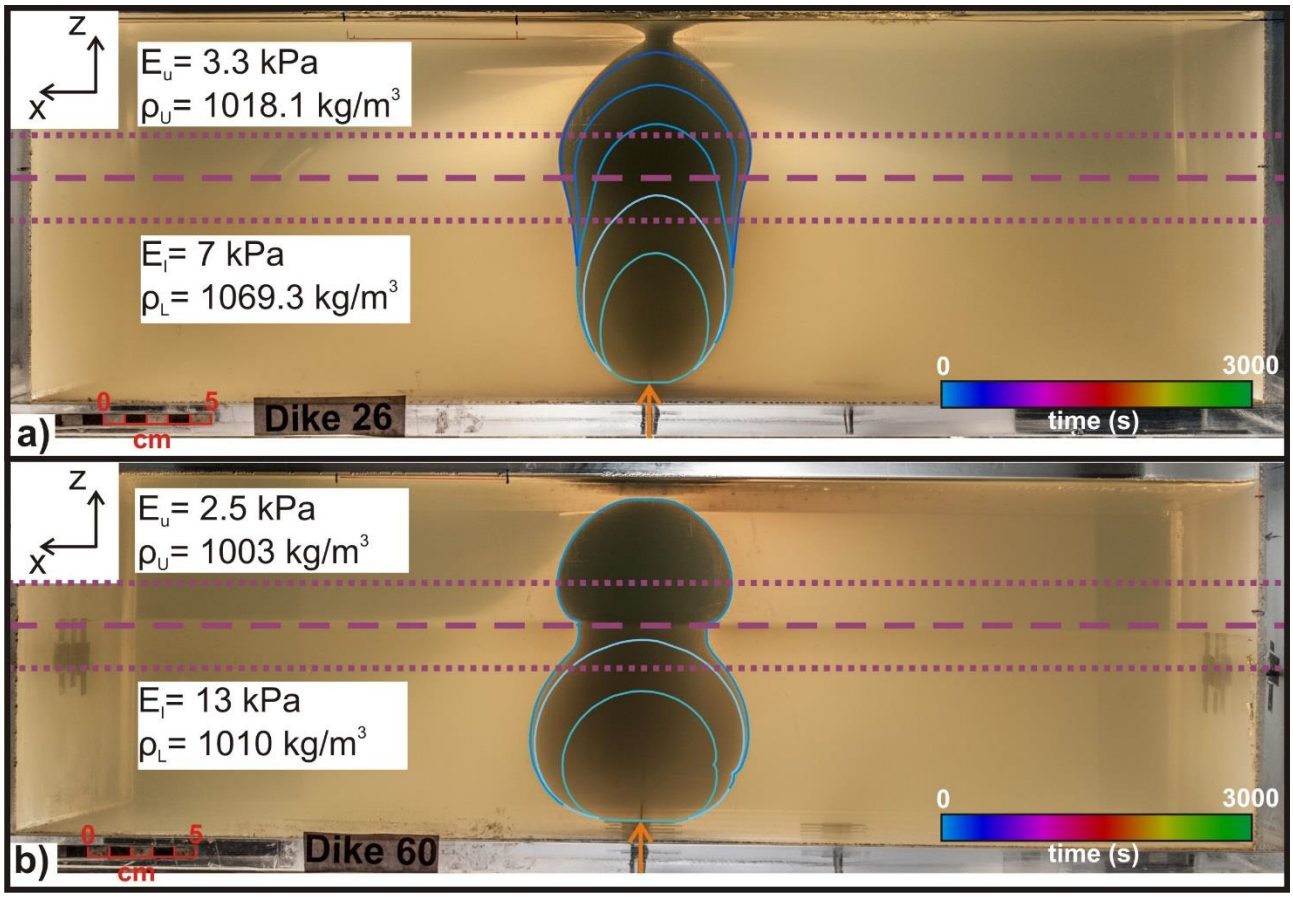

Figure S1. Set 1 experiments showing flat topography and a soft layer overlying the stiff layer. The rigidity ratio is equal to 0.47 and 0.19 in a) and b), respectively. The dashed and dotted purple lines indicate the interface center and the limits of the interface, respectively. The reference system in the top left refers to the box sides and figure 1a. The orange arrows indicate the injection points. The colored lines indicate the dike edge contour every 120 seconds.

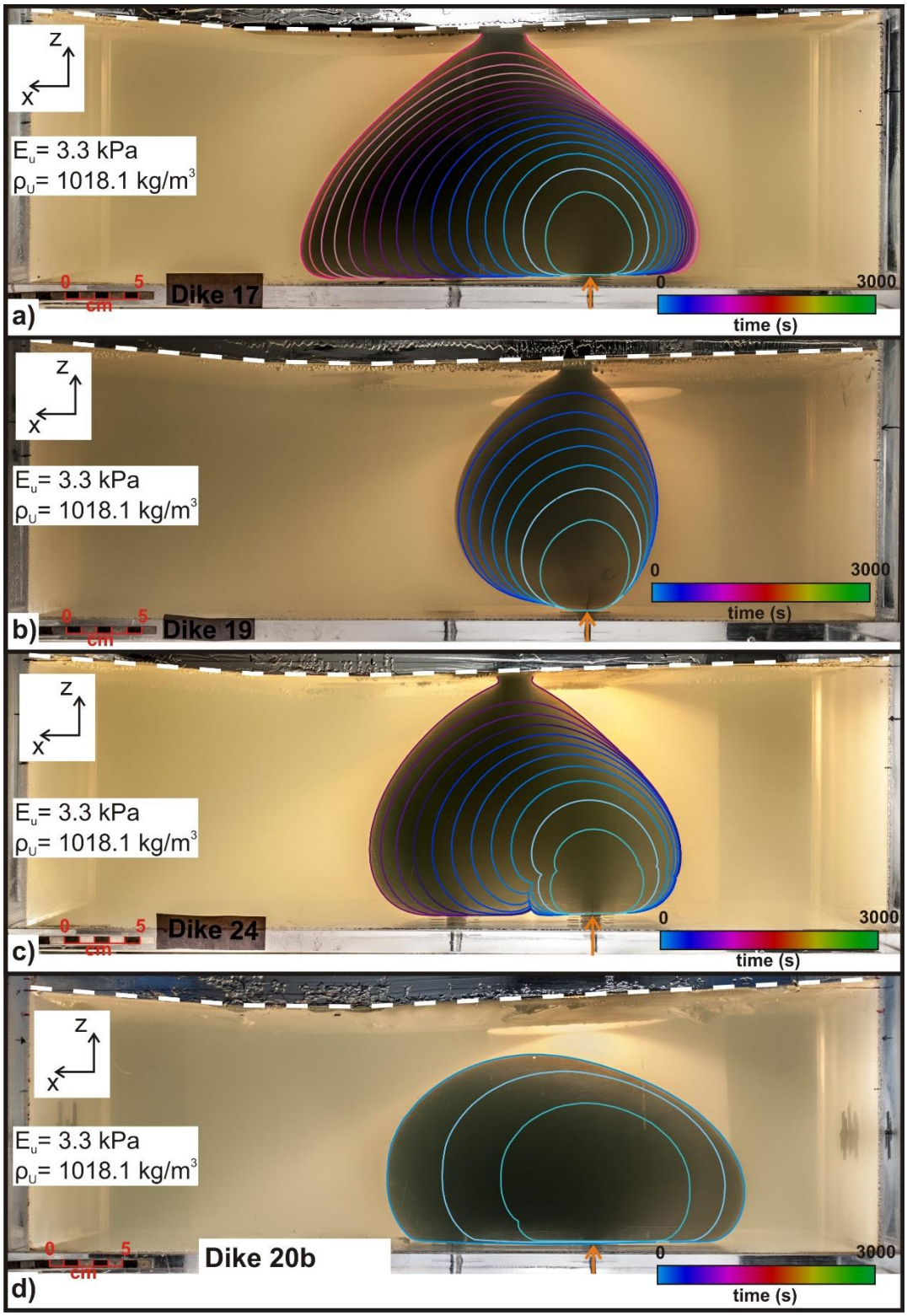

Figure S2. Set 1 experiments with topography and homogeneous gelatin (i.e. no layering). a) Experiment 17: ρ_U/ρ_f= 0.9119; Q= 0.079 ml/s. b) Experiment 19: ρ_U/ρ_f= 1.0247; Q= 0.079 ml/s. c) Experiment 24: ρ_U/ρ_f= 0.9663; Q= 0.079 ml/s. d) Experiment 20b: ρ_U/ρ_f= 0.9119; Q= 0.435 ml/s. The dashed white line indicates the topography profile. The reference system in the top left refers to the box sides and figure 1a. The orange arrows indicate the injection points. The colored lines indicate the dike edge contour every 120 seconds.

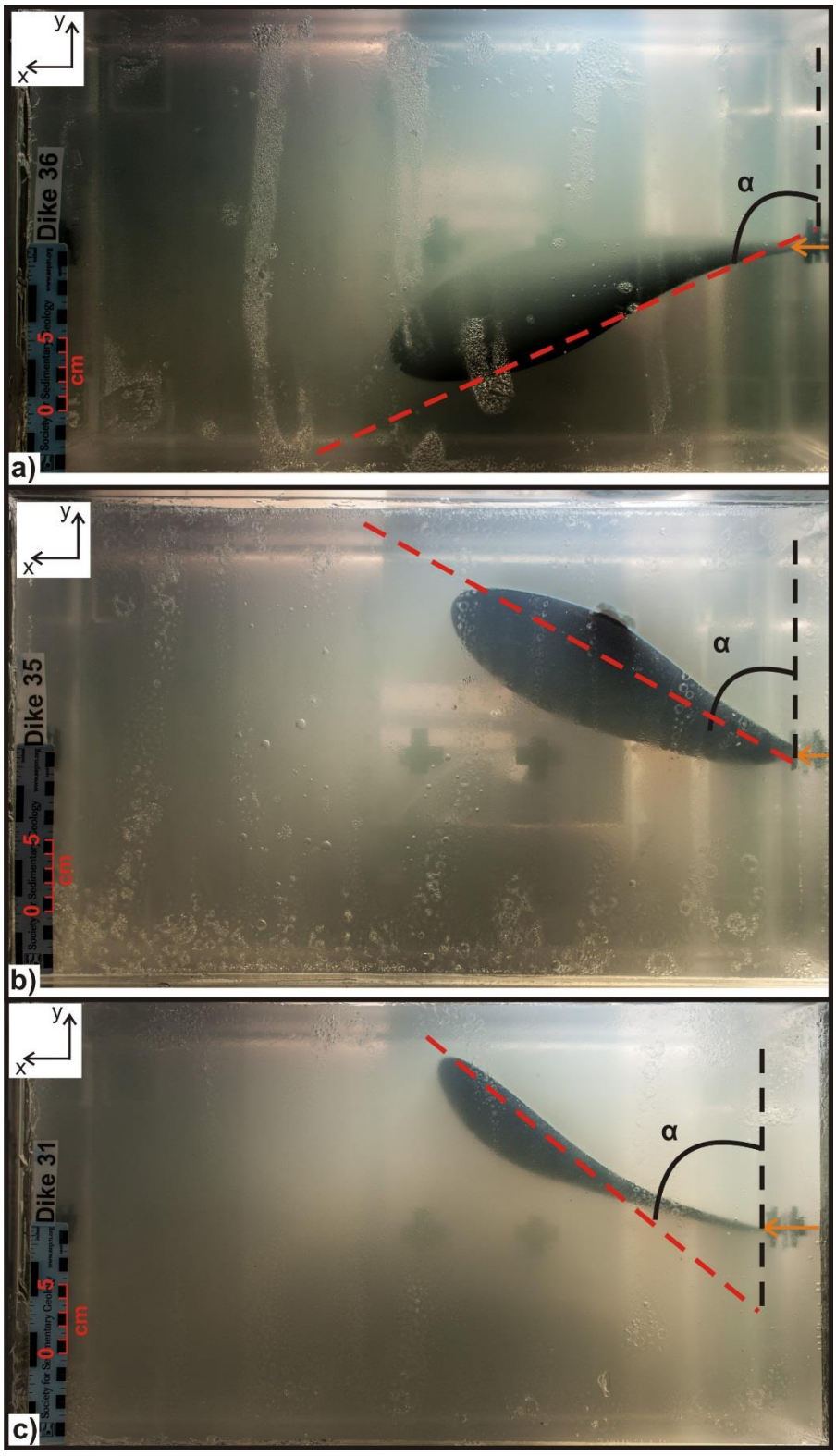

Figure S3. Top view of experiments 36 (a), 35 (b), and 31 (c) showing how the dike tends to be parallel to the imposed topography bending towards the y-axis. α indicates the angle between the slope direction (black dashed line) and the dike strike (red dashed line) which is equal to 114°, 61° and 50° in (a), (b) and (c), respectively. The orange arrow indicates the injection point. Experiments 31 and 35 are excluded from the dataset since they replicate experiments 32 and 36, respectively.

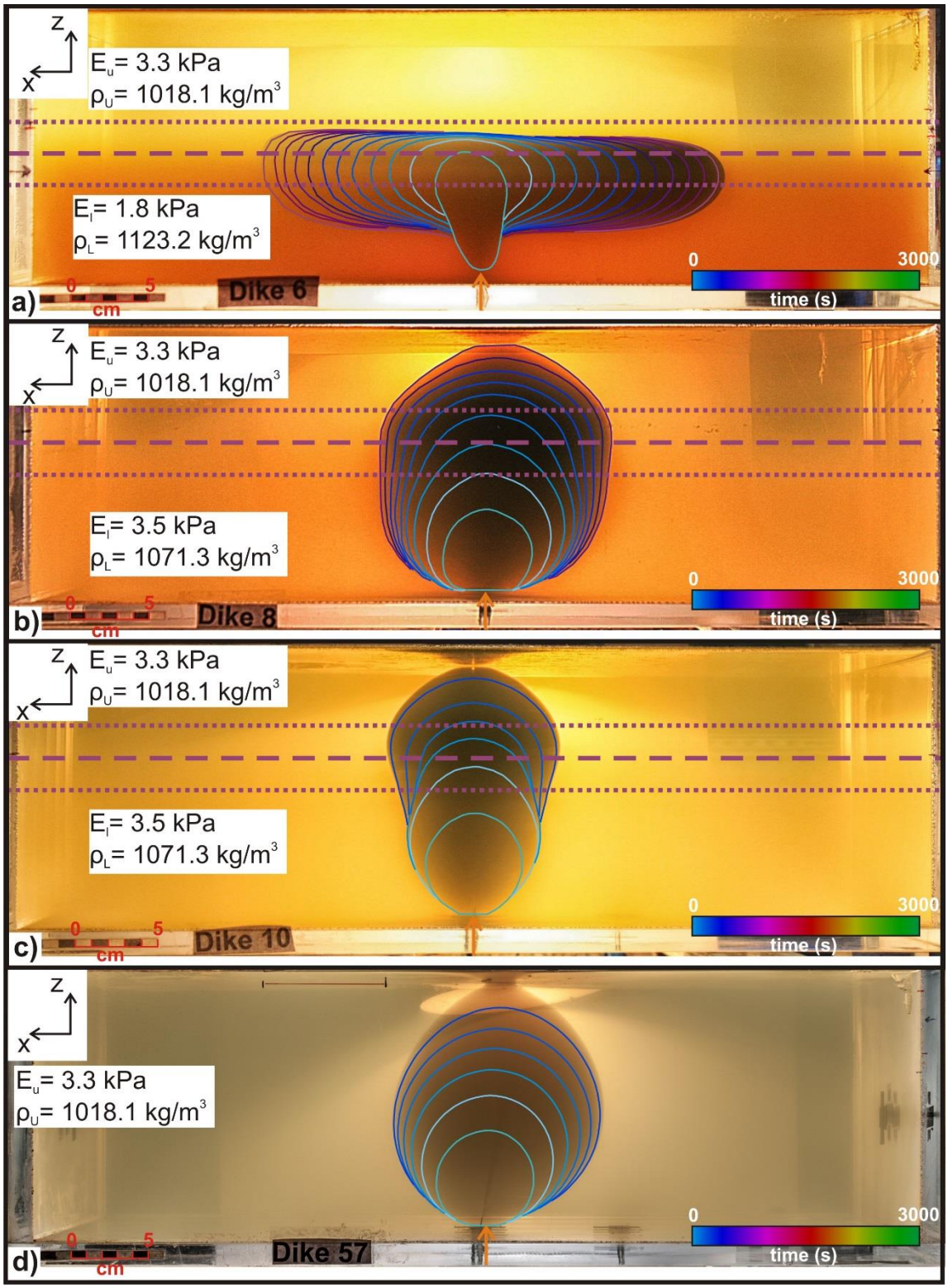

Figure S4. Set 1 experiments showing flat topography, rigidity (a, experiment 6) and density layering (b and c experiments 8 and 10). d) Experiment 57 showing flat topography and no layering. The dashed and dotted purple lines indicate the interface center and the limits of the interface, respectively. The reference system in the top left refers to the box sides and figure 1a. The orange arrows indicate the injection points. The colored lines indicate the dike edge contour every 120 seconds.

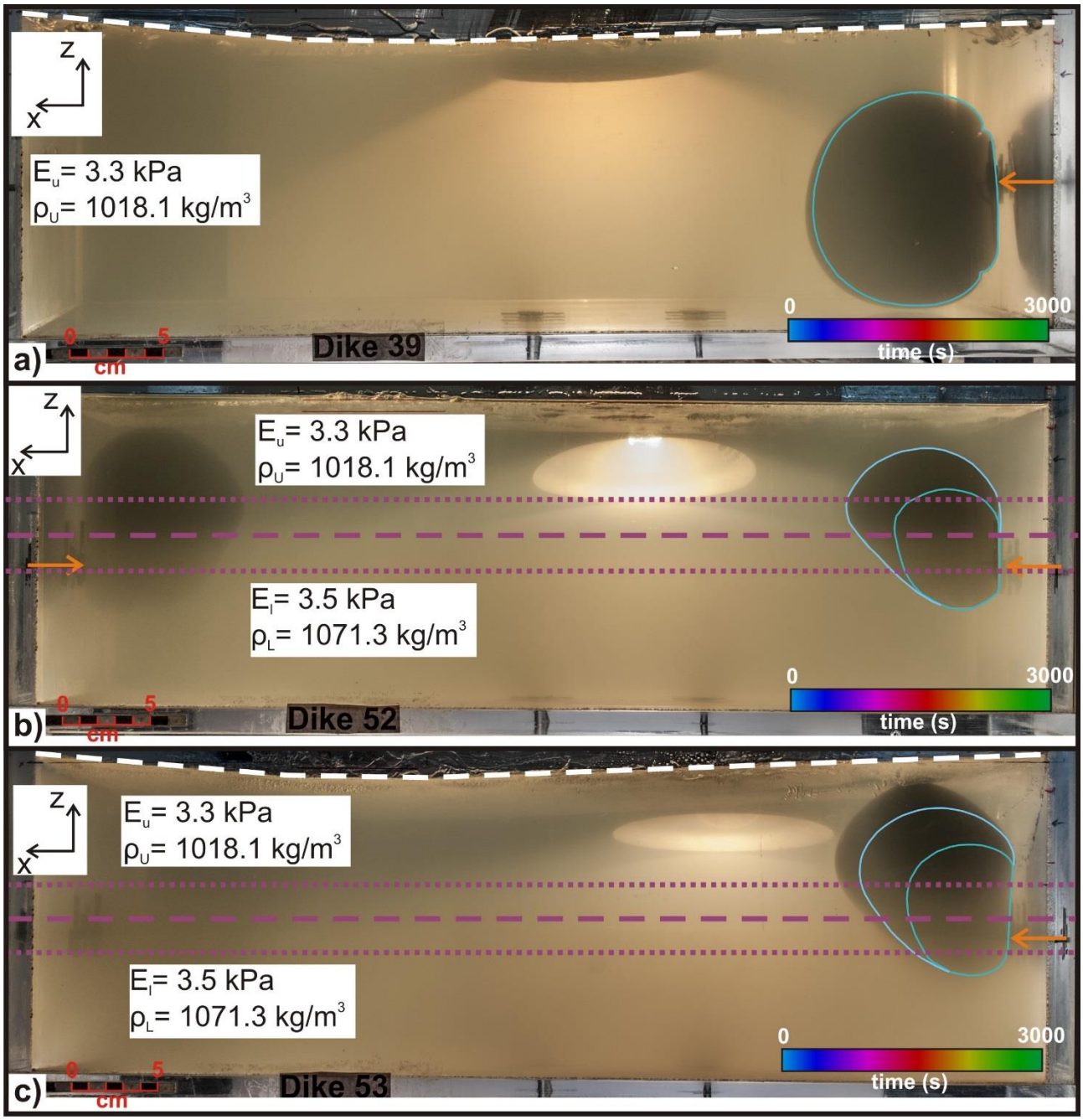

Figure S5. Set 2 experiments with topography and homogeneous gelatin (a, experiment 39), flat topography and density layering (b, experiments 52 and 52b on the right and left side respectively), topography and density layering (c, experiment 53). The dashed white line indicates the topography profile. The dashed and dotted purple lines indicate the interface center and the limits of the interface, respectively. The reference system in the top left refers to the box sides and figure 1a. The orange arrows indicate the injection points. The colored lines indicate the dike edge contour every 120 seconds.

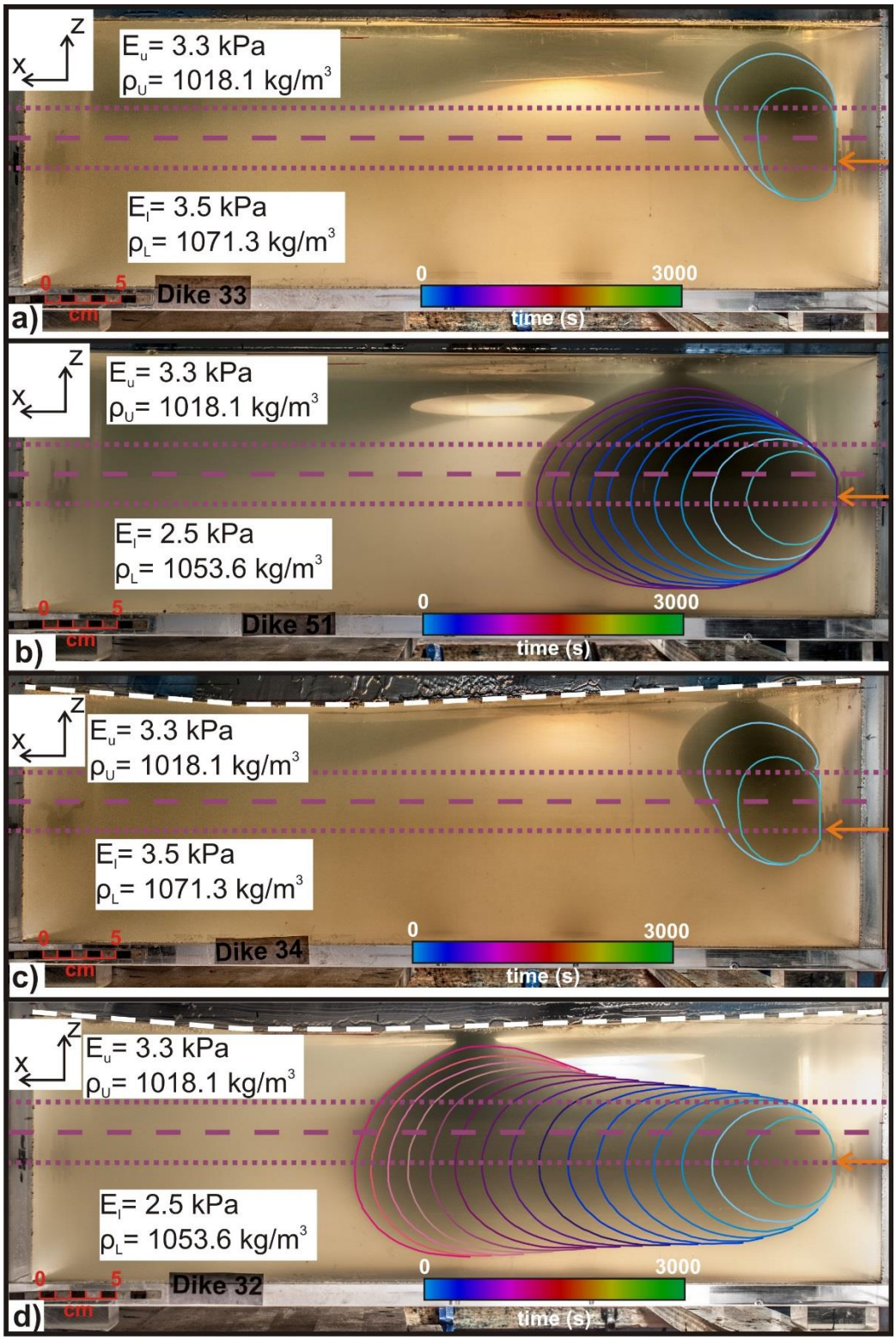

Figure S6. Set 2 experiments with flat topography, density (a, experiment 33) and rigidity layering (b, experiment 51). Experiments with topography, density (c, experiment 34) and rigidity layering (d, experiment 32). The dashed white and purple lines indicate the surface and the center of the interface respectively. Dotted purple lines indicate the limits of the interface. The orange arrows indicate the injection points. The colored lines indicate the dike edge contour every 120 seconds. Modified from [Urbani et al., 2017].

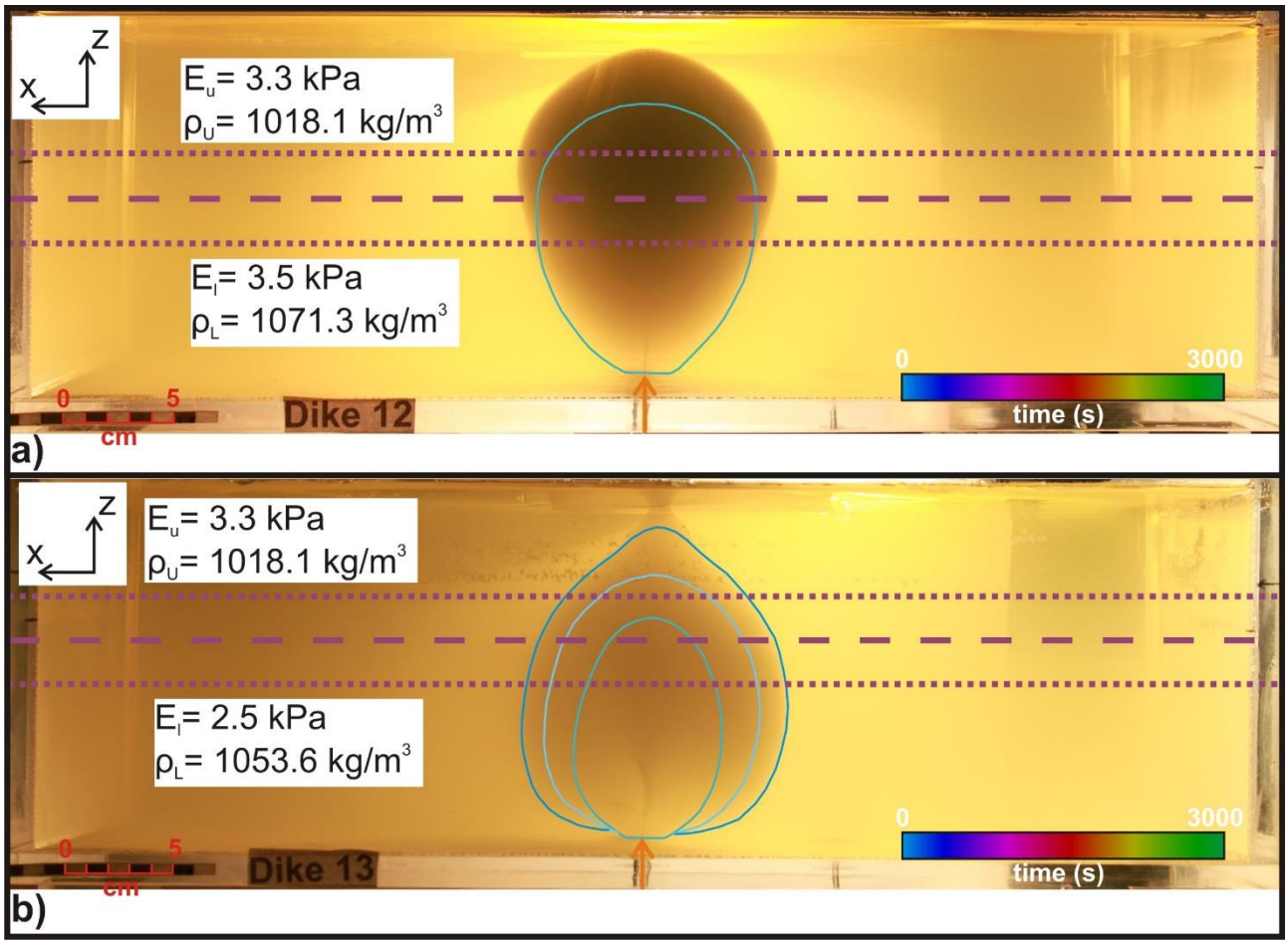

Figure S7. Set 1 experiments with density (a, experiment 12) and rigidity (b, experiment 13) layering, both with high flow rate (Q = 0.435 ml/s). The dashed and dotted purple lines indicate the interface center and the limits of the interface, respectively. The reference system in the top left refers to the box sides and figure 1a. The orange arrows indicate the injection points. The colored lines indicate the dike edge contour every 120 seconds.

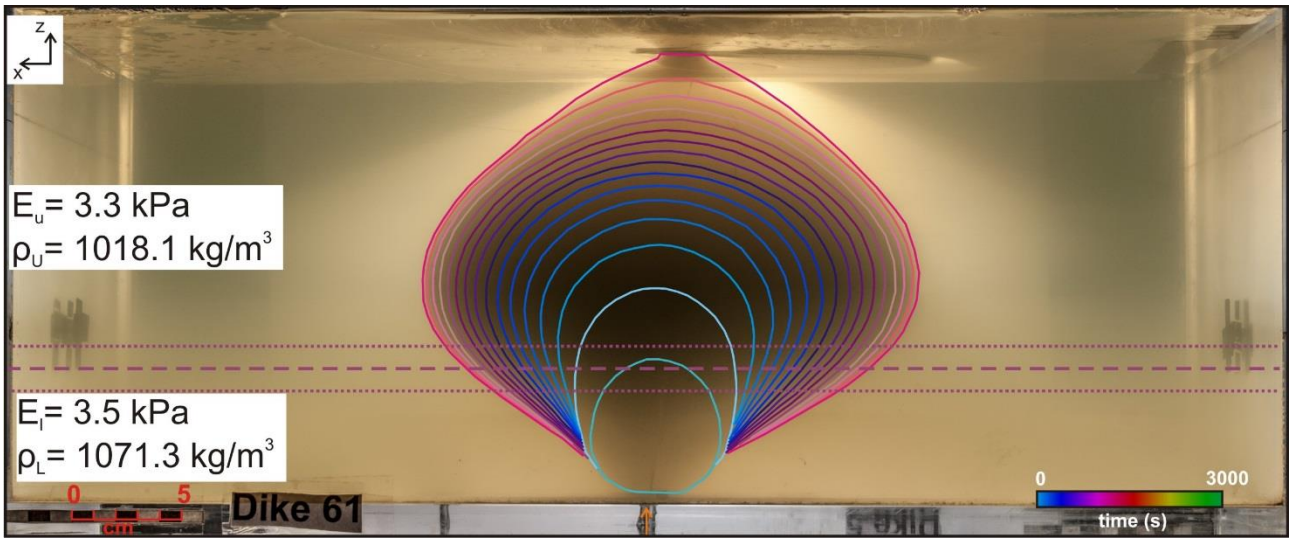

Figure S8. Experiment 61 showing density layering and thickness ratio T_u/T_l= 2.54. The dashed purple line indicates the interface center. The dotted purple lines indicate the limits of the interface. The reference system in the top left refers to the box sides. The orange arrow indicates the injection point. The colored lines indicate the dike edge contour every 120 seconds.

Parameter	Nature	Laboratory	Scaling Factor
$\Delta\rho$	20 kg m^{-3}	20 kg m^{-3}	1
K_c	10^9 Pa m$^{1/2}$	83 Pa m$^{1/2}$	8.3 X 10^{-8}
E	/	/	1.9 X 10^{-7}
V	/	/	7.2 X 10^{-3}
L_b	/	/	1.9 X 10^{-5}
Q	286 m^3 s^{-1}	7.9 X 10^{-8} m^3 s^{-1}	2.76 X 10^{-10}
η	10 Pa s	1.2 X 10^{-3} Pa s	1.2 X 10^{-4}
p_L	/	/	0.6 X 10^{-5}
p_f	/	/	1.9 X 10^{-5}
p_v	/	/	1.1 X 10^{-6}

Table S1. List of the scaled parameters calculated in [Urbani et al., 2017]. $\Delta\rho$= density difference between magma and host rock; K_c= fracture toughness; E= Young modulus; V= propagation velocity; L_b= buoyancy length; Q= flow rate; η= viscosity; p_L= topographic (loading) pressure; p_f= fracture pressure; p_v= viscous pressure.

Chapter 4

General discussion and conclusions

4.1 General discussion

In order to promote lateral propagation, vertical dike ascent needs to be prevented. In this regard, rigidity layering (i.e. a stiff layer overlying a soft one) and topography are the factors that showed the highest effectiveness, being also independent of the depth of injection. In particular, a stiff upper layer provides a strong physical barrier for dike opening in the vertical direction, especially if the rigidity of the upper layer is twice that of the lower layer (i.e. $E_u/E_l \geq 2$), as previously pointed out [Ritter et al., 2013].

On the contrary, a rigidity layering with a soft layer overlying a stiff one may promote vertical ascent, since the upper layer provides less resistance at the tip for dike opening. In particular, the high pressure that builds up at the dike tip to propagate in the lower layer is suddenly released as the dike approaches the interface. This process leads to an abrupt acceleration of the dike in the upper layer until it stabilizes to the rheological proprieties of the surrounding medium.

The imposed topography (i.e. a slope perpendicular to the dike) promotes lateral propagation downslope, since it induces a stress perpendicular to the dike plane (i.e. σ_2, as shown in Urbani et al., 2017) that pushes laterally the dike tip, squeezing its tail. The same process explains also the dike arrest below the plain in front of an opposite relief, since the stress perpendicular to the dike, as it increases upslope, compresses its tip, hindering further propagation.

The proposed hierarchy suggests a subordinate role of density layering and density ratio between host rock and magma on affecting dike propagation. My experiments make clear that the level of neutral buoyancy LNB is not a physical barrier to the vertical magma ascent, but simply the position in which the dike reaches the equilibrium between positive and negative buoyancy (of the lower and

upper layer respectively). The dike will experience a gradually increasing resistance if moving away from this position. At the LNB the total hydrostatic pressure is maximum, implying that the dike will preferentially spread at this level, but still penetrating the lower density layer [Lister, 1990; Rubin 1995 and references therein; Taisne and Jaupart, 2009; Rivalta et al., 2015, Townsend et al., 2017]. This implies that, to obtain a noticeable lateral propagation at the LNB in the experiments, the low-density layer must be thick so that the dike tip can reach the equilibrium prior to erupting. This is confirmed by experiment 61 (Figure S8 in Chapter 3), in which the dike propagated vertically in the lower layer (with positive buoyancy) and then it slowed down in the low-density layer (with negative buoyancy) spreading concentrically (in section view; thus also propagating laterally) before erupting (final B/H=1). However, the lateral propagation obtained in the experiments with high rigidity ratio ($E_u/E_l \sim 2$) is still much higher (B/H ranging from 1.62 to 3.20), even with a thinner stiff upper layer with respect to experiment 61. This confirms that a stiff upper layer is a more effective mechanism to slow down or arrest magma ascent, promoting lateral propagation at the interface, than anti-buoyancy, regardless of the thickness of the intruded layers.

Considering a mean density of basaltic magma $\rho_m = 2700$ kg m^{-3} [Murase and Mc Birney, 1973] and the densities of the most common rocks in the crust (ρ_r) listed in Table 4.1 [Turcotte and Schubert, 2002], I calculate the maximum and minimum natural values for the following ratio:

$$(\rho_r - \rho_m) / \rho_r$$

which ranges between -0.3 to 0.1.

A comparison between this range and the experimental one (ranging between -0.1 to 0.07), shows that the models replicate most of the density variations occurring in nature, excluding the negative extreme values (fig. 4.2). Conversely, natural rigidity ratios (E_u/E_l) span from 0.01 to 11 (Fig. 4.2 and Table 4.1), whereas in the experiments they range between 0.11 to 2, thus showing a difference up to an order of magnitude between each other (fig. 4.2 and table 4.1), with the experimental values covering only a small portion of the natural variability. This implies that the negative buoyancy

occurring in nature may be 3 times more efficient than in the models, thus enhancing the effect of a low density layer shown in fig. 4.1. Thus, at shallow crustal levels, dikes may propagate laterally for larger distances than what observed in the models. However, the 10 times difference between experimental and natural rigidity ratio further supports the strongest effectiveness of a stiff upper layer in preventing vertical ascent and promoting lateral dike propagation at the interface.

Rock type	**ρ (kg m^{-3})**	**E (10^{11} Pa)**
Shale	2100-2700	0.1-0.7
Sandstone	1900-2500	0.1-0.6
Limestone	1600-2700	0.5-0.8
Dolomite	2750-2850	0.5-0.9
Gneiss	2600-2850	0.4-0.6
Amphibole	2800-3150	/
Marble	2670-2750	0.3-0.8
Basalt	2950	0.6-0.8
Granite	2650	0.4-0.7
Diabase	2900	0.8-1.1
Gabbro	2950	0.6-1.0
Diorite	2800	0.6-0.8
Granodiorite	2700	0.7

Table 4.1. Density and rigidity values of the most common rock types in the Earth's crust [Turcotte and Schubert, 2002].

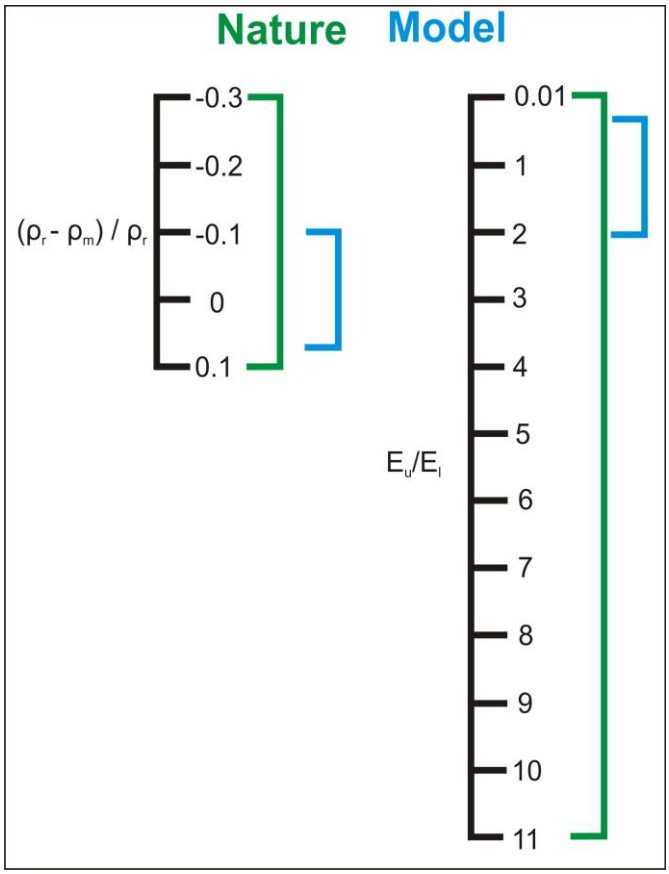

Fig. 4.2 Graphic representation of the studied range of the density and rigidity contrast in the models (blue lines) compared to the ranges occurring in nature (green lines).

One of the assumptions of my experiments is that I consider an unlimited magma availability by feeding the dike with a constant influx rate during the entire duration of the experiments. Even if I have shown that flow rate variations have a negligible effect on dike shape, injecting a limited volume of water would have caused the arrest of some experimental dikes at the interface with a low rigidity layer, as low volume is translated in a lower tensile stress at the dike tip [Gudmundsson 2002, 2003].

Similarly, negative buoyancy in the low-density layers may have stopped the dikes at depth, depending on the amount of positive buoyancy in the lower layer. However, these assumptions will not have changed the main conclusions of this study since, even with a finite amount of water, the dikes should have propagated for shorter distances being influenced by the imposed parameters in the same way observed in the experiments.

Another limitation of my experiments is that I assumed gas-free magma. This implies that the large overpressure due to gas exsolution in magma are underestimated in the experiments. Such large internal pressures in the dike are required to break up the interface with stiff layers, as shown by Rivalta et al., [2005], and may occur in nature especially at shallow depths.

It is important to note that the proposed hierarchy is based on the variations of the final shape of the dikes. The kinematic analysis shows that density ratio variations strongly influence dike velocity (in our case the dike shape evolution with time) with respect to the final geometry (i.e. the dike final shape). This suggests that any hierarchy based on the dike shape may be revisited if based on dike velocity, since density ratio variations, resulting in higher or lower buoyancy, may accelerate or decelerate the dikes.

The models show that an effective barrier to magma ascent (as it is rigidity layering in the models) must assist the effect of topography (i.e. promoting lateral propagation downslope). However, since we investigated the effects of a simplified topographic 2D geometry, models with more complex 3D geometry should be performed as this geometry simulates better the surface loads at stratovolcanoes.

Moreover, in the experiments I neglect the effects of tectonic regional extension, being σ_3 in the plane of the dike. Even if I cannot evaluate the effects of a regional σ_3 perpendicular to the dike, I can assume that this should have favored further lateral propagation, as suggested by the increasing aspect ratio (length/width) of magmatic systems along divergent plate boundaries with increasing extension rate [Acocella, 2014]. Observations from the Iceland Krafla sequence and the Afar Manda-Hararo dikes [Wright et al., 2012] and numerical models [Buck et al., 2006] showed that extensional stress has the effect of preventing eruption of laterally propagating dikes. In fact, the earlier dikes in the sequences had comparatively less eruptive tendency than the later dikes, because the extensional stress accumulated by the tectonics was compensated by the previous dikes. Exploring the role of extensional stress in gelatin experiments is certainly an interesting perspective, however I believe that the hierarchy of factors established here will not be overturned since an extensional stress may have enhanced the effects of rigidity layering and topography further promoting lateral propagation.

Lastly, numerical models should also be performed in this view (i.e. hierarchy definition) to avoid the limitations of the analogue models and test the proposed hierarchy by making different assumptions.

4.2 Conclusions

The take home messages of the PhD thesis are:

1) Rigidity layering (stiff layer above soft layer) promotes lateral dike propagation providing a strong physical barrier to magma ascent. Conversely, reverse layering (soft layer above a stiff layer) promotes vertical ascent by favoring abrupt acceleration of the dike at the interface.

2) A gentle slope, perpendicular to the dike plane, promotes lateral propagation of the dike downslope by compressing its tail. In turn, an opposite topographic pressure gradient (i.e. upslope) favors dike arrest by compressing its tip. This topographic effect will influence dike propagation only if is assisted by other conditions that prevent magma ascent.

3) The joint effect of rigidity layering and topography on dike propagation shows close similarities with recent lateral diking events, suggesting that they should be considered to explain the lateral propagation occurring in nature.

4) Density ratio between host rock and magma, density layering and flow rate show a subordinate influence on lateral dike propagation.

5) In our models we did not observe any significant lateral propagation at the Level of Neutral Buoyancy even with a thick low-density layer, despite what proposed by previous analytical and numerical models considering an infinite thickness of the intruded layers.

References

Acocella, V. (2014), Structural control on magmatism along divergent and convergent plate boundaries: overview, model, problems, *Earth Sci. Rev.*, *136*, 226-288, doi:10.1016/j.earscirev.2014.05.006.

Buck, W.R., P. Einarsson, and B. Brandsdóttir (2006), Tectonic stress and magma chamber size as controls on dike propagation: constraints from the 1975–1984 Krafla rifting episode, *J. Geophys. Res. Solid. Earth, 111*, B12404, doi:10.1029/2005JB003879.

Gudmundsson, A. (2002), Emplacement and arrest of sheets and dykes in central volcanoes, J. *Volcanol. Geotherm. Res., 116*, 279–29, doi:10.1016/S0377-0273(02)00226-3.

Gudmundsson, A. (2003), Surface stresses associated with arrested dykes in rift zones, *Bull. Volcanol., 65*, 606–619, doi:10.1007/s00445-003-0289-7.

Lister, J. R. (1990), Buoyancy-driven fluid fracture: similarity solutions for the horizontal and vertical propagation of fluid-filled cracks, *J. Fluid Mech., 217*, 213-239, doi:10.1017/S0022112090000696.

Murase, T., and A.R. McBirney (1973), Proprieties of some common igneous rocks and their melts at high temperatures, *Geol. Soc. Am. Bull., 84*, 3563-3592, doi:10.1130/0016-7606(1973)84<3563:POSCIR>2.0.CO;2.

Ritter, M. C., V. Acocella, J. Ruch, and S. L. Philipp (2013), Conditions and threshold for magma transfer in the layered upper crust: Insights from experimental models, *Geophys. Res. Lett., 40*, 1–5, doi:10.1002/2013GL058199.

Rivalta, E., M. Bottinger, and T. Dahm (2005), Buoyancy-driven fracture ascent: Experiments in layered gelatine, *J. Volcanol. Geotherm. Res., 144*, 273–285, doi:10.1016/j.jvolgeores.2004.11.030.

Rivalta, E., B. Taisne, A. P. Bunger, and R. F. Katz (2015), A review of mechanical models of dike propagation: Schools of thought, results and future directions, *Tectonophysics*, *638*, 1–42, doi:10.1016/j.tecto.2014.10.003.

Rubin, A. M. (1995), Propagation of magma-filled cracks, *Annu. Rev. Earth Planet. Sci., 23(1),* 439–466, 287–336, doi:10.1146/annurev.ea.23.050195.001443.

Taisne, B., and C. Jaupart (2009), Dike propagation through layered rocks, *J. Geophys. Res., 114*, B09203, doi:10.1029/2008JB006228.

Townsend, M. R., D. D. Pollard, and R. P. Smith (2017), Mechanical models for dikes: A third school of thought, *Tectonophysics*, *703–704*, 98–118, doi:10.1016/j.tecto.2017.03.008.

Turcotte, D. L., and G. Schubert (2002), Geodynamics, Cambridge University Press, Cambridge, England.

Urbani, S., V. Acocella, E. Rivalta, and F. Corbi (2017), Propagation and arrest of dikes under topography: Models applied to the 2014 Bardarbunga (Iceland) rifting event, *Geophys. Res. Lett., 44*, 6692–6701, doi:10.1002/2017GL073130.

Wright, T. J. et al. (2012), Geophysical constraints on the dynamics of spreading centres from rifting episodes on land, *Nat. Geosci., 5(4)*, 242–250, doi:10.1038/ngeo1428.